Copyright

By

Matthew James Bean

2006

Bending Fatigue Performance of Small-Scale Stay Cables

by

Matthew James Bean, B.S.C.E

Thesis

Presented to the Faculty of the Graduate School of

The University of Texas at Austin

in Partial Fulfillment

of the Requirements

for the Degree of

Master of Science in Engineering

The University of Texas at Austin

May 2006

Bending Fatigue Performance of Small-Scale Stay Cables

APPROVED BY
SUPERVISING COMMITTEE:

Sharon L. Wood, Supervisor

Karl H. Frank

Dedication

I want to dedicate this to Stephanie and Preston. All this work is for them.

Acknowledgements

I would like to acknowledge the efforts of my wife, Stephanie Bean. She has supported me and loved me these years as I have worked to finish school. Her unfailing love has kept me going. I love her and I thank God everyday for her.

I would also like to thank Dr. Wood for her guidance and Jun-Ki Lee for his work and support. I acknowledge the contributions of my fellow graduate students as well as those individual who have helped with the physical labor required for this project.

May 5, 2006

Bending Fatigue Performance of Small-Scale Stay Cables

Matthew James Bean, M.S.E.

The University of Texas at Austin, 2006

SUPERVISOR: Sharon L. Wood

This thesis documents the construction and fatigue testing of small-scale specimens designed to model the longest stays on the Fred Hartman Bridge. Transverse stiffness and axial strains were monitored periodically during the fatigue tests to evaluate the degradation of the structural characteristics due to the accumulation of fatigue damage. Also, strand was tested axially to determine the mechanical and fatigue properties and to compare them to published values. The goal of the project is to compare the measured response of the small-scale specimens with analytical models used to evaluate the fatigue response of the bridge stays..

Table of Contents

CHAPTER 1 INTRODUCTION 1

1.1 Fred Hartman Bridge 1

1.2 Who Was Fred Hartman? 4

1.3 Cable Vibrations 5

1.3.1 Vortex Shedding 5

1.3.2 Wake Effects 6

1.3.3 Buffeting 7

1.3.4 Aerodynamic Instability 7

1.3.5 Parametric or Deck Excitation 7

1.3.6 Wind-Rain Induced Vibrations on the Bridge 8

1.4 Damage Research and Repair 8

1.4.1 Bridge Damage and Repair 10

1.4.2 John Hopkins University Research Contribution 11

1.4.3 Texas Tech University Research Contribution 12

1.4.4 University of Texas at Austin Research Contribution 12

1.4.4.1 Field Measurements and Inspection 13

1.4.4.2 Large-Scale Testing in Fatigue Bending 13

1.4.4.3 Characterization of Vibrations Data 14

1.4.4.4 Computational Models 14

1.5 Scope of Investigation 15

CHAPTER 2 SINGLE-STRAND TENSION FATIGUE TESTS 17

2.1 Axial Fatigue Test 17

2.1.1 Test Procedure 18

2.1.1.1 PTI Guide Specifications 19

2.1.1.2 Test Set Up 19
2.1.2 Results…. 23
2.1.2.1 Strand A 23
2.1.2.2 Strand B 25
2.1.3 Summary 26
2.2 Strand Recovered from Large-Scale Bending Fatigue Specimen 27
2.3 Elastic Modulus of Strands 30
2.3.1 Instrumentation and Testing Procedures 30
2.3.1.1 Extensometer 30
2.3.1.2 Strain Gages 31
2.3.1.3 Testing Procedures 32
2.3.2 Measured Modulus of Strand 33
2.3.3 Measured apparent Modulus of Strand 35
2.3.3.1 Results of Apparent Modulus Test 35
2.3.4 Summary 38

CHAPTER 3 CONSTRUCTION OF SMALL-SCALE BENDING FATIGUE SPECIMENS 40

3.1 General Test Setup 40
3.2 Support Conditions for Small-Scale Specimens 41
3.3 Anchor Heads 42
3.4 Materials…. 44
3.4.1 Prestressing Strands 44
3.4.2 Grout…. 45
3.4.3 Duct…… 45
3.5 Construction Sequence 47
3.5.1 Assembly of Test Specimens 47

3.5.2 Grouting 49
3.5.3 Attaching Actuator 50
3.6 Construction Sequence for Specimen 1 51
3.7 Locations of Strain Gages 51
3.7.1 Strain Gage Positions 52
3.7.2 Specimen 1 52
3.7.3 Specimen 2 53
3.7.4 Specimen 3 54
CHAPTER 4 BENDING FATIGUE TESTS 56
4.1 Fatigue Tests 56
4.1.1 Hydraulic Actuator 58
4.1.2 Controller 59
4.2 Fatigue Tests for Specimen 1 60
4.3 Periodic Static Measurements 61
4.3.1 Static Stiffness 62
4.3.2 Strain…. 62
4.4 Free-Vibration Tests 62
4.5 Acoustic Monitoring 63
CHAPTER 5 MEASURED RESPONSE OF SMALL-SCALE SPECIMENS DURING BENDING FATIGUE TESTS 65
5.1 Overview of Fatigue Tests 65
5.2 Acoustic Monitoring 68
5.2.1 Specimen 1 68
5.2.2 Specimen 2 69
5.3 Lateral Stiffness 70
5.3.1 Specimen 1 70

5.3.2 Specimen 2 72
5.3.3 Specimen 3 73

5.4 Measured Strain Response 74
5.4.1 Specimen 3 74
5.4.2 Specimen 2 79
5.4.3 Specimen 1 84

5.5 Comparison with Predicted Response 87

CHAPTER 6 OBSERVED DAMAGE AFTER CONCLUSION OF SMALL-SCALE BENDING FATIGUE TESTS 91

6.1 Wire Fractures due to Fretting 91

6.2 Autopsy Results 93
6.2.1 Specimen 1 93
6.2.2 Specimen 2 99

CHAPTER 7 SUMMARY AND CONCLUSIONS 103

7.1 Summary…. 103

7.2 Conclusions 103
7.2.1 Axial Fatigue Response of Strand 103
7.2.2 Comparison of Small-Scale and Large-Scale 104
7.2.3 SoundPrint System 105
7.2.4 Strain Gages near the Anchor Head 105
7.2.5 Comparison of Measured and Predicted Response 105

APPENDIX A CONSTRUCTION DETAILS 106

A.1 Reaction Frame 106

A.2 Anchor Supports 107

A.3 Prepackaged Grout 108

APPENDIX B RESULTS OF STRAIN MEASUREMENTS 109

B.1 Specimen 1 109

B.1.1 Test 1…. 109

B.1.2 Test 2…. 112

B.1.3 Test 3…. 114

B.2 Specimen 2 117

B.2.1 Test 1…. 117

B.2.2 Test 2…. 119

B.2.3 Test 3…. 122

B.2.4 Test 4…. 124

B.2.5 Test 5…. 127

B.2.6 Test 6…. 129

B.2.7 Test 7…. 131

B.2.8 Test 8…. 133

B.3 Specimen 3 135

B.3.1 Test 1…. 135

REFERENCES 138

VITA.. 140

List of Tables

Table 1-1: Summary of the Fred Hartman Bridge 3
Table 2-1: PTI specifications for strand fatigue Life 19
Table 2-2: Prestressing Strand: Physical Properties 20
Table 2-3: Test Loading and Frequency 21
Table 2-4: Testing Stress Ranges 21
Table 2-5: Strand A axial fatigue test results 24
Table 2-6: Strand B axial fatigue test results 25
Table 2-7: Axial fatigue tests of Strand B and Strand B recovered from bending fatigue specimen 28
Table 2-8: Average elastic modulus of strand 35
Table 2-9: Apparent Modulus of strand 38
Table 3-1: Prestressing properties of Strand B 45
Table 3-2: Strain gage Locations for Specimen 1 53
Table 3-3: Strain gage Locations for Specimen 2 54
Table 3-4: Gage Locations for Specimen 3 55
Table 5-1: Dates of fatigue and static tests 66
Table 5-2 Parameters used to control fatigue tests for Specimen 1 67
Table 5-3: Parameters used to control fatigue tests for Specimen 2 67
Table 5-4: Parameters used to control fatigue tests for Specimen 3 67
Table 5-5: Summary of wire breaks Reported by SoundPrint for Specimen 1 69
Table 5-6: Summary of wire breaks Reported by SoundPrint for Specimen 2 70
Table 5-7: Calculated stiffness for Specimen 1 71
Table 5-8: Calculated stiffness for Specimen 2 73
Table 5-9: Conversion of cut-off stress level to strain 76
Table 5-10: Bending fatigue testing levels 76
Table 5-11: Stress range inferred from measured strain - Specimen 3 77
Table 5-12: Stress range inferred from measured strain - Specimen 2, Test 1 80
Table 5-13: Stress range inferred from measured strain - Specimen 2, Test 2 80
Table 5-14: Strain summary and calculated stresses of Specimen 1 - Test 1 North End 87
Table 5-15: Strain summary and calculated stresses of Specimen 1 - Test 1 South End 88
Table 5-16: Comparison of Pebley's model and Specimen 1-Test 1 88
Table 5-17: Strain summary and calculated stresses of Specimen 1 - Test 2 North End 89
Table 5-18: Strain summary and calculated stresses of Specimen 1 - Test 2 South End 89
Table 5-19: Comparison of Pebley's model and Specimen 1-Test 2 89
Table 6-1: Measured locations of wire breaks – Specimen 1 95

Table 6-2: Measured locations of wire breaks – Specimen 2 100
Table A-1: Grout Properties 108

List of Figures

Figure 1-1 Fred Hartman Bridge 2
Figure 1-3 Vortex shedding 6
Figure 1-4 Wake effects in twin cables 6
Figure 1-5 Wind-rain induced vibrations 8
Figure 1-6 Observed large-amplitude vibrations of stay cables on Fred Hartman Bridge 9
Figure 1-7 Broken guide pipe to anchorage box connections 9
Figure 1-8 Cable restrainers on the Fred Hartman Bridge 11
Figure 1-9 Dampers installed near the deck anchorage regions 11
Figure 1-10 Large-scale bending fatigue tests 14
Figure 2-1 Wire break within grip 18
Figure 2-2 Acceptable wire break along free length 18
Figure 2-3 Sketch of test set-up 20
Figure 2-4 Strand wrapped with copper wire 22
Figure 2-5 Aluminum grips after excessive use 23
Figure 2-6 Strand A: Results of tensile fatigue tests 24
Figure 2-7 Strand B: Results of tensile fatigue tests 26
Figure 2-8 Location of strands recovered large-scale from bending fatigue specimens 28
Figure 2-9 Results of tensile fatigue tests for strand recovered from large-scale bending fatigue specimens 29
Figure 2-10 Photograph of surface of strands 29
Figure 2-11 Modulus Tests 31
Figure 2-12 Strain gages used to determine apparent modulus of strand 32
Figure 2-13 Test 1: Measured stress-strain response 33
Figure 2-14 Test 2: Measures stress-strain response 34
Figure 2-15 Test 3: Measured stress-strain response 34
Figure 2-16 Test 1; Measured response of strain gages 36
Figure 2-17 Test 2; Measured response of strain gages 37
Figure 2-18 Test 3; Measured response of strain gages 37
Figure 3-1 Test Set-up 41
Figure 3-2 Reaction frame and anchor support 42
Figure 3-3 Photographs of anchor heads used for bending fatigue tests 43
Figure 3-4 Dimensions of small-scale anchor head 43
Figure 3-5 Grout cap 44
Figure 3-6 0.6-in. diameter prestressing strand 45
Figure 3-7 Post-tensioning duct 46
Figure 3-8 Wedges used to grip end of strand 47
Figure 3-9 Stressing of strands individually with hydraulic ram 48

Figure 3-10 Strain gages on strands at north end with duct shifted to the side..... 49
Figure 3-11 Strain gage on strand 49
Figure 3-12 Grouting hoses and vents..... 50
Figure 3-13 Strain gage notation..... 52
Figure 3-14 Locations of strain gages for Specimen 1..... 53
Figure 3-15 Locations of strain gages for Specimen 2..... 54
Figure 3-16 Locations of strain gages for Specimen 3..... 55
Figure 4-1 Set-up for fatigue tests..... 57
Figure 4-2 Actuator setup..... 58
Figure 4-3 User interface of controller..... 60
Figure 4-4 Accelerometer..... 63
Figure 4-5 Accelerometer and acoustic sensor locations 64
Figure 4-6 Acoustic sensors 64
Figure 5-1 Measured response of Specimen 1 during static tests 71
Figure 5-2 Measured response of Specimen 2 during static tests 72
Figure 5-3 Measured response of Specimen 3 during static tests 73
Figure 5-4 Measured Strain Response - Specimen 3 74
Figure 5-5 Maximum and minimum loads from fatigue tests superimposed on measured strains from initial static test - Specimen 3..... 77
Figure 5-6 Stress Ranges in Fatigue Test Inferred from Measured Strains in Static Test - Specimen 3; Actuator load is 1.75 k 78
Figure 5-7 Stress Ranges in Fatigue Test Inferred from Measured Strains in Static Test - Specimen 3 for 2 ft from North end; Actuator load is 1.75 k 79
Figure 5-8 Stress Ranges in Fatigue Test Inferred from Measured Strains in Static Test 1 - Specimen 2; Actuator load is 1.8 k 81
Figure 5-9 Maximum and minimum loads from fatigue tests superimposed on measured strains from initial static test - Specimen 2..... 82
Figure 5-10 Summary of Measured Strains; Specimen 2– Static Tests 1 through 4..... 83
Figure 5-11 Summary of Measured Strains; Specimen 2 – Static Tests 1 through 8 84
Figure 5-12 Summary of Measured Strains; Specimen1 – Static Tests 1 through 3 86
Figure 6-1 Initiation points for fretting fatigue 92
Figure 6-2 Fretting fatigue failure between two adjacent outer wires 92
Figure 6-3 North end of Specimen 1 at end of fatigue test 94
Figure 6-4 Fracture of all wires at north end of Specimen 1..... 94
Figure 6-5 Sign convention used to locate wire breaks 95
Figure 6-6 Photographs of wire breaks at north end of Specimen 1 96
Figure 6-7 Comparison of wire breaks detected by SoundPrint with actual locations – Specimen 1 North End..... 97

Figure 6-8 Comparison of wire breaks detected by SoundPrint with actual locations – Specimen 1 Near Midspan 97
Figure 6-9 Photograph of condition of specimen after fracture at north end of Specimen 1 99
Figure 6-10 Typical section through Specimen 1 99
Figure 6-11 Comparison of wire breaks detected by SoundPrint with actual locations – Specimen 2 North End 101
Figure 6-12 Autopsy of specimen 2 101
Figure 6-13 Specimen 2 after grout has been removed 102
Figure A-1 Reaction frame 106
Figure A-2 Reaction frame drawing 107
Figure A-3 Anchor support 107
Figure A-4 Anchor support drawing 108
Figure B-1 Specimen 1 - Test 1- All strain data 110
Figure B-2 Specimen 1 - Test 1- North end strain data 110
Figure B-3 Specimen 1 - Test 1- South end strain data 111
Figure B-4 Specimen 1 - Test 1- Center strain data 111
Figure B-5 Specimen 1 - Test 2- All strain data 112
Figure B-6 Specimen 1 - Test 2- North end strain data 113
Figure B-7 Specimen 1 - Test 2- South end strain data 113
Figure B-8 Specimen 1 - Test 2- Center strain data 114
Figure B-9 Specimen 1 - Test 3- All strain data 115
Figure B-10 Specimen 1 - Test 3- North end strain data 115
Figure B-11 Specimen 1 - Test 3- South end strain data 116
Figure B-12 Specimen 1 - Test 3- Center strain data 116
Figure B-13 Specimen 2 - Test 1- All strain data 117
Figure B-14 Specimen 2 - Test 1- North end strain data 118
Figure B-15 Specimen 2 - Test 1- South end strain data 118
Figure B-16 Specimen 2 - Test 1- Center strain data 119
Figure B-17 Specimen 2 - Test 2- All strain data 120
Figure B-18 Specimen 2 - Test 2- North end strain data. 120
Figure B-19 Specimen 2 - Test 2- South end strain data 121
Figure B-20 Specimen 2 - Test 2- Center strain data 121
Figure B-21 Specimen 2 - Test 3- All strain data 122
Figure B-22 Specimen 2 - Test 3- North end strain data 123
Figure B-23 Specimen 2 - Test 3- South end strain data 123
Figure B-24 Specimen 2 - Test 3- Center strain data 124
Figure B-25 Specimen 2 - Test 4- All strain data 125
Figure B-26 Specimen 2 - Test 4- North end strain data 125
Figure B-27 Specimen 2 - Test 4- South end strain data 126
Figure B-28 Specimen 2 - Test 4- Center strain data 126
Figure B-29 Specimen 2 - Test 5- All strain data 127

Figure B-30 Specimen 2 - Test 5- North end strain data 128
Figure B-31 Specimen 2 - Test 5- South end and Center strain data 128
Figure B-32 Specimen 2 - Test 6- All strain data 129
Figure B-33 Specimen 2 - Test 6- North end strain data 130
Figure B-34 Specimen 2 - Test 6- South end and Center strain data 130
Figure B-35 Specimen 2 - Test 7- All strain data 131
Figure B-36 Specimen 2 - Test 7- North end strain data 132
Figure B-37 Specimen 2 - Test 7- South end and Center strain data 132
Figure B-38 Specimen 2 - Test 8- All strain data 133
Figure B-39 Specimen 2 - Test 8- North end strain data 134
Figure B-40 Specimen 2 - Test 8- South end and Center strain data 134
Figure B-41 Specimen 3- All strain data 135
Figure B-42 Specimen 3- North end strain data at 2 in and 6 in 136
Figure B-43 Specimen 3- North end strain data at 12 in and 18 in 136
Figure B-44 Specimen 3- Center strain data 137
Figure B-45 Specimen 3- South end strain data 137

CHAPTER 1
Introduction

1.1 FRED HARTMAN BRIDGE

During the construction of the Fred Hartman Bridge, near Baytown, Texas, large-amplitude vibrations of the stay cables were observed. These vibrations occurred during various conditions, including light wind and rain. Large-amplitude vibrations can cause fatigue damage and shorten the life of the bridge. These conditions have also been observed in other cable-stayed bridges around the world, including the Veterans Memorial Bridge in Texas. In 1997, the Texas Department of Transportation (TxDOT) initiated a coordinated research project to limit further damage to the stay cables, repair observable damage caused by the large-amplitude vibrations, and estimate the extent of the fatigue damage caused by the repetitive motions. This thesis documents the results of small-scale, fatigue tests conducted in the Ferguson Structural Engineering Laboratory to understand the fatigue response of the stay cables.

Figure 1-1 Fred Hartman Bridge (texasexplorer.net, 2006)

Construction of the Fred Hartman Bridge began in 1986 and was completed in September of 1995 at a cost of over $100 million. The cable-stay bridge spans the Houston Ship Channel and carries Texas State Highway 146 from LaPorte to Baytown.

The twin double diamond shaped towers support the deck 174 ft above the water surface and the tops of the towers are 440 ft above the ground. Each of the two decks are 78 ft wide making the total deck area 353,000 ft^2. The Fred Hartman Bridge was one of the largest cable-stayed bridges in the world when it was constructed. The bridge is 2,475 ft long with a main span of 1,250 ft. This span provides 600 ft of navigable channel while allowing ten times the road traffic as the Baytown-LaPorte Tunnel, which was decommissioned after completion of the bridge.

Table 1-1: Summary of the Fred Hartman Bridge (texasexplorer.net, 2006)

Built:	1986-1995
Designed by:	District 12 of the Texas Department of Highways and Public Transportation
Owner:	Texas Department of Transportation
Original Design:	Leonhardt, Andra Und Partner, URS Greiner
Structural Engineer:	Woodward Clyde
Subcontractor:	Holger S. Svensson, DRC
Consultant:	Robert H. Scanlan
Cost:	$117,500,000
Tower Height:	440 ft
Maximum Span:	1,250 ft
Crosses:	Houston Ship Channel
Carries:	Texas State Road 146

Each of the two bridge decks contains four lanes of traffic and two emergency lanes. The decks are supported by 192 stay-cables, arranged in fan patterns along each of the diamond shaped concrete towers. The cables of the bridge are parallel strand cables, with outside diameters between 4-½ and 7-5/8 in. and lengths between 195 and 650 ft (TxDOT). Each stay cable has between 19 and 61 prestressing strands. The prestressing strands have a diameter of 0.6 in. Polyethylene (PE) pipe surrounds the strands and portland cement grout was used to fill the space between the wires and the pipe. The pipe and the grout were selected to provide two layers of corrosion protection for the prestressing strands.

1.2 WHO WAS FRED HARTMAN?

Figure 1-2 Fred Hartman (TDNA, 2006)

Fred Hartman was a newspaper owner and community leader in the Baytown area. He was born May 20, 1908, in Marlin, Texas. He first became interested in newspapers in the 1920s in high school in Springfield, Missouri (AP, 1991).

Hartman later attended Baylor University and received his Masters in Journalism in 1931. After graduating, he accepted a job as editor-business manager of a news publishing company in La Porte, Texas. The company printed six newspapers in the Houston area along the ship channel (Hornswell, 1983).

In 1935, Hartman become the sports editor for the Baytown Sun. By 1944, Hartman was editor of the newspaper and six years later he also served as publisher. He held these positions for 24 years (Hornswell, 1983).

Hartman received a law degree from the Houston Law School ten years after graduating from Baylor. He had chances to work for larger newspapers but opted to stay with community newspapers. He served as chairman of the board of Southern Newspapers. He believed that local newspapers should be independent and not try to compete with the city papers on national coverage (Hornswell, 1983). He felt that the hometown-news should be emphasized. At its zenith, his newspaper corporation owned more that two dozen papers in Texas.

The bridge is named for Fred Hartman in recognition of his contributions to the area. Hartman had the idea to build the bridge years before its construction, and he used his influence in the community and state to help get residents and

officials involved. Fred Hartman died in 1991 during the construction of the bridge (AP, 1991).

1.3 CABLE VIBRATIONS

Cable-stay bridges have become increasingly popular in the last 50 years, with huge advances in cable-stay bridge technology and increasing bridge span in the last 15 years. However, it has been observed that the stay cables experience vibrations, sometimes large-amplitude, which may cause fatigue damage or damage to other structural bridge members. Several different causes for the vibrations have been identified and are summarized briefly in the following sections. Methods for controlling these vibrations include installing cable dampers in the anchorage region or cable restrainers that connect adjacent cables and reduce vibration in fundamental modes.

1.3.1 Vortex Shedding

Vortex shedding is observed when a smooth flow of air passing around an object produces vortices (Zou, 2005). These vortices form on alternating sides of the stay cable and create alternating forces perpendicular to the direction of the wind (Figure 1-3). When the frequency of the vortex shedding matches a natural frequency of the stay cable, visible vibrations occur. The stay cables have relatively small diameters, so the critical wind velocities needed to produce these vortices are very low. Because of low critical wind velocity, vortex shedding was not considered to be a cause of the large-amplitude vibrations observed on the Fred Hartman Bridge.

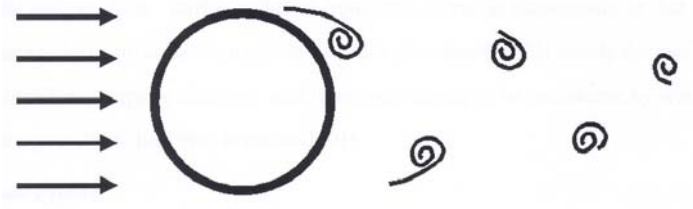

Figure 1-3 Vortex shedding (Dowd, 2001)

1.3.2 Wake Effects

This phenomenon occurs when a cable is in the wake of a structural element or another cable. Vortices form around and behind an object, similar to vortex shedding. If a cable lies in the path of these vortices then that cable can experience vibration. If one cable is in the wake of another cable, the second cable is affected by the wind flow around the first cable, and then in turn the first one is affected by the change in flow around the second one (Virlogeux, 1998). Again, because of the relatively low wind velocities, wake effects were not considered to be the cause of the large-amplitude vibrations.

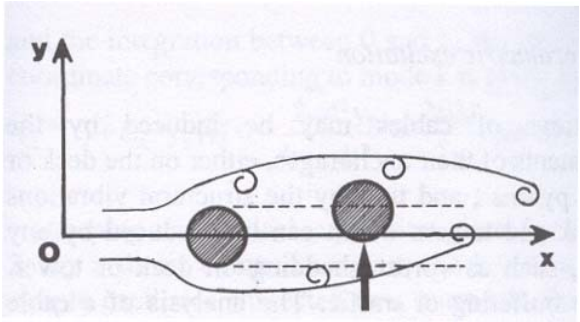

Figure 1-4 Wake effects in twin cables (Virlogeux, 1998)

1.3.3 Buffeting

Turbulent wind flow conditions cause buffeting vibrations. This type of vibration can occur from direct turbulent wind flow on the stay cable or a wake turbulent flow from a nearby structural element. Buffeting is likely to affect bridge decks more than the stay cables (Virlogeux, 1998).

1.3.4 Aerodynamic Instability

Aerodynamic instability, also known as galloping, causes vibrations that are induced by wind on stay cable with irregular shapes or cross-sections. Pipes generally have circular cross-sections so this is usually not a problem. If the cable pipe has an odd cross-section or if ice has formed along the pipe then wind can force vibrations to occur. To avoid this incident, stay pipes have been designed with different cross-sections to allow wind to flow more smoothly around the stay cable. Also, they are designed so that water cannot stay on the cable long enough to freeze (Virlogeux, 1998).

1.3.5 Parametric or Deck Excitation

Parametric excitation vibrations are induced by the movements of the cable anchorages, propagating from the bridge deck or tower. These movements in the structural elements can be caused by wind on the element, traffic, or other means. This type of vibration can be avoided by separating the natural frequencies of the major structural elements (Virlogeux, 1998).

1.3.6 Wind-Rain Induced Vibrations on the Bridge

Wind-rain induced vibrations are similar to vibrations of galloping. During rainy and windy conditions, water collects to form one or two small rivulets on the sides of the stay cable at a perpendicular axis to the direction of the wind. These water rivulets change the cross-sectional shape and aerodynamics of the stay cable. As the wind blows and the cable moves the rivulets also shift causing cyclic oscillations (Zou, 2005).

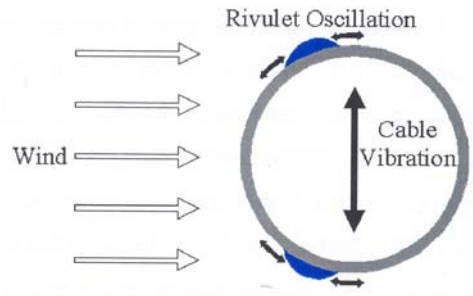

Figure 1-5 Wind-rain induced vibrations (Dowd, 2001)

1.4 DAMAGE RESEARCH AND REPAIR

Large-amplitude vibrations on the Fred Hartman Bridge were observed for the first time during construction. Photos of large-amplitude stay cable vibrations are shown in Figure 1-6. The longest cables have experienced vibrations with amplitudes on the order of ±20 in. (Poston, 1998). The frequency of the vibrations was between 1 to 3 Hz. These large-amplitude vibrations were observed under low to moderate wind speeds (10-45 mph) and rainy conditions (Zou, 2005).

Figure 1-6 Observed large-amplitude vibrations of stay cables on Fred Hartman Bridge (TxDOT, 1997)

These large-amplitude vibrations caused 101 of 192 anchorage guide pipes to fracture during the time between construction was completed and 1998 when the research project was initiated (Figure 1-7). The damage to the guide pipes was a clear illustration that large-amplitude vibrations of the say cables can cause structural damage.

Figure 1-7 Broken guide pipe to anchorage box connections (TxDOT, 1997)

TxDOT established the following set of objectives when it initiated the study of the Fred Hartman Bridge:

- Design the repair of the anchor guide pipes and any other damage caused by the large-amplitude vibrations.

- Control and minimize these vibrations with an effective engineered design.
- Characterize the vibrations such that effective dampers can be designed and installed.
- Characterize the fatigue properties of the stay cables.
- Estimate the amount of fatigue damage in the stay cables caused by the vibrations.

Researchers and engineers from Whitlock, Dalrymple, Poston, and Associates (WDP), John Hopkins University (JHU), Texas Tech University (TTU), and the University of Texas at Austin (UT) formed the project team.

1.4.1 Bridge Damage and Repair

Engineers at WDP designed the modifications to the Fred Hartman Bridge to repair observed damage and prevent further damage due to large-amplitude vibrations of the stay cables.

The guide pipes fractured because the stays cables came in contact with the guide pipes. This caused a fracture of the weld in most of the pipes (Figure 1-7). The guide pipes were repaired and stiffeners were added to help withstand lateral forces resisted by the pipes.

To limit the vibrations in the stay cables, cable restrainers and dampers were installed. The cable restrainers connect adjacent stay cables and restrict relative motion between them. The cable restrainers were installed at key locations to reduce the effective length of the stay cables, which reduces the vibration amplitude that a cable might experience. Viscous dampers were also installed near the lower anchorage points to limit the vibrations.

Figure 1-8 Cable restrainers on the Fred Hartman Bridge (Ridd 2004)

Figure 1-9 Dampers installed near the deck anchorage regions (Ridd 2004)

1.4.2 John Hopkins University Research Contribution

The research team at JHU instrumented the stay cables of the Fred Hartman Bridge to collect weather and vibration data. Their goal was to understand the mechanisms of vibrations that the Fred Hartman is experiencing. They also assessed the effectiveness of viscous dampers and cable restrainers in mitigating the large-amplitude vibrations (Zou, 2005).

Accelerometers were installed on the stays to monitor vibrations. JHU worked closely with WDP to design effective dampers for the cable stays. Understanding the characteristics of the cables and the observed vibrations helped

to design the dampers. A weather station was also installed at the bridge to determine the conditions when these vibrations occur. All this information was been monitored and recorded between October 1997 and August 2005.

After years of monitoring, JHU found that many mechanisms cause vibration of the stay cables, including vortex shedding, wind-rain induced, and parametric deck induced vibrations. They also found that the dampers and cable restrainers have been generally effective in reducing large-amplitude vibrations in the stay cables. (Zou, 2005)

1.4.3 Texas Tech University Research Contribution

Researchers at TTU developed a passive aerodynamic damping system for the stay cables of the Fred Harman Bridge. The system consists of rings placed around the stay cables at a spacing of two to four times the diameter of the stay cable. The rings have circular cross-sections a small fraction of the diameter of the stay cable. The rings were designed to reduce the chances of the formation of water rivulets. These rivulets are necessary to have wind-rain induced vibrations. This damping system did not function as designed and was not installed on the bridge.

1.4.4 University of Texas at Austin Research Contribution

The responsibility to characterize the fatigue properties of the stay cables to help estimate the amount of fatigue damage has been given to researchers at UT. This has been done by taking field measurements, testing full-scale stay cables in fatigue, developing computational models, and testing small-scale stay cables in fatigue.

1.4.4.1 Field Measurements and Inspection

Attempts to inspect damage to existing stays and measure field conditions have been made. Since inspection of the wire cables themselves is impossible, small sections in the PE pipe were removed in the anchorage areas to inspect the grout. Small radial cracks were found in the grout and the pipe was replaced. In some cases, strain gages were applied directly to the grout at different axis on the same cable. Strains showed that the stay cable was acting predominantly axially and no beam actions were recorded. Strain measurements were not recorded during high amplitude conditions and the efforts were discontinued.

1.4.4.2 Large-Scale Testing in Fatigue Bending

Large-scale tests were conducted at the Ferguson Structural Engineering Laboratory. Twelve, 32-ft long specimens, both grouted and ungrouted were tested. The specimens were constructed and tested in a reaction frame. Most tests were conducted on a 19-strand grouted specimen representing the smallest cables on the Fred Hartman Bridge. The design of the specimens was based on the geometry of the shortest stays on the bridge.

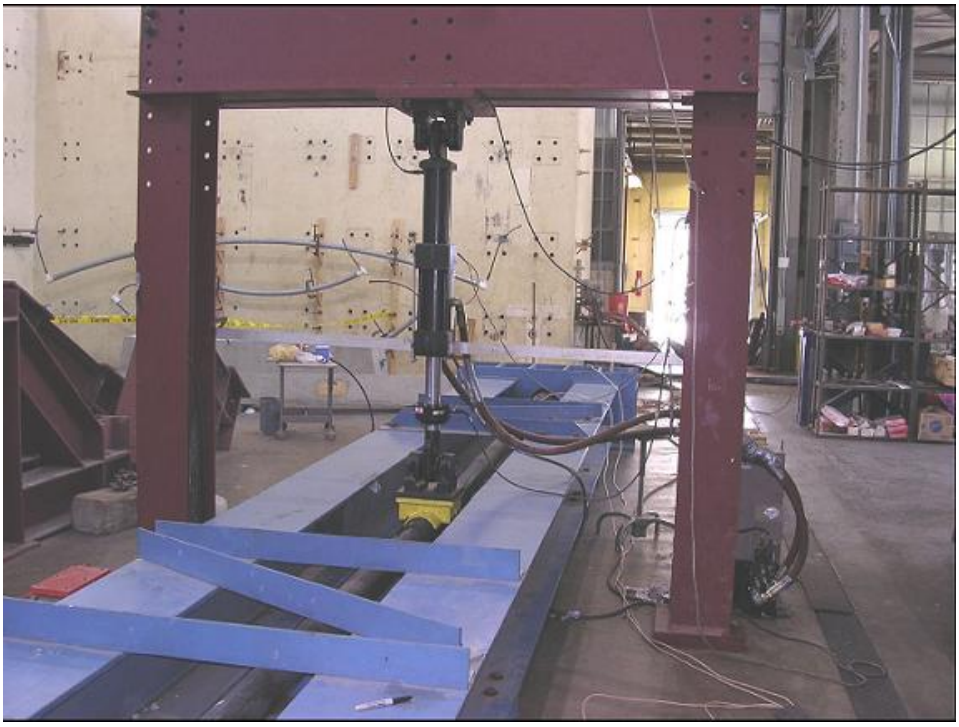

Figure 1-10 Large-scale bending fatigue tests (Ridd, 2004)

1.4.4.3 Characterization of Vibrations Data

Eggers (2003) used data collected by Johns Hopkins University to characterize the cable vibrations. In his work, the displacement of the cables at the location of the accelerometer is determined. In addition, the number of cycles seen by the cables is estimated and the primary modes in which the cables vibrate are presented. This information is important in estimating the extent of fatigue damage already accumulated on the bridge.

1.4.4.4 Computational Models

Computational models are useful in comparing the results obtained from the test specimens to the longer, larger cables on the Fred Hartman Bridge. Finite

element models were created by Dowd (2001) and Pebley (2005) to compare characteristics in the bridge to the testing in the laboratory.

Dowd developed a finite element model of the laboratory test specimens using beam elements. This was done to understand the stress concentrations near the anchorage regions. However, comparison of the FEM and test results showed that the model created by Dowd overestimates the stiffness of the cable by a factor of two.

Pebley created two, 3-D finite element models. The first model, of the longest stays on the bridge, was created to corroborate the video footage taken of the stays in large-amplitude vibrations (Figure 1-6). Pebley found that the displaced shapes of the cables could be modeled using parametric deck excitation as the input motion.

The second model was developed to assist with the design of the specimens for the small-scale bending fatigue tests. This model is the guide for the test specimens discussed in this thesis.

1.5 SCOPE OF INVESTIGATION

This thesis includes descriptions of testing and results of bending fatigue tests of small-scale specimens and axial fatigue tests of single strands. The scope of each investigation is summarized below.

Axial fatigue tests of the strands used to construct the large-scale bending fatigue specimens were previously reported by Eggers (2003) and Ridd (2004). However, those results were questioned when the controller malfunctioned in a subsequent series of fatigue tests. Samples of the two types of strands used to construct the twelve large-scale bending fatigue specimens were reevaluated to confirm the original findings. The testing procedures and results are discussed in Chapter 2.

Three small-scale stay specimens were subjected to bending fatigue loads. Construction of the specimens is discussed in Chapter 3 and the procedures used to control the fatigue tests are summarized in Chapter 4. Periodically during the fatigue tests, static tests were conducted to monitor strain response and assess variations in stiffness. The results of these tests are presented in Chapter 5. The observed damage at the completion of the fatigue tests is presented in Chapter 6. Chapter 7 summarizes the results of the entire investigation.

CHAPTER 2
Single-Strand Tension Fatigue Tests

Two sets of tests were conducted to determine the physical properties of the prestressing strands used to construct the large-scale and small-scale specimens. The results of the axial fatigue tests are summarized in Section 2.1 and the results of static axial tests to determine the elastic modulus are presented in Section 2.2.

2.1 AXIAL FATIGUE TEST

A series of axial fatigue tests were conducted in air to determine the baseline response of the prestressing strand. The results will be compared with the measured fatigue response of the test specimens in Chapter 5.

Two types of 0.6-in. diameter strand were tested. Strand A was used to construct large-scale specimens 1 through 6 (Poser 2001 and Ridd 2004) while strand B was used to construct large-scale specimens 7 through 12 (Ridd 2004) and the small-scale specimens described in this thesis.

Eggers (2003) and Ridd (2004) had previously reported the fatigue characteristics of both types of strand. According to Ridd, Strand A was unacceptable and Strand B was acceptable. However, shortly after those tests were concluded a problem was discovered with the controller that was used to set the force limits during the fatigue tests. That controller has been replaced, and the fatigue tests were repeated to verify the response of the strand.

A total of twenty-four specimens were tested in fatigue. Three stress ranges were selected for investigation: 20, 30, and 40 ksi. Testing was conducted following the Post-Tensioning Institute recommendations for stay cables (2001). The tests were conducted under load control and the maximum stress was set to

be 45% of the guaranteed ultimate tensile strength (GUTS) of the strand or 121.5 ksi. Testing was concluded when one of the following events occurred:

a) A single wire break along the free length.
b) A single wire break in grips
c) Run-out (specimen survived more than 2 million cycles)

2.1.1 Test Procedure

The testing objective was to obtain three acceptable tests for each strand at each stress range. An acceptable test is one that results in a run-out or with a break along the free length, between the grips. The tests that broke in the grips are not considered an acceptable break because the grips may have shortened the fatigue life by increasing friction on the strand or artificially increasing the fatigue damage.

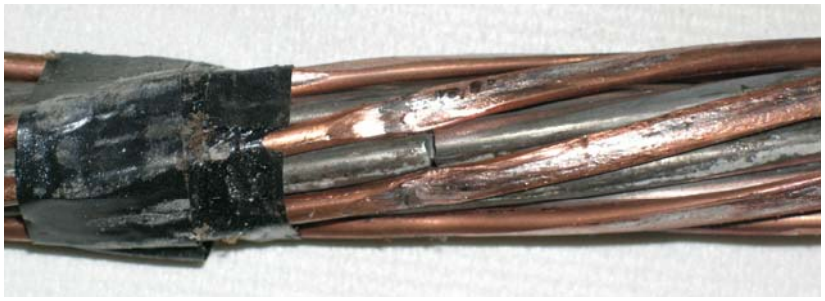

Figure 2-1 Wire break within grip

Figure 2-2 Acceptable wire break along free length

2.1.1.1 PTI Guide Specifications

The Post-Tensioning Institute has recommendations for the fatigue testing of strands used to construct stay cables (PTI, 2001). The specifications require that he fatigue tests be conducted with a maximum stress of 45% of GUTS. The guide also included a summary of minimum fatigue life for various stress ranges (Table 2-1).

Table 2-1: PTI specifications for strand fatigue Life (PTI, 2001)

No. of Cycles (N)	Component Fatigue Test Stress Range	
	MPa	ksi
2×10^6+	213	30.9
2×10^6	228	33.1
5×10^5	302	43.8
1×10^5	443	64.2

2.1.1.2 Test Set Up

The axial tensile tests were performed in a 220-kip MTS load frame. This load system consists of two heads with hydraulically controlled clamps which may be used to fix a specimen in the load frame. Once a specimen is clamped in place, the bottom head may be moved to load the specimen.

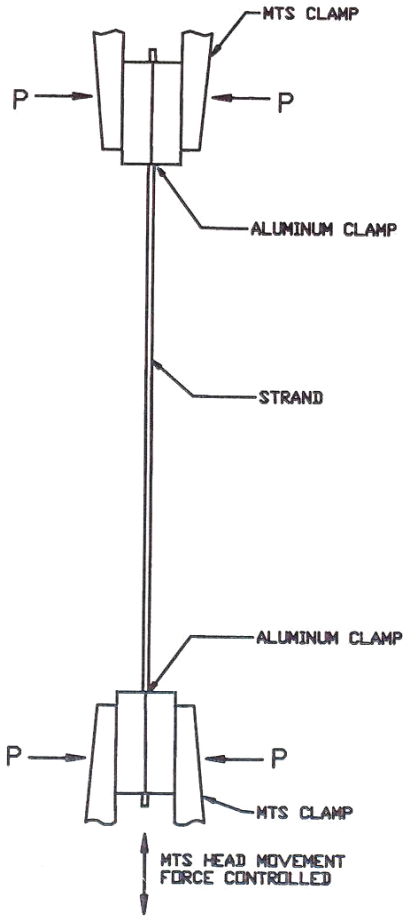

Figure 2-3 Sketch of test set-up

The loading was controlled by MTS software. Each test was run under load control with the necessary loads being calculated based on the area of the strand as measured by Ridd (2004).

Table 2-2: Prestressing Strand: Physical Properties (Ridd, 2004)

Grade 270	Strand A		Strand B	
	Mill Certificate	Measured	Mill Certificate	Measured
Area	0.2185 in^2	0.220 in^2	0.2204 in^2	0.223 in^2
Area - Outer Wire	-	0.0311 in^2	-	0.0313 in^2
Area - Center Wire	-	0.0334 in^2	-	0.0352 in^2

A sinusoidal loading function was used. Peak-valley compensation was also selected to compensate for the error between the extreme values of the input command and the actual load measured by the test specimen. The error was consistently less than 100 lbs or 4% of the smallest load range. The test frequency was determined by the capacity of the test machine and the hydraulic power supply. The parameters used to define each test are summarized in Table 2-3. The maximum load corresponds to the levels indicated in the PTI Guide Specifications. The set point is the mean load and the load range is one half the amplitude of the sine wave.

Table 2-3: Test Loading and Frequency

Stress Range (ksi)	Set Point (k)	Load Range (k)	Max. Load (k)	Min. Load (k)	Test Frequency
20	24.860	2.230	27.09	22.63	6.5 Hz
30	23.745	3.345		20.40	6.5 Hz
40	22.630	4.460		18.17	5.0 Hz

The area of strand B was used to calculate loads for the predetermined stress ranges. The same load limits were used for both types of strand, although the area of strand A is less. The corresponding stress range for Strand A are reported in table 2-4.

Table 2-4: Testing Stress Ranges

Stress Range (ksi)*	
Strand A	Strand B
20.27	20.0
30.41	30.0
40.55	40.0

*Corrected for differences in cross-sectional area.

Each specimen was approximately 60 in. long. Aluminum grips were used to clamp the strand at each end, so the clamps from the MTS machine did not directly compress the prestressing strand.

Figure 2-4 Strand wrapped with copper wire

Copper wires were placed between the aluminum grips and the steel prestressing strands to fill the space between the steel strand and the aluminum grips, to distribute the gripping force to the strand more evenly (Figure 2-4). The wire is 8-gage solid copper wire. Six pieces, 8-in. long were cut and formed to follow the helical wrap of the strand at each end. The copper wire was taped into place to secure them while the MTS clamps gripped the specimen. It was found that when the copper wires were formed to fit the strand properly, the gripping process and the testing were much easier to conduct and the specimen was much less likely to experience a wire break in the grip area.

The strand was loaded into the machine with 1 to 1½ in. of the aluminum grip left outside of the MTS clamp at the top and bottom. This was done to provide a transition in the stiffness between the grip and the specimen to reduce chances of fatigue fractures in the grip region. The grips are the same used by Ridd (2004).

The original aluminum grips were smooth along the inside where the grip came in contact with the aluminum strands. As these tests continued the smooth surfaces became worn. Helical groves formed around the inside of the grips (Figure 2-5). The outside of the grips also became worn from being clamped in the MTS clamps.

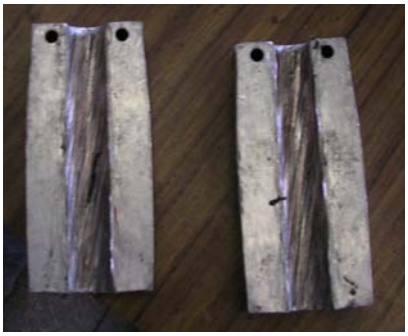

Figure 2-5 Aluminum grips after excessive use

2.1.2 Results

Summaries for all of the tests are presented in Tables 2-5 and 2-6). Because of time constraints, two specimens were not tested, one for Strand A at 20 ksi and one for Strand B at 30 ksi. The reason for terminating each test is listed in the last column of the tables.

2.1.2.1 Strand A

Eight axial fatigue tests were conducted using Strand A (Table 2-5). Only tow tests were completed at a nominal stress range of 20 ksi, but both resisted were than 2 million cycles. Of the six tests at higher stress ranges, four of the specimens failed after resisting fewer cycles than required in the PTI Guide Specifications (2001). Most notably, all three specimens tested at a nominal stress range of 40 ksi survived fewer than 500,000 cycles (Figure 2-6).

Table 2-5: Strand A axial fatigue test results

Test	S_r (ksi)	N (cycles)	PTI cycle Requirements	Notes
1	40	408,528	817,607	Wire Break
2	40	224,965	817,607	Wire Break
3	40	245,637	817,607	Wire Break
4	30	547,314	2,000,000	Wire Break
5	30	2,345,514	2,000,000	Run-out
6	30	2,375,834	2,000,000	Run-out
7	20	3,308,952	2,000,000	Run-out
8	20	2,477,752	2,000,000	Run-out

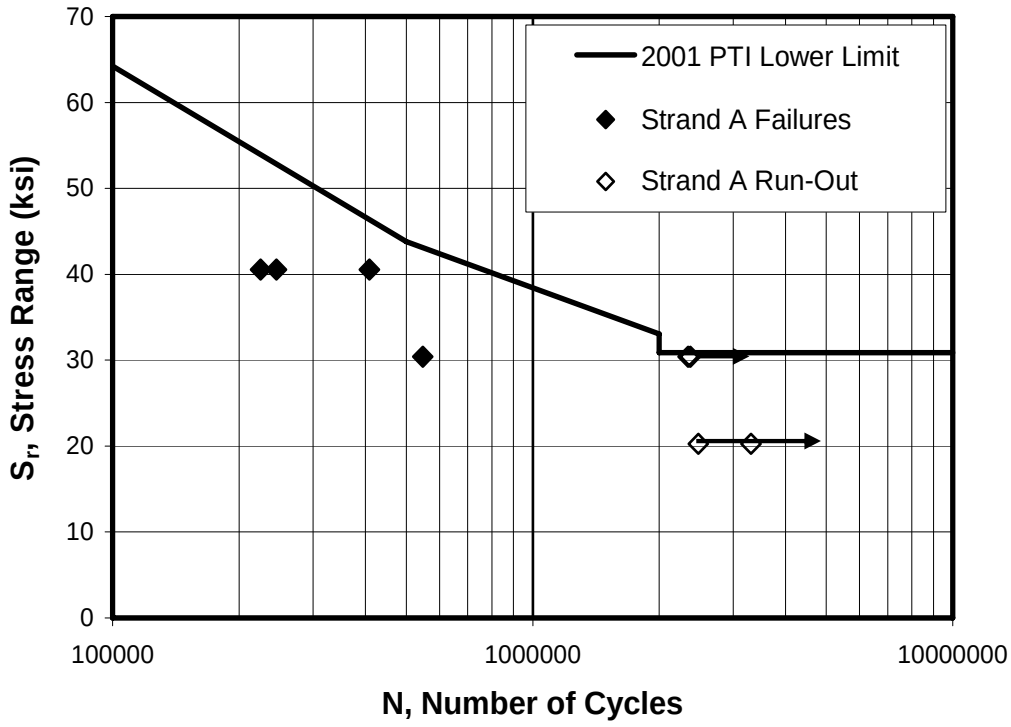

Figure 2-6 Strand A: Results of Tensile Fatigue Tests

2.1.2.2 Strand B

A total of eleven axial fatigue tests were conducted using strand B (Table 2-6). Three specimens failed in the grips, and those results are not considered in the evaluation of the data. All three specimens tested at a nominal stress range of 20 ksi and both specimens tests at a nominal stress range of 30 ksi resisted more than 2 million cycles (Figure 2-7). For specimens tested at 40 ksi stress range, Test 2 did not satisfy the PTI specifications, Test 1 was just at the requirement and Test 5 acceptable.

Table 2-6: Strand B axial fatigue test results

Test	S_r (ksi)	N (cycles)	PTI cycle Requirements	Notes
1	40	815,018	817,607	Wire Break
2	40	667,259	817,607	Wire Break
3	40	651,006	817,607	Grip failure
4	40	193,411	817,607	Grip failure
5	40	2,153,379	817,607	Run-out
6	30	2,306,750	2,000,000	Run-out
7	30	851,507	2,000,000	Grip failure
8	30	2,149,275	2,000,000	Run-out
9	20	2,318,197	2,000,000	Run-out
10	20	2,677,051	2,000,000	Run-out
11	20	2,164,075	2,000,000	Run-out

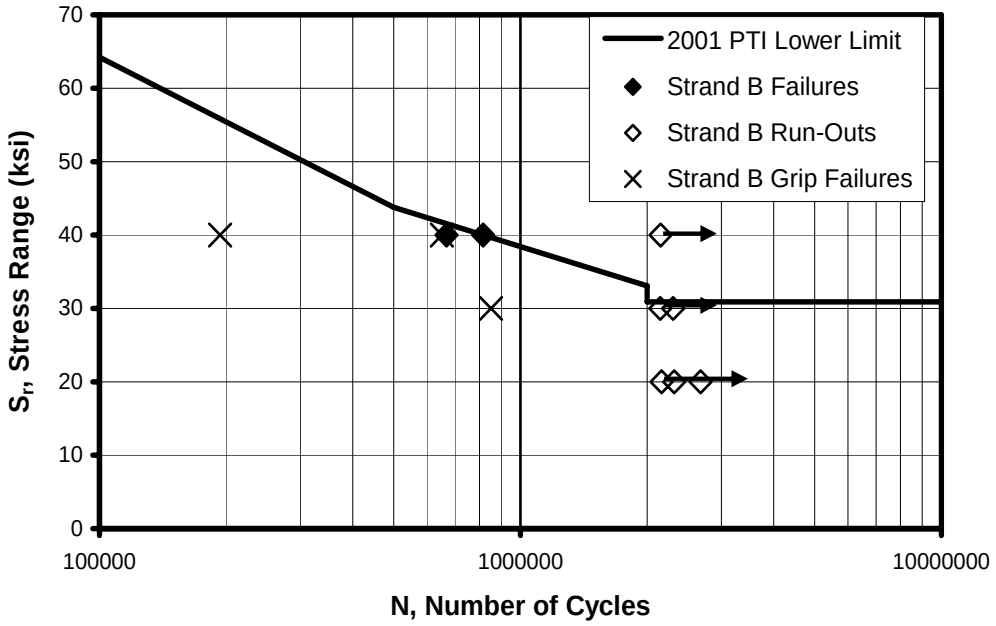

Figure 2-7 Strand B: Results of Tensile Fatigue Tests

2.1.3 Summary

The axial fatigue response of Strand A and Strand B may be evaluated by comparing Figures 2-6 and 2-7. At a nominal stress range of 40 ksi, the axial fatigue performance of Strand B was significantly better than that of Strand A. At a nominal stress range of 20 ksi, all specimens resisted more than 2 million cycles, so no differences could be attributed to the type of strand.

PTI Guide Specifications 3.2.2.1-E defines acceptable requirements for strands. In summary, if more than one tests specimen fails at the designated stress range before the specified number of cycles, then the strand is considered unacceptable. Strand A did not satisfy PTI minimum specifications for fatigue. Strand B performed substantially better than strand A and is to be considered acceptable by the PTI specifications for fatigue (2001).

One possible explanation for the observed differences in the fatigue response of the strand is the size of the center wire. As indicated in Table 2-2, the diameter of the center wire on Strand A is less than that for Strand B; however, the nominal diameter of the two strands is the same. This means that the interstitial space is larger for Strand A, and that the wires move more relative to each other during fatigue loading. This increased relative movement of wires may be the cause of the reduced fatigue life for strand A at a higher stress range.

Another difference in the two strands was the outer surface. Figure 2-10 shows the surfaces of the strands tested in axial fatigue. Strand A has a much darker outer surface. These small can cause fretting of the outer strands. It is noted that all of the wire breaks occurred on the outer wires, none were observed on the center wire

These results are similar to those by Ridd (2004) and Eggers (2003). Ridd previously reported that Strand A was unacceptable and Strand B was acceptable.

2.2 STRAND RECOVERED FROM LARGE-SCALE BENDING FATIGUE SPECIMEN

Axial fatigue tests were also performed on sections of strand recovered from a large-scale bending fatigue specimen. Strand B was used to construct Specimen 12. Although the strand used in the axial fatigue tests did not experience high fatigue stresses during the bending fatigue tests (Figure 2-8), the strand had been encased in portland-cement grout. Therefore, grout filled the interstitial spaced between the wires for these specimens.

Five tests were conducted at a nominal stress range of 40 ksi. Results are summarized in Table 2-7 and Figure 2-9. None of the specimens satisfied the PTI specifications (2001); however, only one specimen resisted significantly fewer cycles than Strand B (Figure 2-7). This degradation in performance is attributed to the presence of the grout. Contact between the grout and the surface of the

wires caused minor abrasions which reduced the fatigue life. But, the difference is very slight. In terms of cycle count the two strands are very similar. More tests of the used strand would be required to determine a difference.

Table 2-7: Axial fatigue tests of Strand B and Strand B recovered from bending fatigue specimen

Strand B				
Test	**S_r (ksi)**	**N (cycles)**	**PTI cycle Requirements**	**Notes**
1	40	815,018	817,607	Wire Break
2	40	667,259	817,607	Wire Break
3	40	651,006	817,607	Grip failure
4	40	193,411	817,607	Grip failure
5	40	2,153,379	817,607	Run-out
Strand B recovered from bending fatigue specimen				
1	40	501,052	817,607	Grip failure
2	40	756,826	817,607	Grip failure
3	40	697,665	817,607	Wire Break
4	40	325,913	817,607	Wire Break
5	40	746,674	817,607	Wire Break

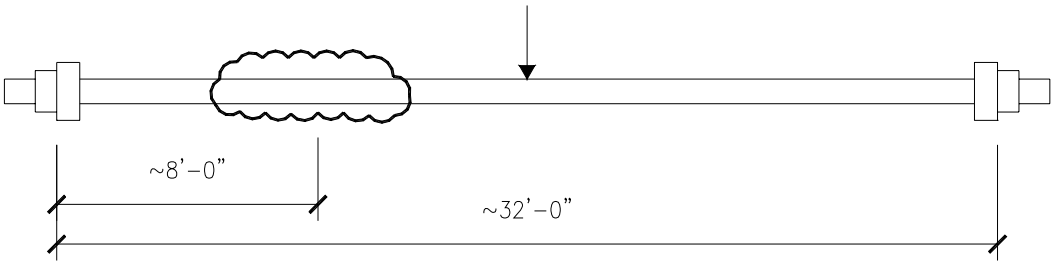

Figure 2-8 Location of strands recovered large-scale from bending fatigue specimens

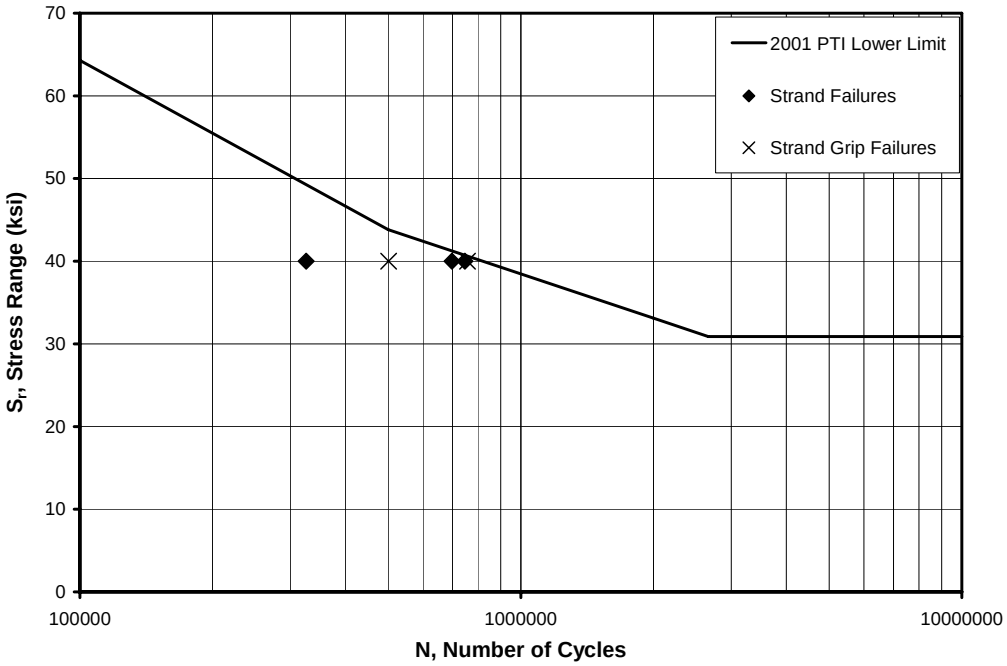

Figure 2-9 Results of tensile fatigue tests for strand recovered from large-scale bending fatigue specimens

Figure 2-10 Photograph of surface of strands: (a) Strand A, (b) Strand B, (c) Recovered from bending fatigue specimen

2.3 ELASTIC MODULUS OF STRANDS

A primary objective of the tests discussed in this thesis was to determine the stresses experienced by a strand when a stay cable is subjected to bending. Strain gages attached to the surface of the strand represent the only direct way to measure the strand response. The elastic modulus tests were performed to relate the strains measured along an individual wire to axial strains in a strand. The axial stress in the strand can then be calculated from the axial strain.

During the static tests, two types of instrumentation was used to measure the response of the strand: (a) an extensometer was used to measure axial deformation of the strand and (b) strain gages were used to measure strains along the axes of individual wires.

Instrumentation and testing procedures are summarized in Section 2.3.1. The measured values of elastic modulus are reported in Section 2.3.2 and the measured values of apparent modulus are presented in Section 2.3.3

2.3.1 Instrumentation and Testing Procedures

2.3.1.1 Extensometer

The extensometer used to determine the elastic modulus of the strand was developed by Heller (2003). Ridd (2004) and Eggers (2003) used the same instrumentation. The extensometer measures the axial displacement of a strand in tension over a gage length of 24 in. Two linear voltage displacement transducers (LVDTs) with a range of +/- 0.05 in. are used to measure the response of the strand.

The extensometer is constructed from three blocks and two rods (Figure 2-11). The top and bottom blocks are attached to the rods and separated by up to 3 ft. The top block is also attached to the strand, but the strand is free to pass through the bottom block, therefore the distance between the top and bottom

blocks does not vary during the test. The bottom block also supports the two LVDTs, one on each side of the strand.

The middle block is attached only to the strand. The distance between the center of the top and the middle blocks represents the gage length of the extensometer. The LVDTs recorded the movement of the middle block relative to the bottom block, which is the same as the top block.

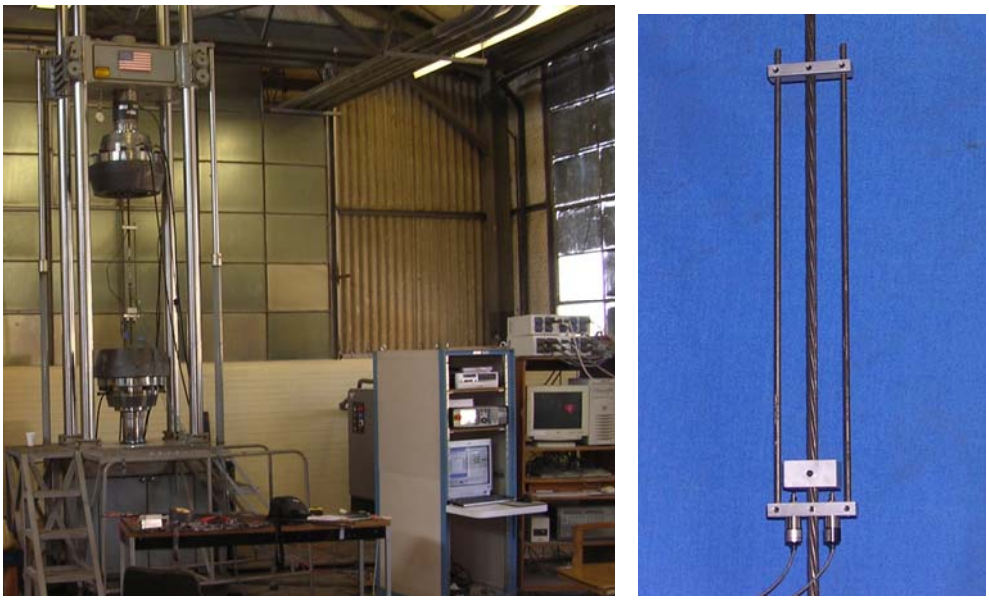

(a) ***(b)***

Figure 2-11 Modulus Tests (a) Setup for modulus tests (b) Extensometer (Ridd, 2004)

2.3.1.2 Strain Gages

Strain gages were used to determine the apparent modulus of the strand. The gages were attached to individual wires along their own axes (Figure 2-13).

Strain gages from Tokyo Sokki Kenkyujo Company were used in these tests. The gages have a 3-mm gage length, gage factor 2.13, and are type FLA-3-11-5LT.

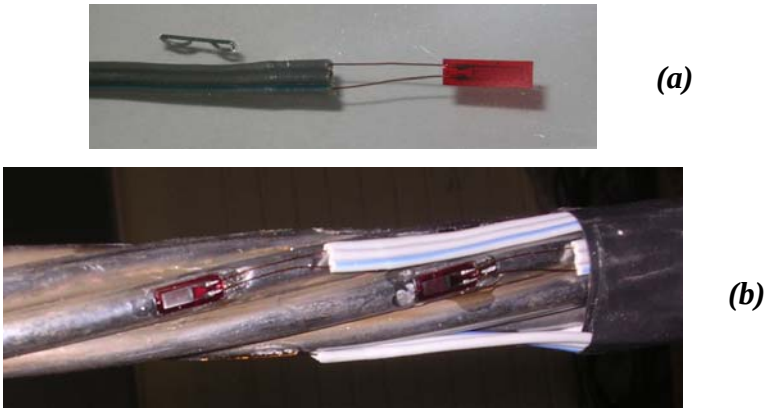

(a)

(b)

Figure 2-12 Strain gages used to determine apparent modulus of strand: (a) 3-mm strain gage, (b) alignment of strain gages along axes of wires

2.3.1.3 Testing Procedures

The static tests were conducted in the same 220-kip testing machine that was used for the axial fatigue tests. The aluminum grips and copper wires discussed in Section 2.1.1.2 were also used in these tests; however, the results were not as sensitive to the technique used to grip the strand.

Three specimens were tests statically. Data from the extensometer and the strain gages were recorded by a data acquisition system (DAQ), but the load was recorded manually. The strands were loaded to approximately 48% of GUTS (approximately 122 ksi) in increments. At each increment, load was maintained long enough to record the load and capture the corresponding displacement and strain. The samples were then unloaded in increments, and the process was repeated. This loading and unloading repetition was done to ensure that the specimen was positioned properly in the testing machine and that the response would to as linear as possible.

2.3.2 Measured Modulus of Strand

The measured stress-strain response of the three test specimens is shown in Figures 2-13 through 2-15. For the first test, data were only recorded during one loading cycle (Figure 2-13). Both loading and unloading were recorded for the second specimen (Figure 2-14) and two complete loading and unloading cycles were recorded of the third specimen (Figure 2-15). The slope of the data recorded by the two LVDTs is not the same in any of the tests, indication that the aluminum blocks rotated slightly during testing.

A slight hysteresis was also observed between loading and unloading cycles. The elastic modulus was taken as the average of the slopes from the loading curves (second cycle for the third specimen). The results were in a narrow band between 29,620 and 29,680 ksi with an overall average of 29,650 ksi.

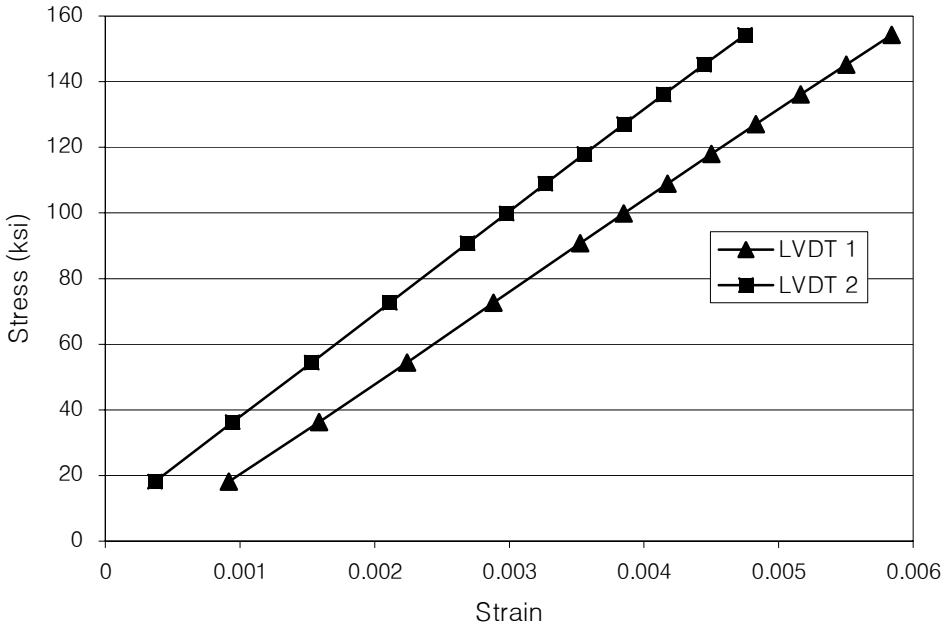

Figure 2-13 Test 1: Measured stress-strain response

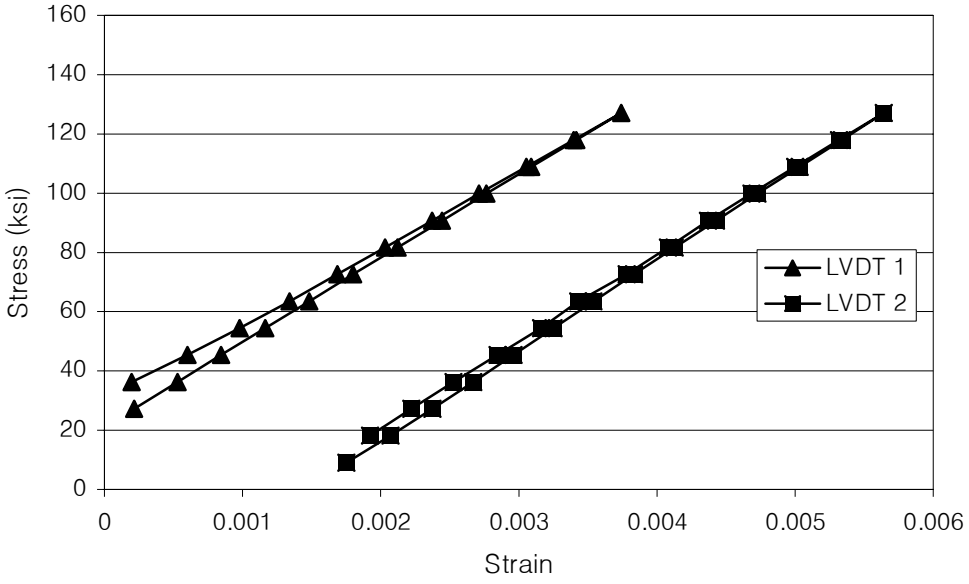

Figure 2-14 Test 2: Measures stress-strain response

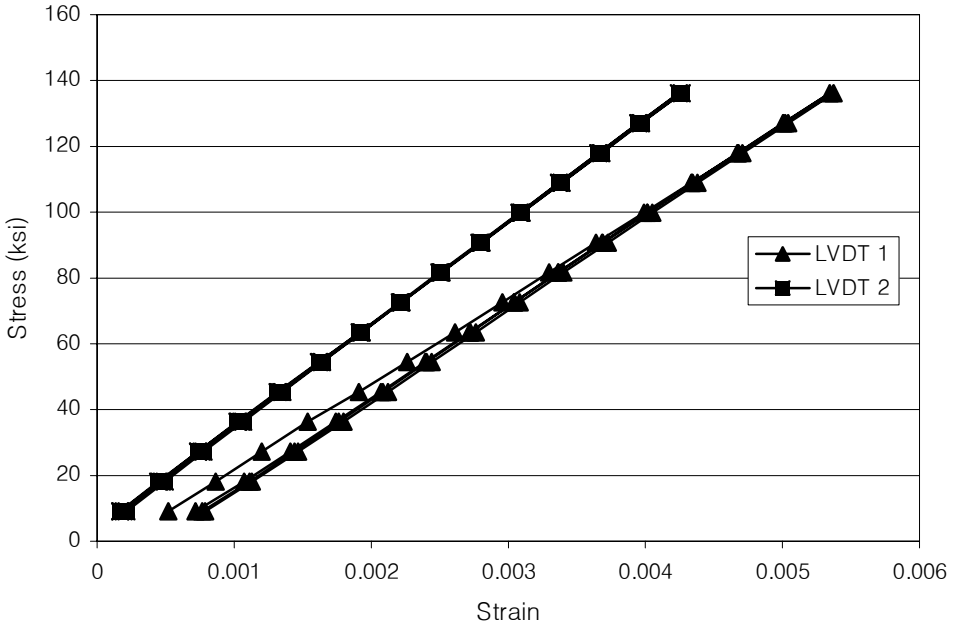

Figure 2-15 Test 3: Measured stress-strain response

Table 2-8: Average Elastic Modulus of Strand

LVDT	test 1 (ksi)	test 2 (ksi)	test 3 (ksi)
1	31,260	28,400	31,030
2	27,980	30,970	28,290
Average	29,620	29,680	29,660
	Overall	Average	29,650

2.3.3 Measured apparent Modulus of Strand

The apparent modulus of the strand was determined from the strain data. Strain gages were attached to all six outer wires for Specimen 1, to two outer wires for specimen 2, and to three outer wires for specimen 3. Data from the strain gages were recorded at the same time as the data from the extensometer. Therefore, data are available from one loading cycle for specimen 1, from one loading/unloading cycle for specimen 2, and for two loading/unloading cycles for specimen 3. Data are plotted in Figures 2-16 through 2-18.

2.3.3.1 Results of Apparent Modulus Test

The least square fit was used to calculate a linear stiffness value for each strain gage. If a small but noticeable change in the stress-strain relationship occurred during the test, that data were not used to calculate the stiffness. In all tests, the smallest measurements were not used in the stiffness calculation because of irregularities from slipping. In test 2 (Figure 2-17), there is a noticeable divergence of the stress-strain relationship on one of the unloading cycles. This portion was not used to calculate the overall stress-strain relationship for this test.

Some divergence or large differences in strain measurements are seen in the graphs. This may be because the gages were not positioned directly in line with the axis of the wires. These differences account for the variability in the data.

A summary of the results is given in Table 2-9. The values from each strain gage were averaged for each test. The resulting three values were averaged to determine the apparent modulus. The average apparent modulus for the strands is E_a = 30,960 ksi.

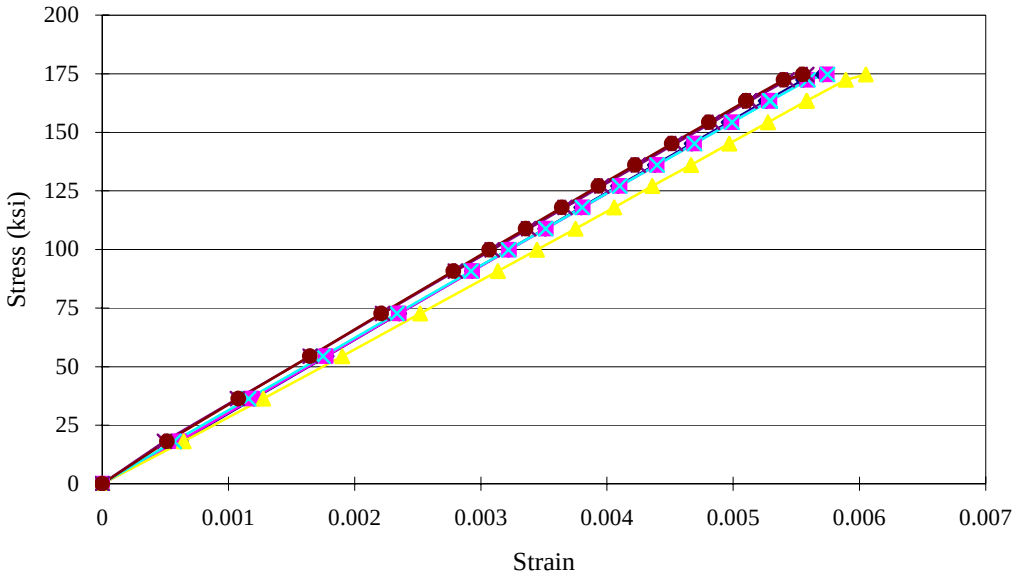

Figure 2-16 Test 1; Measured response of strain gages

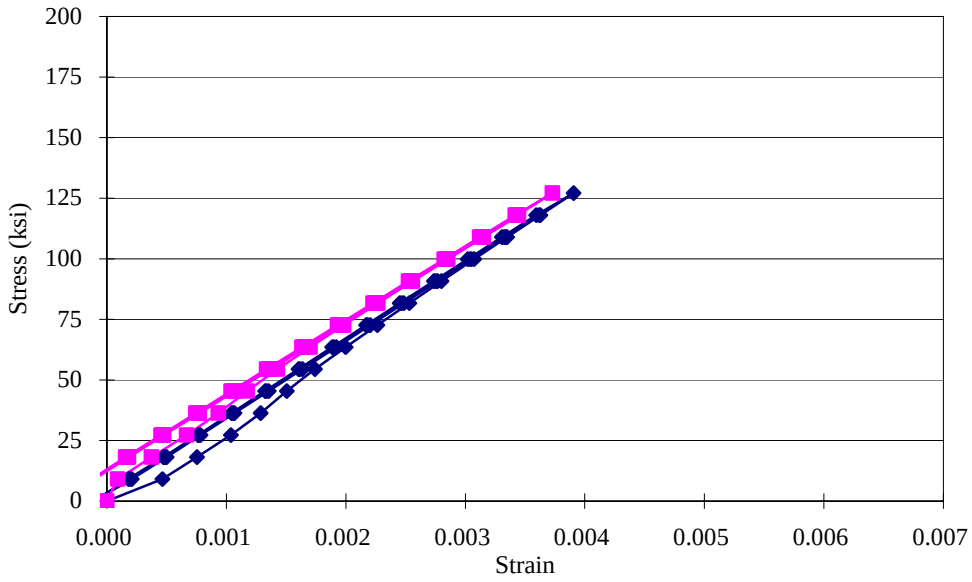

Figure 2-17 Test 2; Measured response of strain gages

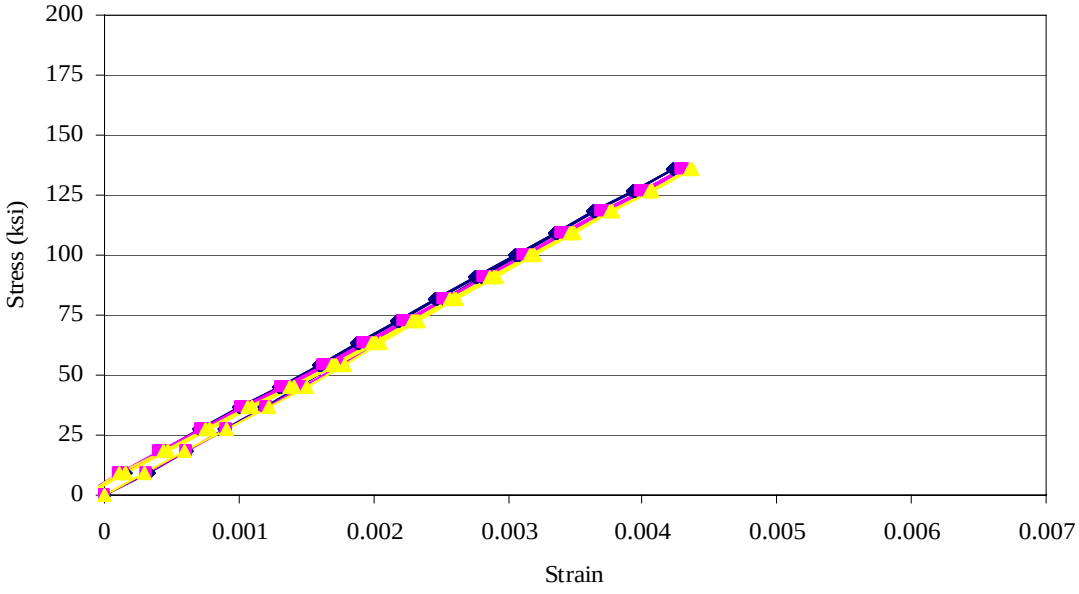

Figure 2-18 Test 3; Measured response of strain gages

Table 2-9: Apparent Modulus of strand

Strain Gage	test 1 (ksi)	test 2 (ksi)	test 3 (ksi)
1	31,260	30,550	31,100
2	30,940	32,120	30,390
3	29,650		30,561
4	30,710		
5	31,200		
6	31,420		
average	30,860	31,340	30,680
Overall	Average	Ea =	30,960 ksi

2.3.4 Summary

Average values of the elastic and apparent moduli of Strand B were determined during the static tests. As expected, the apparent modulus is larger than the elastic modulus because the apparent modulus is measured along the axis of the wires.

In the fatigue tests of the stay cables, strains can only be measured along the wires. However, the effective axial strain in the strand, ε, can be calculated by multiplying the strain measured along the axis of an individual wire, ε_a, by the modular ratio E/E_a:

$$\varepsilon_a\left(E/E_a\right) = \varepsilon \qquad \text{(Equation 2-1)}$$

Based on the results of the static tests, the modular ratio may be taken as 0.958 for strand B.

Heller (2003) reported a similar value for apparent modulus for 0.5-in strand. Heller used a similar test procedure. The resulting average apparent modulus (E_a) of Heller's test was 31,200 ksi, a less than 1% difference from the value calculated in these tests. It is noted that the angle of the wire wrap around

the center wire is different for the two strand types. The distance along the strand for a wire to wrap around one time is called the lay length (MacDougall, 2003). The lay length is one way to quantify the angle of the wire wrap. The lay length for the 0.5-in. strand is approximately 8 in. and for the 0.6-in. strand, approximately 8.5 in.

CHAPTER 3
Construction of Small-Scale Bending Fatigue Specimens

This chapter discusses the materials and procedures used to construct the small-scale bending fatigue specimens. These specimens were designed to have similar structural characteristics as the longest stays on the Fred Hartman Bridge. The large-scale bending fatigue specimens were relatively short with larger moment of inertias. Because of these properties, the large-scale specimens behaved more like a beam in tension than a cable in bending (Pebley 2005). The small-scale specimens were longer and had smaller moment of inertia. These specimens were intended to behave more like a cable in bending, similar to the large stays on the bridge.

3.1 GENERAL TEST SETUP

The test specimens are simplified representations of stay cables. The specimens are 49-ft long (Figure 3-1). Two, 0.6-in. diameter strands were used to construct each specimen and the specimens were grouted after the strands were tensioned. Corrugated, post-tensioning duct was used to encase the grout. The specimens were loaded transversely at one point along the length of the cable using a hydraulic actuator. Initially, the actuator was located at midspan of the specimen (Location 1), but most tests were conducted with the actuator located near the quarter-span (Location 2).

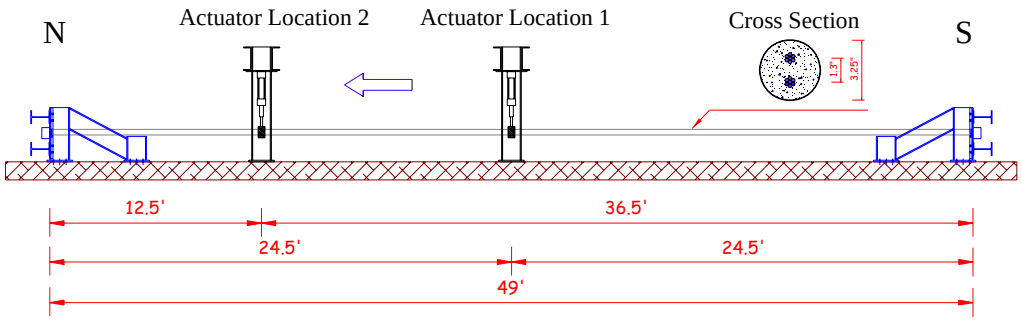

Figure 3-1 Test Set-up

In an earlier phase of this research project, Poser (2001) and Ridd (2004) tested twelve large-scale stay specimens in bending fatigue (Figure 1-10). The large-scale specimens were 32-ft long and the cross-sectional dimensions were selected to match those of the shortest stays on the Fred Hartman Bridge.

The large-scale test set-up could not be used for the small-scale fatigue tests due to the increased length of the small-scale specimens. In the description of the specimens tested in this investigation, some comparisons are made between the small-scale specimens and the large-scale specimens tested previously.

3.2 SUPPORT CONDITIONS FOR SMALL-SCALE SPECIMENS

A self-reacting frame was used to support the large-scale specimens during the bending fatigue tests (Figure 1-10). The primary advantage of this arrangement was that the specimen could be moved after the strands were stressed. For example, the large-scale specimens were inclined during grouting, which reproduced the conditions in the field and reduced the likelihood of voids along the length of the specimen.

The idea of a self-reacting frame was abandoned for the small-scale specimens due to the increased length. Four independent reaction frames were fabricated and attached to the strong floor (Figure 3-1). Anchor support spanned

between the reaction frames and provided the reaction for the anchor heads. The dimensions of reaction frames and anchor supports are described in Appendix A.

Figure 3-2 Reaction frame and anchor support

Because the reaction frames were attached to the laboratory floor and the supports at the two ends of the specimen were independent, the specimens could not be moved after the stands were stressed. As a result, the specimens were grouted in a horizontal position.

3.3 ANCHOR HEADS

The anchor heads for the small-scale bending fatigue tests were fabricated to accommodate a maximum of four strands. The spacing of the holes was selected to match that in the large-scale tests (Figure 3-3). The large-scale anchor head has a diameter of 10 in. and can accommodate 19 strands. The diameter of the small-scale anchor head was 7 in. The thickness of both types of anchor heads was 5 in.

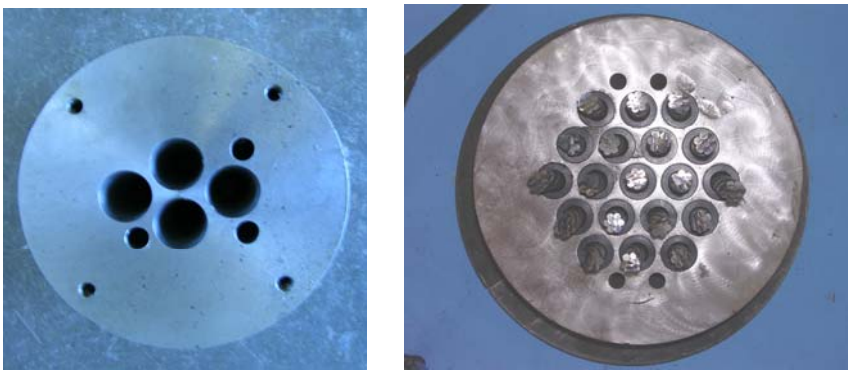

(a) ***(b)***

Figure 3-3 Photographs of anchor heads used for bending fatigue tests: (a) Small-scale anchor head; (b) Large-scale anchor head with prestressing strands (Ridd 2004)

Because only two strands were used to construct the small-scale bending fatigue specimens, the extra holes in the anchor head were plugged with caulk or epoxy before construction of the specimens (Figure 3-4). One grout hole was left open.

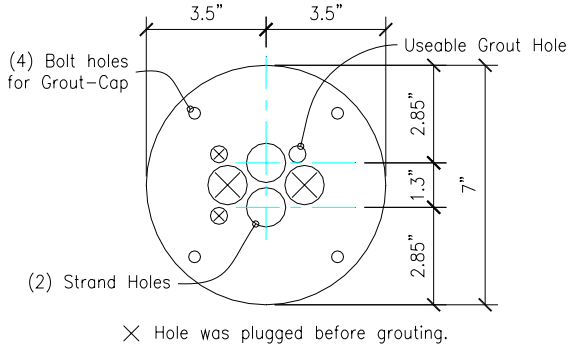

Figure 3-4 Dimensions of small-scale anchor head

Grout caps were fabricated from steel plate and steel pipe for the small-scale specimens (Figure 3-5). The flange of the grout cap was bolted to the end of the anchor head after the strands were stressed. A styrofoam seal was placed between the flange of the grout cap and the anchor head to minimize leakage of

the grout. The grout caps were fabricated with a single vent, which was positioned on the top of the specimen, to ensure that the grout completely filled the grout cap.

(a) After fabrication *(b) Bolted to anchor head*

Figure 3-5 Grout cap

3.4 MATERIALS

The small-scale stay cables were constructed using three materials: prestressing strand, grout, and duct. The properties of each are described in the sections below.

3.4.1 Prestressing Strands

Two types of 0.6-in. diameter prestressing strand were tested in the large-scale bending fatigue tests (Ridd 2004). Strand B was used to fabricate all three small-scale specimens. Table 3-1 summarizes the ASTM A416 specifications for this weldless, low-relaxation strand and corresponding values provided on the mill certificate values. Strand B was designed specifically for stay cable applications and was manufactured with a larger center wire than is typically used for 0.6-in. diameter strand (Figure 3-6).

Table 3-1: Prestressing Properties of Strand B

Grade 270 Strand	ASTM Standard	Mill Certificate
Modulus of Elasticity	27,500 ksi	28,300 ksi
Breaking Strength	58.6 kip	60.3 kip
Yield Point (1% Extension)	52.7 kip	54.0 kip
Nominal Area	0.217 in^2	0.220 in^2

Figure 3-6 0.6-in. diameter prestressing strand

3.4.2 Grout

A prepackaged grout (SikaGrout 300 PT) was used to construct the test specimens. Portland cement is the primary constituent of the prepackaged grout. The grout also contains admixtures for minimizing shrinkage and increasing the flow ability (water reducer/plasticizer). Additional information is provided in Appendix A.

3.4.3 Duct

The large-scale bending fatigue specimens were constructed using black, polyethylene (PE) pipe. This material was also used to construct the stays on the Fred Hartman Bridge. A white post-tensioning duct was selected for the small-scale tests. The decision to use a different material was based on the desire to

minimize grout voids. The post-tensioning duct is ribbed and includes three longitudinal flow channels (Figure 3-7). In addition, the duct is semi-transparent, so the level of the grout can be observed during the grouting process.

The post-tensioning duct is a blend of polyethylene and polypropylene. The outside diameter is 4 in. (based on the top of the rib). The inside diameter is 3.35 in., and the wall thickness is approximately 3/16 in. The spacing of the transverse ribs is 1.5 in. (Figure 3-7).

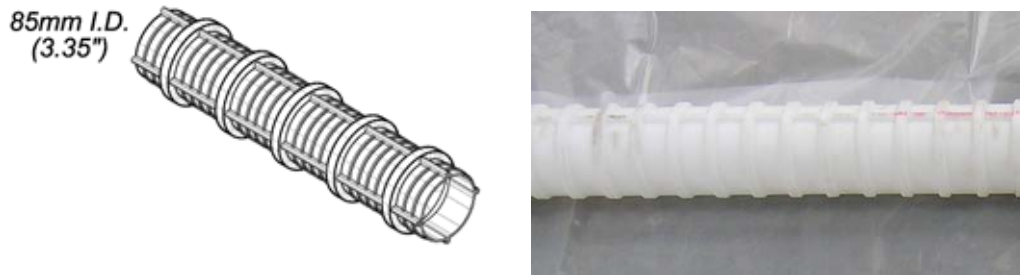

Figure 3-7 Post-tensioning duct (General Technologies, Inc., 2006)

A second reason for selecting the post-tensioning duct was the availability of commercial couplers for connecting sections of duct. The splices were hard plastic cylinders with an inner diameter slightly larger than the outer diameter of the duct. A shrink-wrap sleeve was then placed over the splice region to ensure a water-tight connection

Plastic welding had been used to connect all sections of PE pipe in the large-scale specimens. Welding was more difficult with the post-tensioning duct due to the thinner wall thickness and the lower melting temperature of the duct material. Small sections of the post-tensioning duct were welded, but the region was also encased with the shrink-wrap sleeves.

The third reason for using the post-tensioning duct is that strain gages could be easily applied to the strands after the strands were stressed. The process of attaching strain gages is discussed in Section 3.5.1.

3.5 CONSTRUCTION SEQUENCE

The construction process for the small-scale bending fatigue specimens may be divided into three steps: assembling the components, grouting the ducts, and attaching the actuator to the test specimen. Stressing the strands, splicing the ducts, and installing the strain gages are included in the first step. All steps are described briefly in the following sections.

3.5.1 Assembly of Test Specimens

Two, 55-ft sections of prestressing strand were used to construct each specimen. The strands were pushed through the holes in the anchor head at one end of the specimen. Several sections of duct and couplers were slid over the strand. The number varied depending on the number of locations that were instrumented with strain gages. The total length of the sections of duct was approximately 18 in. less than the length of the specimens.

The strands were then pushed through the holes in the anchor head at the other end of the specimen. Wedges were inserted into the south anchor head to hold the strands in place (Figure 3-8).

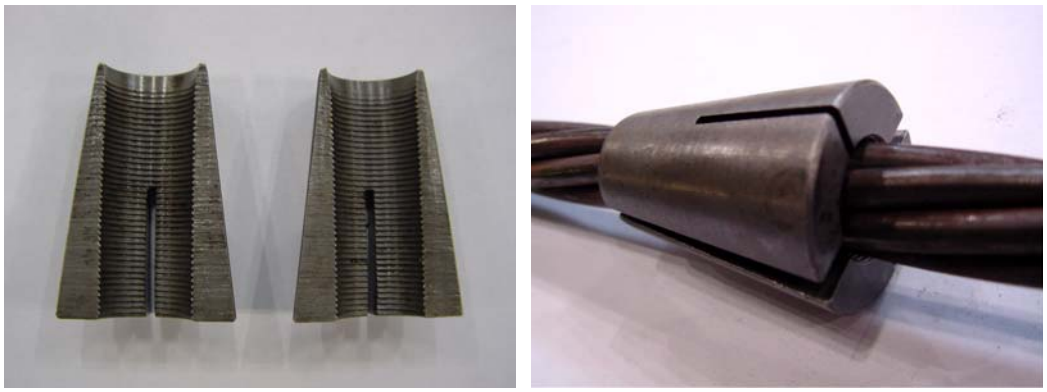

(a) Two-part wedges ***(b) Wedges around strand***

Figure 3-8 Wedges used to grip end of strand (Ridd, 2004)

The strands were then stressed individually from the north end (Figure 3-9). The hydraulic ram used to stress the strands has a seating jack that applies uniform pressure to the wedges, which reduces the seating losses. A pressure gage was used to monitor the applied force. The target stress level in each strand was 50% of GUTS.

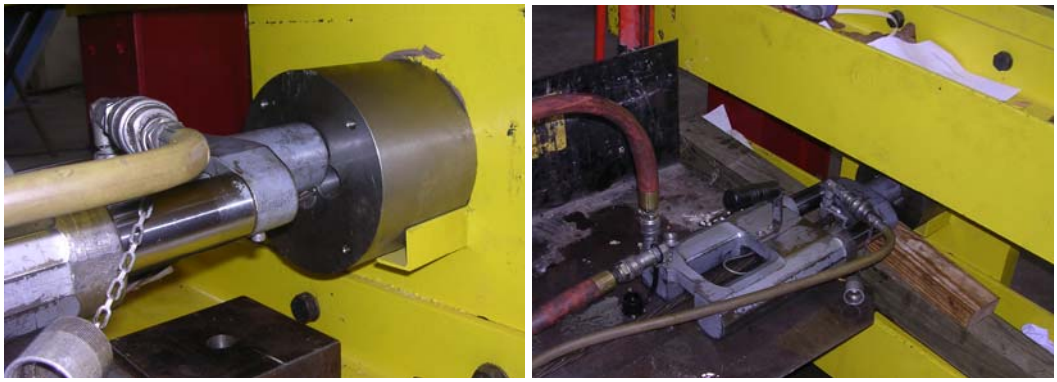

Figure 3-9 Stressing of strands individually with hydraulic ram

After stressing the strand, strain gages were attached to the surface of the strand. Access to the desired location was obtained by sliding the sections of duct along the strands. Different locations were used for each specimen because the best locations for the gages were determined as testing progressed. Section 3.7 describes the locations of strain gages on each specimen. Figure 3-10 shows the position of the duct when the strain gages were attached to the north end of the specimen.

Figure 3-10 Strain gages on strands at north end with duct shifted to the side

The number of strain gages attached to each specimen varied, and is presented in Section 3.7. However, at each gage line, stain gages were attached to wires on the top and bottom of each strand (Figure 3-10 and Figure 3-13). Holes had been drilled in the duct to accommodate the wires from the strain gages.

Figure 3-11 Strain gage on strand

3.5.2 Grouting

A pre-packaged grout was used to construct the specimens. Grout was pumped into the duct near the center of the specimen. Air vents were placed at several locations along the length and at each grout cap. Three-ft sections of hose were attached to each of the air vents (Figure 3-14).

Grout was pumped continuously into the specimen flowed through each of the air vents. The ends of the hoses were then capped to prevent air from returning into the duct.

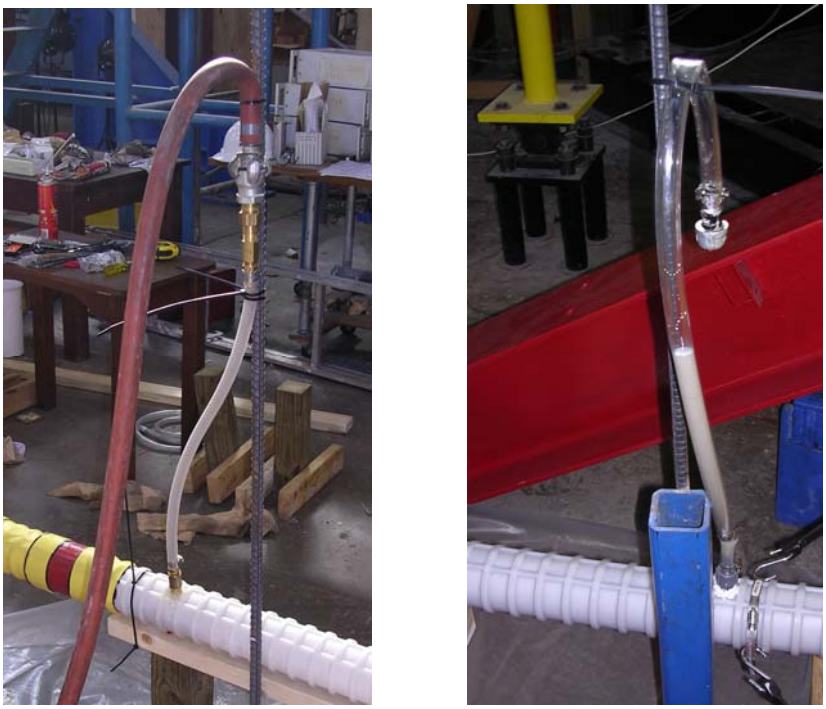

(a) Grout hose from pump *(b) Vent hose after grouting*

Figure 3-12 Grouting hoses and vents

3.5.3 Attaching Actuator

The grout was allowed to cure for approximately seven days before attaching the actuator. In preparation, a soft, spongy styrofoam was wrapped around the specimen to use as padding between the actuator grip and the duct. The styrofoam was cut into strips narrow enough to fit in between the ribs on the duct. The actuator setup was assembled (Section 4.1.1) without the bottom of the actuator grip. The ram was lowered and a small amount of load was applied on

the specimen to allow the grip to fit securely on the specimen. The bottom of the grip was then attached by bolting it to the top of the grip.

3.6 CONSTRUCTION SEQUENCE FOR SPECIMEN 1

The actual construction sequence for Specimen 1 varied from the idealized procedure described in Section 3.5. Two important differences, one intended and one unintended, are discussed in this section.

During construction of Specimen 1, four strain gages were attached to the strand before stressing. The strains were monitored during stressing to determine if the stress calculated from the pressure gage was consistent with the stress calculated from the measured strains. The pressure gage proved to be accurate.

The pre-packaged grout was mixed with almost double of the amount of required water. The mixture had a very low viscosity and a large amount of bleed water was observed after grouting was completed. Because of the bleed water, small voids were observed at the top of the specimen along most of the length. It was possible to detect the presence of the voids through the translucent duct and vent holes before testing. However, the extent of the voids was not known until the specimen was dismantled after the conclusion of the test. The autopsy results are discussed in Chapter 6.

3.7 LOCATIONS OF STRAIN GAGES

Strain gages were used to monitor the response of the strands at various locations along the length during the fatigue tests. The number of gages increased with each specimen. Information about the locations of the strain gages is summarized below.

3.7.1 Strain Gage Positions

Throughout this paper, the gages are designated by letters and numbers to identify the location of each strain gage. The first letter refers to the location along the length of the stay. The second letters refers to the top strand (T) and the bottom strand (B). The number refers to the position the gage is on the strand: 1 for the top of the strand and 2 for the bottom of the strand. For example refer to Figure 3-16. The strain gage at the north end on the bottom side of the top strand is designated at A-T2.

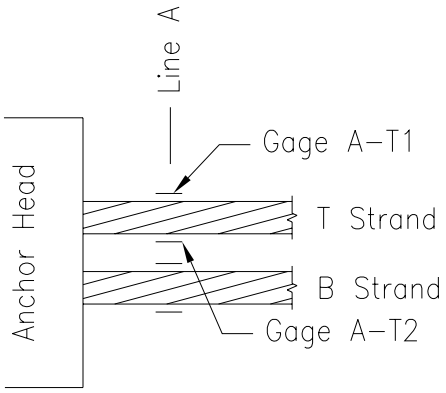

Figure 3-13 Strain gage notation

3.7.2 Specimen 1

Strain gages were positioned near each anchor head and near the midspan of Specimen 1. Four strain gages were positioned at each of the sections shown in Figure 3-14. The midspan gages were attached to the strands before stressing, as discussed in Section 3.6, and the gages near the ends were attached to the strands after stressing. Only ten gages survived the grouting process.

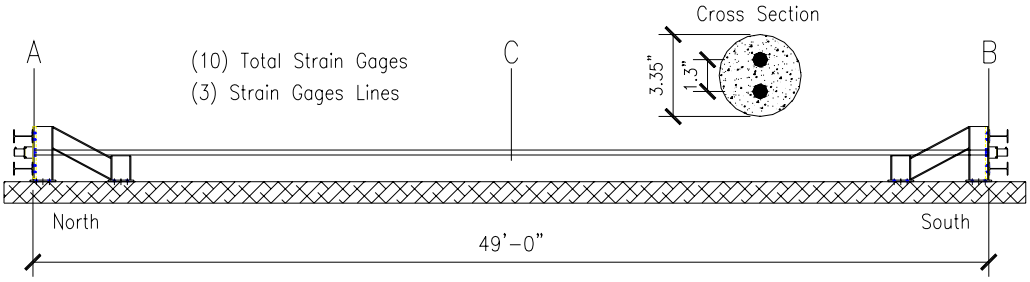

Figure 3-14 Locations of strain gages for Specimen 1

Table 3-2: Strain gage Locations for Specimen 1

Gage	Distance to Nearest Anchor Head
A-T1	1/4 in
A-T2	1/4 in
A-B1	1/4 in
A-B2	5/16 in
B-T1	1/4 in
B-T2	1/4 in
B-B1	3/16 in
B-B2	5/16 in
C-T1	Near Center
C-B2	Near Center

3.7.3 Specimen 2

The actuator was moved to Location 2 (Figure 3-1) during the fatigue tests for Specimen 1 and Specimens 2 and 3 were tested using this configuration. Therefore, more strain gages were positioned near the north end of Specimen 2 that near the south end, because the damage was expected to be concentrated in this area. In addition, two sets of strain gages were positioned near the point of load application. The six locations selected for the strain gages are shown in Figure 3-17. Strain gage designations are given in Table 3-3 for all 16 gages. Fifteen gages survived the grouting process.

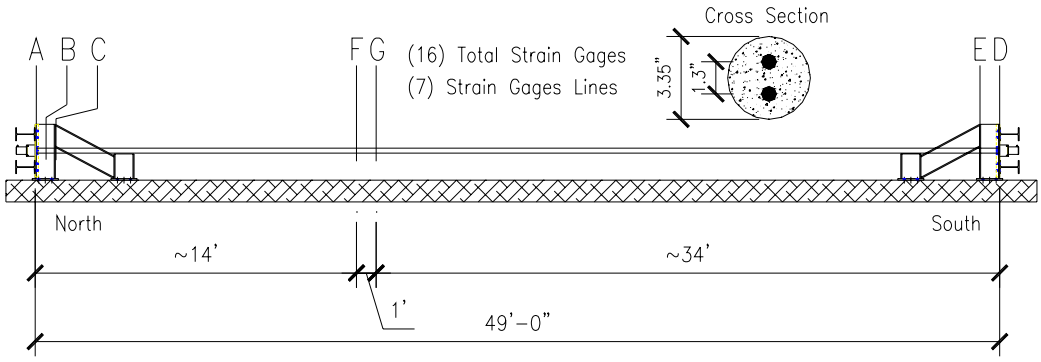

Figure 3-15 Locations of strain gages for Specimen 2

Table 3-3: Strain gage Locations for Specimen 2

Gage	Distance to Nearest Anchor Head
A-T1	1-1/16 in
A-T2	1-1/16 in
A-B1	1/2 in
A-B2	1/2 in
B-T1	6-1/8 in
B-B2	5-7/8 in
C-T1	12-3/8 in
C-B2	12-1/2 in
D-T1	1-1/16 in
D-B2	1/2 in
E-T1	5 in
E-B2	5 in
F-T1	~14 ft
F-B2	~14 ft
G-T1	~15 ft
G-B2	~15 ft

3.7.4 Specimen 3

As shown in Figure 3-18, strain gages were positioned at nine locations along Specimen 3. The designations used to identify the 32 gages are summarized in Table 3-4. Thirty-one gages survived the grouting process.

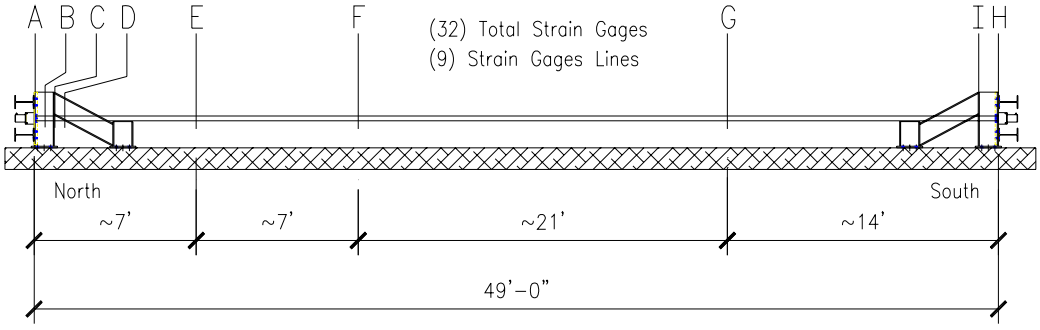

Figure 3-16 Locations of strain gages for Specimen 3

Table 3-4: Gage Locations for Specimen 3

Gage	Distance to Nearest Anchor Head	Gage	Distance to Nearest Anchor Head
A-T1	1-5/8 in	E-T1	7'-1"
A-T2	2-1/2 in	E-T2	7'-1"
A-B1	2-1/8 in	E-B1	7'-1"
A-B2	2-3/8 in	E-B2	7'-1"
B-T1	6-1/2 in	F-T1	14'-2"
B-T2	6-1/2 in	F-B2	14'-2"
B-B1	6-1/4 in	G-T1	14'-3"
B-B2	6-5/8 in	G-B2	14'-3"
C-T1	12 in	H-T1	2-1/2 in
C-T2	12 in	H-T2	2 in
C-B1	12-1/4 in	H-B1	2 -7/8 in
C-B2	12-1/4 in	H-B2	2-1/2 in
D-T1	16-3/4 in	I-T1	13-7/8 in
D-T2	17-5/8 in	I-T2	13-5/8 in
D-B1	16-3/4 in	I-B1	13-1/8 in
D-B2	17-1/2 in	I-B2	12-7/8 in

CHAPTER 4
Bending Fatigue Tests

This chapter summarizes the procedures used to conduct the small-scale bending fatigue tests. Although the primary objective was to evaluate the fatigue response of the specimens, several other tests were conducted periodically. The transverse stiffness and strain response was monitored by loading the specimens statically. Free-vibration tests were conducted by detaching the actuator from the specimen, and exciting the specimen with a low-amplitude impulsive force. In addition, the specimens were continually monitored acoustic sensors to detect for wire breaks.

The procedures used to control the fatigue tests are discussed in Section 4.1, the periodic static tests are summarized in Section 4.3, the free vibration tests are presented in Section 4.4, and the acoustic monitoring system is addressed in Section 4.5. The fatigue testing procedures for Specimen 1 were more complicated than the other those for the other two specimens, because the hardware was changed during the test. Those changes are discussed in Section 4.2.

4.1 FATIGUE TESTS

The procedures and hardware discussed in this section were used in the fatigue tests of Specimens 2 and 3 and for the last 1.5 million cycles of Specimen 1. Several modifications were made during the first 3.5 million cycles of Specimen 1, and those changes are discussed in Section 4.2.

Fatigue loads were applied to the specimens by a single hydraulic actuator (Figure 4-1). The actuator was positioned near the north quarter point (Location 2 in Figure 3-1) for most tests. For stability reasons, the specimens were loaded in

one direction only. The actuator pulled the specimen up and allowed the specimen to almost return to the neutral position during each loading cycle. Specimens were loaded in both directions during the large-scale fatigue tests (Poser 2001, Ridd 2004), but the small-scale specimens were significantly longer and had a much smaller cross section. As a result, the small-scale specimens were extremely flexible and it was not possible to maintain alignment of the actuator if the specimen was pushed beyond the neutral position. The procedure used to setup the actuator is discussed in Section 4.1.1.

Figure 4-1 Set-up for fatigue tests

The controller unit was programmed such that the actuator would impose the desired displacement history to the specimen. The loading cycle followed a sinusoidal waveform. The controller maintained a constant amplitude and frequency during the tests. The controller is discussed in Section 4.1.2.

4.1.1 Hydraulic Actuator

A 5-kip hydraulic actuator with a 12-in. stroke was used for all fatigue tests (Figure 4-1). The actuator was manufactured by Miller Fluid Power Division. The force imposed by the actuator was monitored by an external load cell and an external displacement transducer was used to monitor the position of the actuator (Figure 4-2).

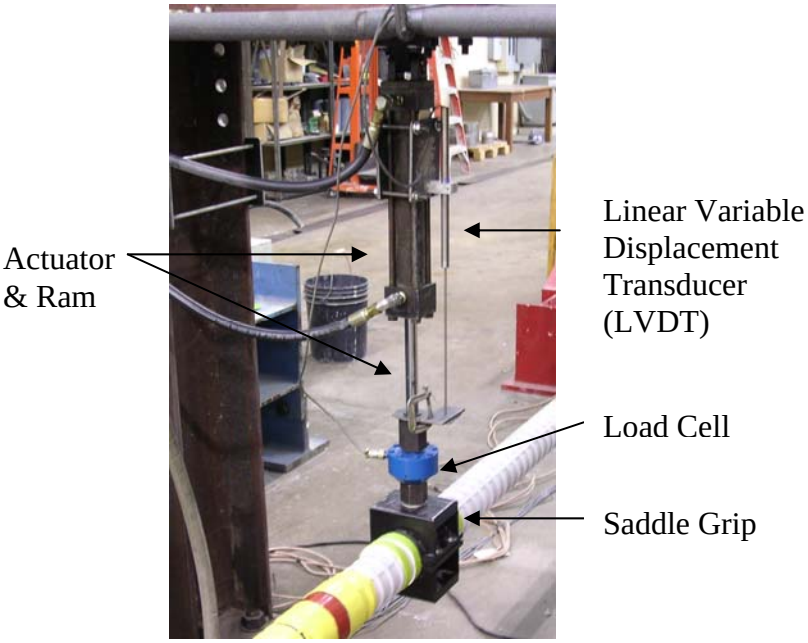

Figure 4-2 Actuator setup

The load cell also had a capacity of 5 kip. The load cell was manufactured by Interface (model number 1010AF-5K-B, serial number 159490A, and calibration factor 2.177mV/V). The displacement transducer had a stroke of ±3 in. and was manufactured by G.L. Collins Corporation (part number A5453 and serial number 718218).

The hydraulic power was supplied by a 6-gpm hydraulic pump. This pump was sufficient to test at a frequency of 1.5 Hz.

4.1.2 Controller

A PC-based controller (MTS FlexTest SE system, software release MTS 793.00) was used to control the movement of the actuator during the fatigue tests. A typical dialog box for sinusoidal response is shown in Figure 4-3. The user must define the frequency, amplitude, and target setpoint to control the test. The setpoint is the zero position for the sinusoidal displacement and the amplitude represents the displacement from the zero position to the maximum and minimum values during the cycle.

The “Meter 1” display box shows the peak values of axial force and displacement measured during the cycle, and the data are plotted in the “Scope 1” display box. A time delay usually exists between the displacement signal sent by the controller and the displacement of the actuator.

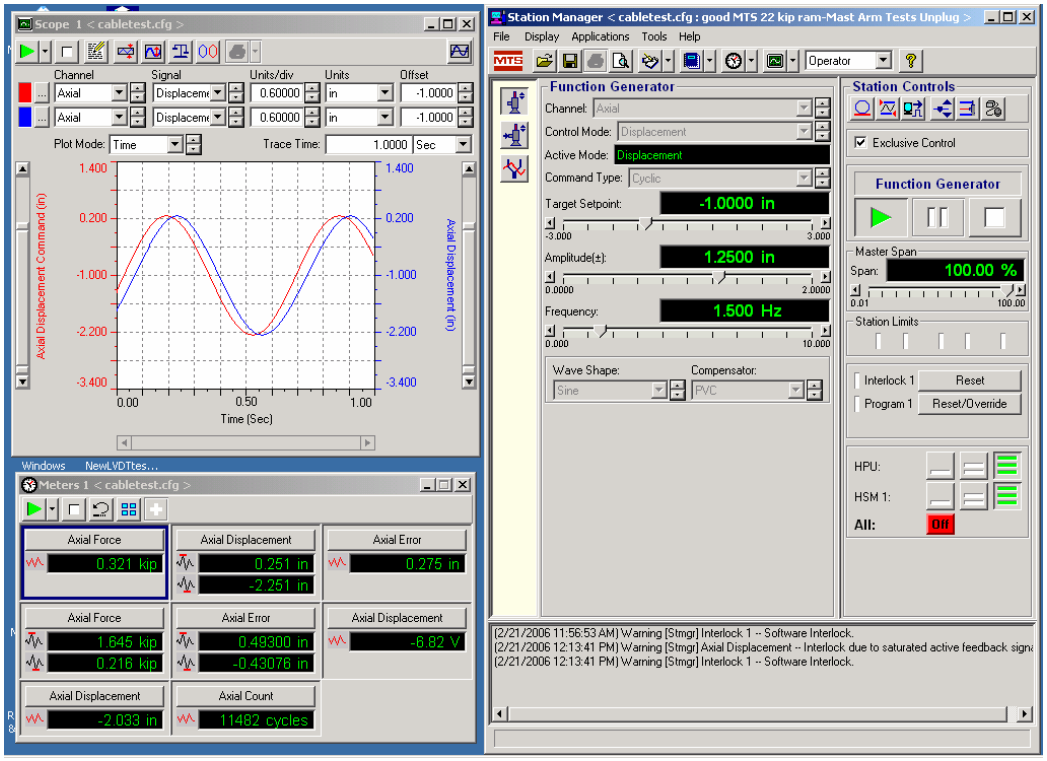

Figure 4-3 User interface of controller

During the fatigue tests, strict error limits were imposed on the system, ensuring that the loading cycles stayed within closely-defined parameters. If the load, deflection, or error between the controller and actuator output drifted out of range, the system would shut off automatically.

4.2 FATIGUE TESTS FOR SPECIMEN 1

Two problems were identified during the early stages of the fatigue tests for Specimen 1: the actuator could not be operated in displacement control and the testing frequency was severely limited by the size of the hydraulic pump. A larger capacity pump was installed after approximately 550,000 cycles and the testing frequency was increased from 0.6 Hz to 1.25 Hz. The frequency was

increased to 1.5 Hz after approximately 880,000 cycles, and this frequency was used for the remainder of this test and for the later two specimens.

Correcting the problems that prevented the actuator from being operated in displacement control proved to be more problematic. Therefore, the fatigue test for Specimen 1 was run in load control for nearly 3,400,000 cycles. Resolving this issue required replacement of a PC board in the controller and acquisition of a displacement transducer that was compatible with the MTS control software. It was possible to monitor the displacement response of the actuator during the first 3,400,000 cycles, but the displacement signal could not be used to control the actuator. After changing the displacement transducer, all subsequent tests were run under displacement control.

The actuator was positioned at midspan (Location 1 in Figure 3-1) at the beginning of the fatigue tests for Specimen 1. However, after more than six weeks of testing, no wire breaks had been detected near the anchor heads by the acoustic monitoring system (Section 4.5). Therefore, the decision was made to move the actuator closer to the north anchor head (Location 2 in Figure 3-1) after nearly 3,500,000 cycles.

4.3 PERIODIC STATIC MEASUREMENTS

The fatigue tests were stopped periodically and static tests were conducted to assess the extent of the damage caused by the fatigue loading. As wires fracture, the tension in the strands is expected to decrease. Because the transverse stiffness of the specimen depends on the axial tension force, reductions in transverse stiffness should be detected as wires break during the fatigue tests. During each static test, the applied load, transverse displacement, and strain response along the specimen were monitored.

4.3.1 Static Stiffness

The neutral position of the specimen was determined by finding the actuator displacement that corresponded to zero applied load. The actuator displacement was increased incrementally under displacement control from the neutral position to a predetermined level near the cycle maximum for the fatigue tests. Load and displacement values were recorded at each displacement level.

4.3.2 Strain

The strains were monitored to determine if the distribution of stress varied as damage increased. Strains were measured at each displacement level during the static tests.

4.4 FREE-VIBRATION TESTS

The natural frequency of the specimens was also expected to decrease as the tension in the strands decreased. Accelerometers were attached to the surface of the duct at various locations (Figure 4-4).

The actuator was disconnected from the specimen and a rubber mallet was used to impose an impulsive load at several locations along the span. The natural frequencies were easily detected by converting the measured acceleration data into the frequency domain. The results of the dynamic tests are not reported in this thesis, but will be presented in a dissertation by Jun-Ki Lee.

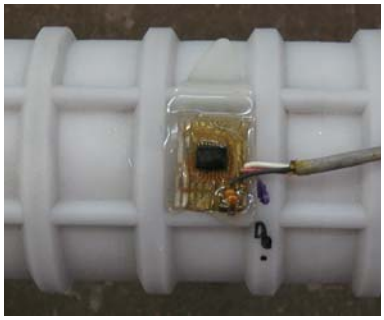

Figure 4-4 Accelerometer

4.5 ACOUSTIC MONITORING

The fatigue tests were monitored continuously using a system provided by SoundPrint, a division of Pure Technologies, Ltd. Acoustic sensors were placed on each anchor head and at two points along the free length as shown in Figures 4-5 and 4-6. Sensor locations are also summarized in Figure 4-5. The sensors were connected to a computer that was monitored remotely by SoundPrint. The sensors were set up to trigger automatically and were calibrated to detect wire breaks. Wire break events were recorded and time stamped by the system.

SoundPrint made the data available to the research team on the company's website. SoundPrint also approximated the location of each wire break. Because many false events occurred, SoundPrint used data filters to identify the actual wire breaks. False events were likely generated by routine construction and testing activities in the Ferguson Structural Engineering Laboratory.

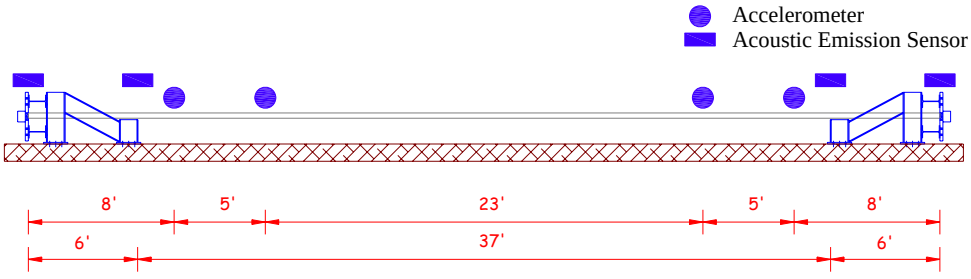

Figure 4-5 Accelerometer and Acoustic Sensor Locations

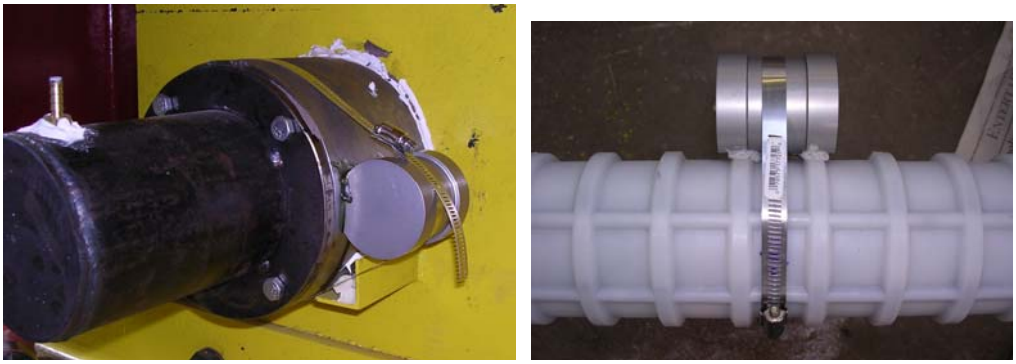

(a) Sensor attached to anchor head *(b) Sensor attached along stay length*

Figure 4-6 Acoustic sensors

CHAPTER 5

Measured Response of Small-Scale Specimens During Bending Fatigue Tests

This chapter summarizes the measured response of Specimens 1, 2 and 3 during the bending fatigue tests. The measured strain and stiffness response is presented for all three specimens. SoundPrint data are also summarized for Specimens 1 and 2.

On a daily basis, researchers recorded the cycle count, maximum and minimum displacements, and maximum and minimum loads. These data provided an approximate means of monitoring degradation of the specimens and also allowed the time of wire breaks, monitored by SoundPrint, to be correlated with the number of fatigue cycles.

5.1 Overview of Fatigue Tests

The starting and ending dates for the fatigue tests and the dates of the static tests are summarized in Table 5-1. Specimen 1 was subjected to more than 5 million loading cycles. A total of seven static tests were conducted. Strains were monitored during only the first three static tests, and stiffness data were collected in tests one and three through seven. Specimen 2 sustained more than 4.7 million loading cycles. Strains and stiffness data were recorded during all eight static tests. Specimen 3 was subjected to four static tests before May 1, 2006. The fatigue tests are ongoing and only the results of the first static test are reported in this thesis.

Table 5-1: Dates of Fatigue and Static Tests

Specimen	Date	Cycle Count	Comments
1	8/30/05	-	Static test 1
1	8/31/05	1000	Static test 2
1	9/01/05	8,305	Begin fatigue test
1	9/06/05	258,597	Static test 3
1	9/16/05	967,854	Static test 4
1	9/27/05	2,328,000	Static test 5
1	10/3/05	3,123,500	Static test 6
1	10/5/05	3,261,997	Static test 7
1	10/17/05	3,409,405	Move Actuator to Location 2
1	11/1/05	5,044,194	End of fatigue test
2	2/21/06	-	Static test 1
2	2/21/06	0	Begin fatigue test
2	2/28/06	~857,200	Static test 2
2	3/8/06	1,871,180	Static test 3
2	3/15/06	2,780,862	Static test 4
2	3/21/06	3,568,128	Static test 5
2	3/24/06	3,924,975	Static test 6
2	3/27/06	4,323,526	Static test 7
2	3/30/06	4,603,980	Static test 8
2	3/31/06	4,715,555	End of fatigue test
3	4/25/06	-	Static test
	4/25/06	0	Begin fatigue test

As discussed in Chapter 4, the fatigue tests were controlled by specifying the set point, frequency, and amplitude of the actuator movement. These data are summarized in Tables 5-2 through 5-4.

Table 5-2 Parameters used to control fatigue tests for Specimen 1

Date	Cycles (N)	Frequency (Hz)	Set Point*	Amplitude	Control Method	Max.	Min.
9/1/05	0	0.6	0.8 k	0.5 k	Force	2.937 in	0.836 in
9/12/05	552,688[+]	1.25	0.8 k	0.5 k	Force	3.182 in	0.492 in
9/15/05	879,999	1.5	0.8 k	0.5 k	Force	3.237 in	0.422 in
10/6/05	3,398,082§	1.5	1.96 in	1.5 in	Displ.	1.767 k	0.244 k
10/17/05	3,484,840**	1.5	1.96 in	1.25 in	Displ.	1.770 k	0.382 k
10/27/05	4,532,472	1.5	1.96 in	1.25 in	Displ.	1.450 k	0.118 k
10/28/05	4,538,130	1.5	1.96 in	1.25 in	Displ.	0.506 k	0.128 k
11/1/05	5,044,194	1.5	1.96 in	1.25 in	Displ.	0.492 k	0.111 k

[+] Connected higher capacity pump.
§ Installed new LVDT and switched to displacement control.
** Moved actuator from position 1 to position 2.
* Set point given in inches represents displacement level above neutral position.

Table 5-3: Parameters used to control fatigue tests for Specimen 2

Date	Cycles (N)	Frequency (Hz)	Set Point (in)*	Amplitude (in)	Control Method	Max. (k)	Min. (k)
2/21/06	0	1.5	1.519	1.25	Displ.	1.624	0.218
3/5/06	1,524,939	1.5	1.519	1.25	Displ.	1.511	0.195
3/16/06	2,909,696	1.5	1.719	1.25	Displ.	1.620	0.308
3/24/06	3,925,204	1.5	1.919	1.25	Displ.	1.577	0.279
3/27/06	4,323,719	1.5	2.119	1.25	Displ.	1.577	0.392
3/31/06	4,715,555	1.5	2.119	1.25	Displ.	1.386	0.363

* Set point displacement level above neutral position.

Table 5-4: Parameters used to control fatigue tests for Specimen 3

Date	Cycles (N)	Frequency (Hz)	Set Point (in)*	Amplitude (in)	Control Method	Max. (k)	Min. (k)
4/25/06	0	1.5	1.5	1.4	Displ.	1.685	0.066
5/1/06	748,855	1.5	1.5	1.4	Displ.	1.604	0.023

* Set point represents displacement level above neutral position.

The many changes that occurred during the fatigue test for specimen 1 are discussed in Section 4.2. The amplitude and frequency of the cycles did not vary

for specimen 2. However, several times during the tests, the set point was increased such that the applied force at the maximum displacement was approximately 1.6 k. As fatigue damage increased, the displacement required to induce a larger applied force decreased. The set point was increased to keep the applied load approximately the same. The last two columns of Tables 5-2 through 5-4 represent the displacement or load that was required by the actuator to keep the specimen cycling around the set point at the designated amplitude.

5.2 ACOUSTIC MONITORING

The test specimens were monitored continuously during the fatigue tests with the SoundPrint system. The data reported on the SoundPrint website included the date and time that each suspected wire break was recorded and the approximate location of the wire break. The number of cycles corresponding to each wire break was estimated for the daily logs.

5.2.1 Specimen 1

A total of fourteen wire breaks were recorded for Specimen 1 (Table 5-5). The first two were recorded 34 days after the beginning of the test. The last twelve breaks occurred in the last nine days of testing. The duration of the fatigue test was 61 days.

Table 5-5: Summary of Wire Breaks Reported by SoundPrint for Specimen 1

Date	Approximate Number of Cycles (N)	Wire Break	Comment	Approximate Distance from Inner Face of Anchor Head (in.)	
				N Anchor	S Anchor
9/01/05	8,305		Begin test		
10/03/05	3,101,000	10/03/05 11:42 AM	Wire break (1)	295	293
10/04/05	3,250,000	10/04/05 06:10 PM	Wire break (2)	295	293
10/24/05	4,219,000	10/24/05 6:50 PM	Wire break (3)	0.5	587.5
10/25/05	4,338,000	10/25/05 1:22 AM	Wire break (4)	3	585
10/25/05	4,382,000	10/25/05 6:43 PM	Wire breaks (5) & (6)	-1	589
10/26/05	4,430,472	10/26/05 6:30 PM	Wire break (7)	7	581
10/26/05	4,431,000	10/26/05 9:56 PM	Wire break (8)	4	584
10/27/05	4,513,500	10/27/05 12:46 PM	Wire break (9)	7	581
10/27/05	4,532,500	10/27/05 4:36 PM	Wire break (10)	11	577
10/27/05	4,545,670	10/27/05 8:28 PM	Wire break (11)	12	576
10/28/05	4,560,395	10/28/05 1:09 AM	Wire break (12)	4	584
10/28/05	4,588,000	10/28/05 3:35 PM	Wire break (13)	9	579
11/01/05	5,044,000	11/01/05 3:15 AM	Wire break (14)	4	584
11/01/05	5,044,194		End of fatigue test		

5.2.2 Specimen 2

A total of six wire breaks were reported for Specimen 2 (Table 5-6). The first two were within the first four days of the fatigue test. The last four breaks occurred in the final seven days of testing. The duration of the fatigue test was 32 days.

Table 5-6: Summary of Wire Breaks Reported by SoundPrint for Specimen 2

Date	Cycles (N)	Wire Break	Comment	Approximate Distance from Inner Face of Anchor Head (in.)	
				N Anchor	S Anchor
2/21/06	0		Start actuator		
3/02/06	1,000,000	3/2/2006 12:53 PM	Wire break (1)	5.5	582.5
3/03/06	1,300,000	3/3/2006 5:32 PM	Wire break (2)	6	582
3/22/06	3,600,000	3/22/2006 10:28 AM	Wire break (3)	19	569
3/23/06	3,780,000	3/23/2006 8:22 AM	Wire break (4)	23	565
3/23/06	3,850,000	3/23/2006 6:27 PM	Wire break (5)	11.5	576.5
3/28/06	4,449,500	3/28/2006 5:32 PM	Wire break (6)	24	564
3/31/06	4,715,555		End of fatigue test		

5.3 LATERAL STIFFNESS

The procedures used to collect load and displacement data during the static tests were discussed in Section 4.1. The lateral stiffness was calculated by using a least-squares fit to determine the line most closely represented by the data. The lateral stiffness was taken as the slope of this line.

5.3.1 Specimen 1

The lateral stiffness of Specimen 1 was measured six times before the actuator was moved to location 2 (Table 5-1). The lateral stiffness values calculated during each test are reported in Table 5-7. The data are also plotted in Figure 5-1.

The initial stiffness was the highest. The stiffness was slightly lower in Tests 2 through 5. Tests 6 and 7 were conducted after the first two wire breaks were detected, but the change in stiffness were still very small. Static tests were not conducted after the actuator was moved to location 2.

Table 5-7: Calculated stiffness for Specimen 1

Static Test	Cycles (N)	Stiffness (k/in)	Total Wire Breaks*
1	0	0.408	
3	258,597	0.399	
4	967,864	0.400	
5	2,328,000	0.399	
6	3,123,500	0.393	1
7	3,261,997	0.390	2

* Identified by SoundPrint

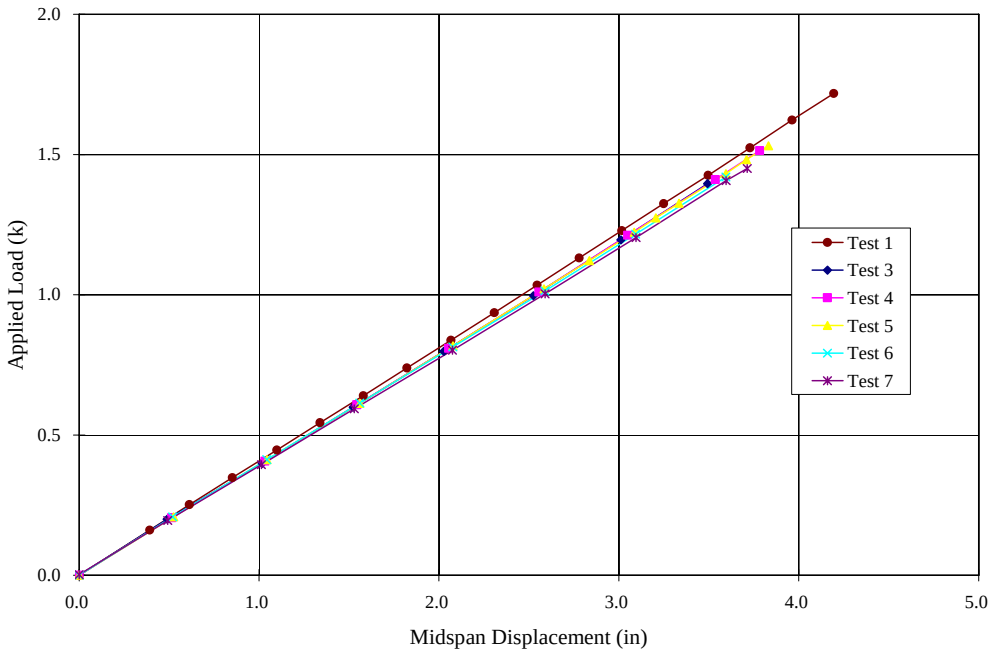

Figure 5-1 Measured response of Specimen 1 during static tests

5.3.2 Specimen 2

The lateral stiffness of Specimen 2 was measured eight times, but the tests were more uniformly distributed throughout the duration of the fatigue test (Table 5-8).

Data form the first two tests indicate that the stiffness of the specimen did not change during the first 850,000 cycles. A distinct change in stiffness was observed in Test 3, which was conducted after two wire breaks were reported. The stiffness continued to decrease in subsequent tests (Figure 5-2). At the conclusion of the fatigue tests, the lateral stiffness was approximately 15% less than the initial lateral stiffness.

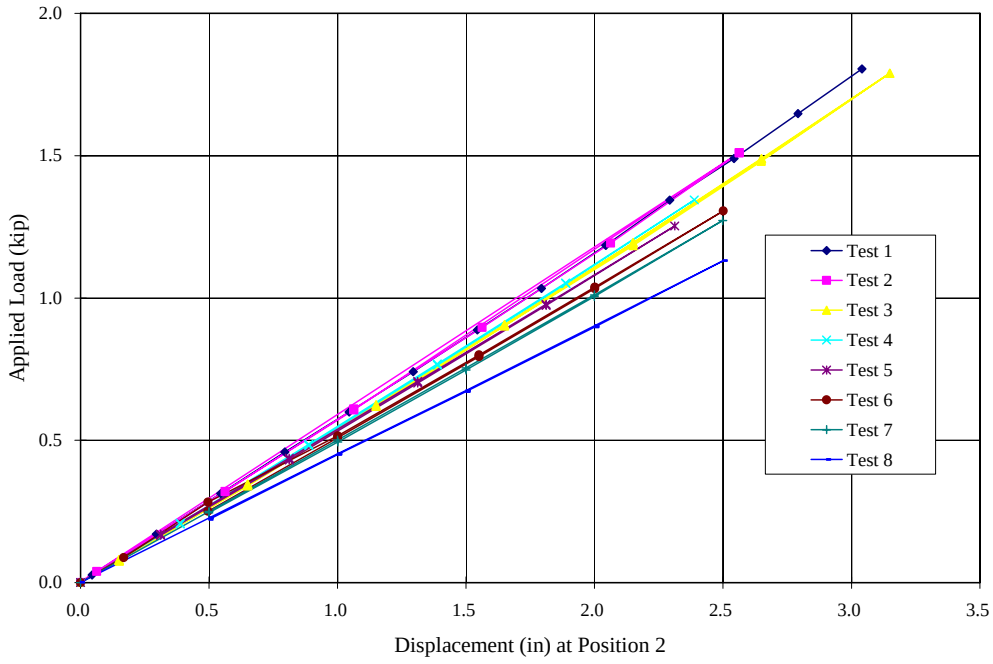

Figure 5-2 Measured response of Specimen 2 during static tests

Table 5-8: Calculated stiffness for Specimen 2

Static Test	Cycles (N)	Stiffness (k/in)	Total Wire Breaks*
1	0	0.591	
2	857,200	0.592	
3	1,871,180	0.566	2
4	2,780,862	0.563	
5	3,568,128	0.541	
6	3,924,975	0.517	5
7	4,323,526	0.508	
8	4,603,980	0.451	6

5.3.3 Specimen 3

The stiffness for Specimen 3 is reported only at the beginning of the fatigue test. The measured stiffness was 0.580 k/in (Figure 5-3), which is less than the initial stiffness of specimen 2.

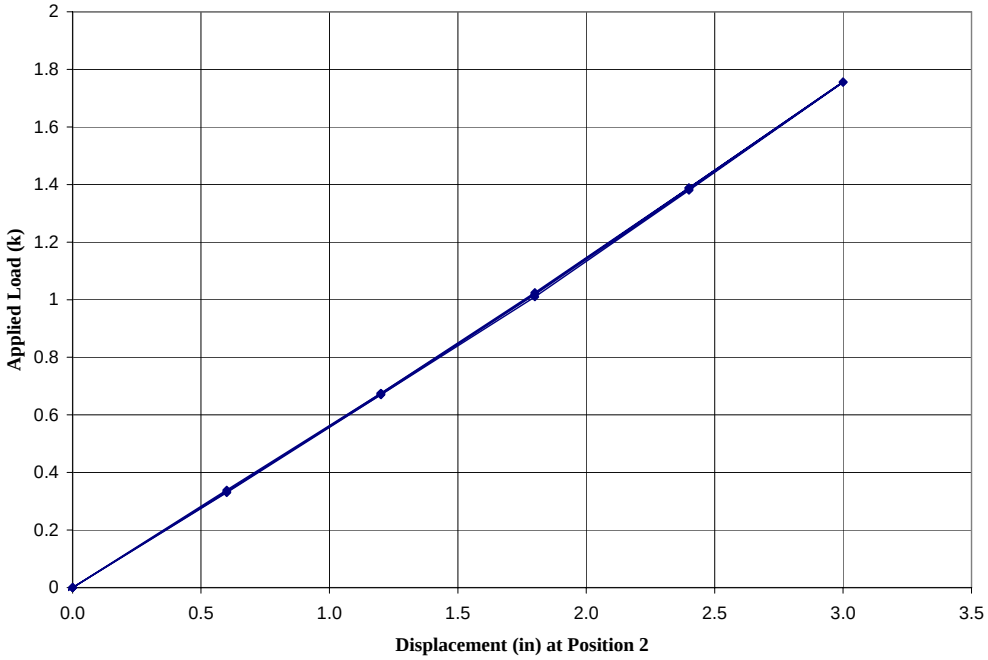

Figure 5-3 Measured response of Specimen 3 during static tests

5.4 MEASURED STRAIN RESPONSE

Strains in the strand were measured during most of the static tests. All the strain data are presented in Appendix B. The results are summarized in this section.

Specimen 3 is discussed first, because the largest numbers of gages were used to monitor this specimen. Strain gages will be identified using the designations given in Section 3.7.

5.4.1 Specimen 3

A total of 32 strain gages were used to monitor the response of Specimen 3. Thirty-one gages survived the grouting process. Strain data from the first static test are plotted in Figure 5-4. Zero strain corresponds to the strain in the undeflected strand after stressing.

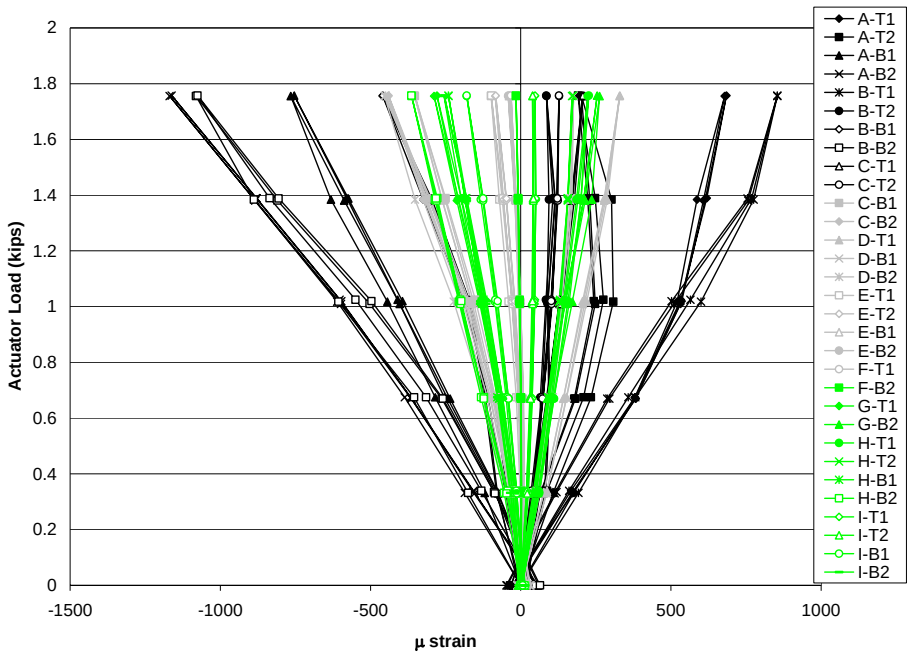

Figure 5-4 Measured Strain Response - Specimen 3

The strain in approximately half the gages increased as the specimen was pulled upward. Therefore, the total tensile strain increased in these gages. In contrast, the negative strains shown in Figure 5-4 indicate that the initial tensile strain was reduced. In no case did the change in strain due to bending of the specimen exceed the average strain due to prestressing (4360 $\mu\varepsilon$).

The strain gages values tended to increase or decrease linearly as the applied load was increased. However, many gages exhibited nonlinear behavior and the loading and unloading paths were different. This response is not unexpected because the strain gages were oriented along the individual wires of the strand. Slight shifting of the wires relative to each other could cause the observed strain response.

The largest variations in strains were measured in gages A-T1, A-B1, A-B2, B-T1, and B-B2. Variations exceeded 500 $\mu\varepsilon$ in these five gages which were located within 6 in. of the north anchor head (Figure 3-16). Maximum measured strain variations did not exceed 350 $\mu\varepsilon$ at any other location.

As discussed in Chapter 2, the fatigue life of the strand is normally assumed to decrease as the stress range increases. Significant variations in the axial fatigue life of the strand were observed in Chapter 2, but no fatigue failures were observed for a stress range of 20 ksi. Wire breaks, therefore, are expected to occur in the regions where the stress variation due to fatigue exceeds 20 ksi. This stress threshold is divided by the apparent modulus of the strand, E_a, to determine the corresponding strain along the axis of the wires (Table 5-9). The corresponding strain threshold is 645 $\mu\varepsilon$. Only five strain gages recorded strain variations during the static tests that exceeded this threshold.

Table 5-9: Conversion of Cut-Off Stress level to Strain

Stress level	20 ksi
Apparent Modulus, E_a	31,000 ksi
Calc. Apparent Strain, $\mu\varepsilon_a$	645

During the fatigue tests, the actuator displacement was varied relative to the set point. It was necessary to keep the actuator in tension to avoid stability problems. The displacement limits used at the beginning of the fatigue tests for specimen 3 and the corresponding force levels are reported in Table 5-10. These load levels are plotted in Figure 5-2 along with the measured strain data. The measured strain range between these force levels are reported in Table 5-11 for the five strain gages that exceeded the 645 $\mu\varepsilon$ threshold during the static tests.

Table 5-10: Bending Fatigue Testing Levels

	Displacement (in.)	Load (k)
Minimum	0.10	0.06
Maximum	2.90	1.67

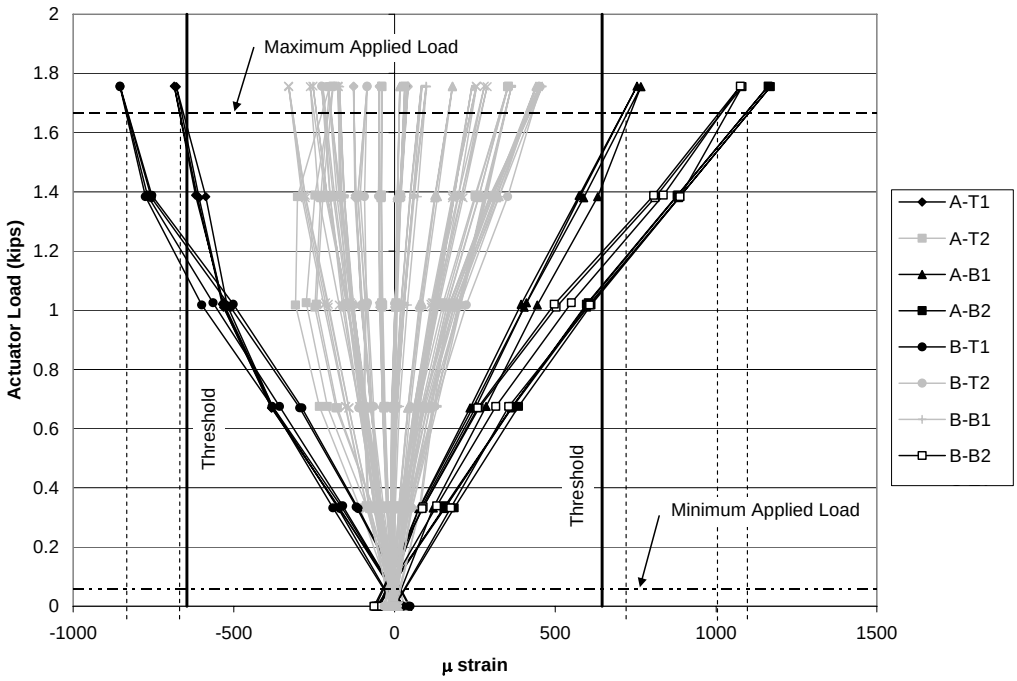

Figure 5-5 Maximum and minimum loads from fatigue tests superimposed on measured strains from initial static test - Specimen 3

Table 5-11: Stress Range Inferred from Measured Strain - Specimen 3

Gage	Measured Strains (με)		Inferred Stresses (ksi)		Stress Range (ksi)
	Min. Load (0.06 k)	Max. Load (1.67 k)	Min. Load (0.06 k)	Max. Load (1.67 k)	
A-T1	-18	-660	-0.6	-20.4	19.9
A-B1	12	720	0.4	22.3	21.9
A-B2	19	1100	0.6	34.1	33.5
B-T1	-19	-830	-0.6	-25.7	25.1
B-B2	18	1020	0.6	31.6	31.0

A maximum stress range of 33.5 ksi was calculated for the bottom wire in the bottom strand located 2 in. from the north anchor head (A-B2. This location is not surprising, as the highest induced moment is expected at the north end of the specimen. If the specimen behaves as a composite member, then the largest increase in strain would be on the bottom fiber at the north end of the specimen.

The same approach was used to relate the measured strain response during static test to the stress range in the strand for all specimens. However, only the data summarized in Table 5-11 will be presented.

The variation of the maximum and minimum stress ranges as a function of location is shown in Figure 5-6. A larger view of the north end is shown in Figure 5-7. The inferred stresses near the north anchor head are not reported directly at the anchor head. About 2-in. of gradient was not measurable because of the location of the strain gages. An unexpectedly high stress value is shown near 35 ft along the specimen. Because it is between the point of loading and the anchor it is expected to have a much lower inferred stress value. In general, stress is expected to be highest at the north end where there is a large change in curvature.

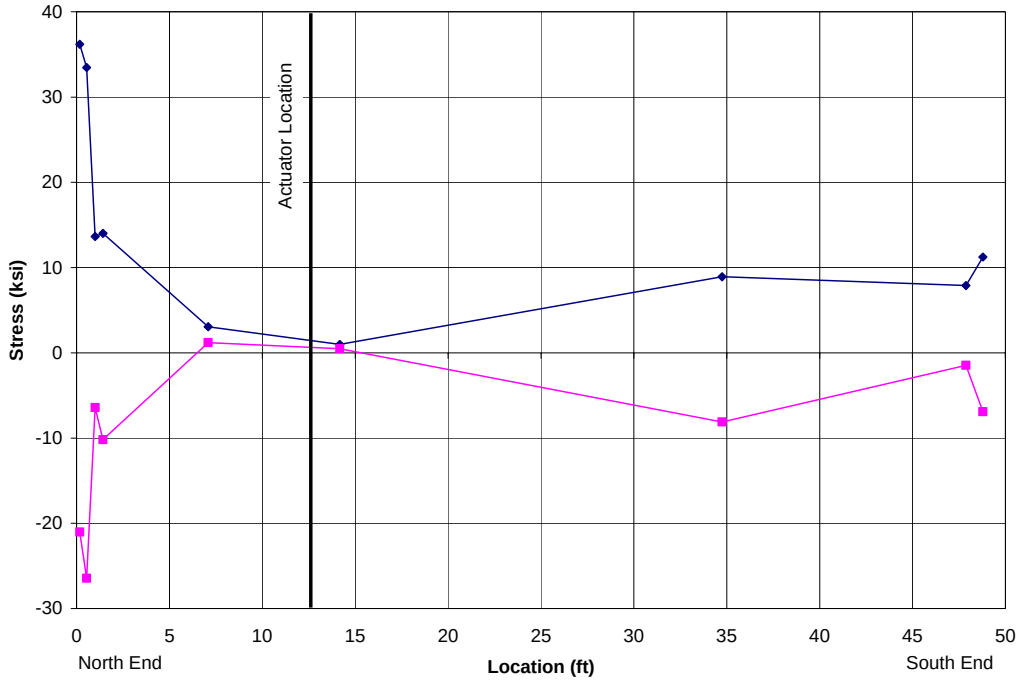

Figure 5-6 Stress Ranges in Fatigue Test Inferred from Measured Strains in Static Test - Specimen 3; Actuator load is 1.75 k

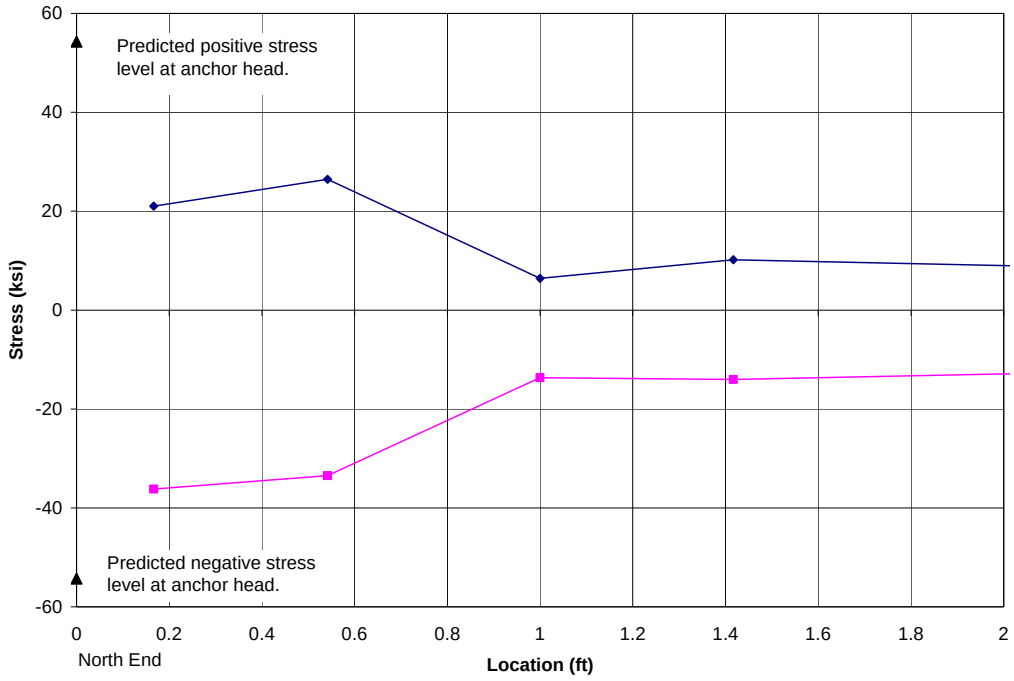

Figure 5-7 Stress Ranges in Fatigue Test Inferred from Measured Strains in Static Test - Specimen 3 for 2 ft from North end; Actuator load is 1.75 k

5.4.2 Specimen 2

Eight static tests were conducted for Specimen 2, and strains were measured during each static test. Stress values above the threshold of 20 ksi were only reported by two strain gages during the first two static tests. These strain gages malfunctioned before the third static test so it was not possible to monitor how the strain in the most highly stressed areas varied as fatigue damage accumulated.

The stress ranges inferred from the measured strain data are summarized in Tables 5-12 and 5-13 for the first two static tests. The stress range approaches 50 ksi in the strain gage A-B1, which was 1 in. from the north anchor head, in the first static test. However, the stress range inferred from the strain gage was less

than 20 ksi in the second static test. In contrast, the stress range in gage C-B2 increased from 18 to 32 ksi during the same two static tests.

Table 5-12: Stress Range Inferred from Measured Strain - Specimen 2, Test 1

Gage	Measured Strains ($\mu\varepsilon_a$)		Inferred Stresses (ksi)		Stress Range (ksi)
	Min. Load (0.06 k)	Max. Load (1.67 k)	Min. Load (0.06 k)	Max. Load (1.67 k)	
A-B1	90	1680	2.79	52.01	49.2
C-B2	20	675	0.62	20.90	20.3

Table 5-13: Stress Range Inferred from Measured Strain - Specimen 2, Test 2

Gage	Measured Strains ($\mu\varepsilon_a$)		Inferred Stresses (ksi)		Stress Range (ksi)
	Min. Load (0.06 k)	Max. Load (1.67 k)	Min. Load (0.06 k)	Max. Load (1.67 k)	
A-B1	65	660	2.01	20.43	18.4
C-B2	100	1130	3.10	34.98	31.9

The variation of inferred stress range along Specimen 2 is plotted in Figure 5-7. The trends are similar to those observed for Specimen 3; however, the stress ranges are larger for Specimen 2.

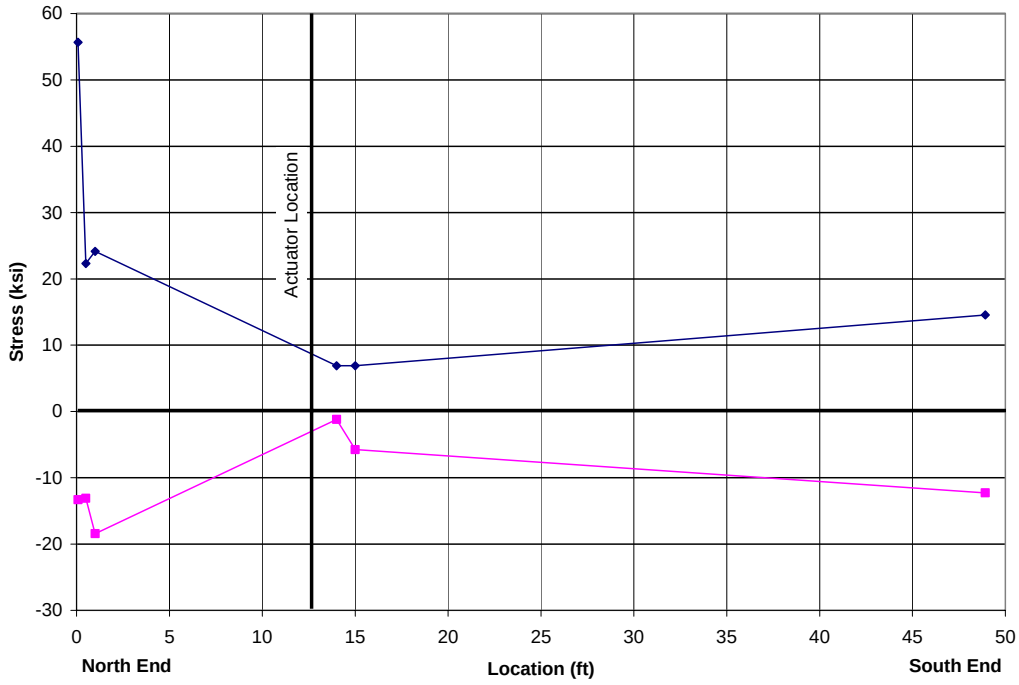

Figure 5-8 Stress Ranges in Fatigue Test Inferred from Measured Strains in Static Test 1 - Specimen 2; Actuator load is 1.8 k

It should be noted that many of the strain gage did not exhibit linear variations during the static test for Specimen 2. Data from the first static test are plotted in Figure 5-8. In many cases, the strain would increase with increasing load at low load levels and decrease with increasing load at higher loads levels. However, the strain levels corresponding to the maximum and minimum load measured during the fatigue tests were used to calculate the stress range.

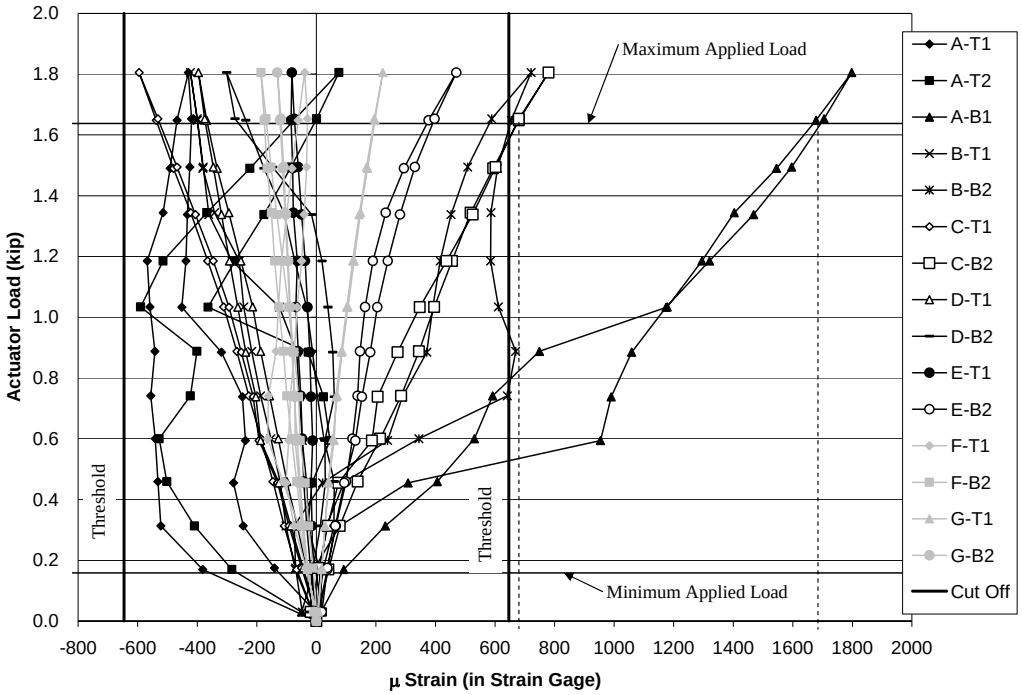

Figure 5-9 Maximum and minimum loads from fatigue tests superimposed on measured strains from initial static test - Specimen 2

Measured strain data from all eight static tests are plotted in Figures 5-9 and 5-10. Data from strain gages attached to the top strand are plotted above the horizontal axis and data from the strain gages attached to the bottom strands are plotted below the horizontal axis. When strains were recorded for gages on top and bottom of the strand then a line connects the values. If only one gage was on the strand then only a point value is shown for the strain measurement. The strain measurements were summarized in Figures 5-9 and 5-10 to show the strain values at different locations along the length of the specimen.

In general, the sections experience decreasing strain on the top of the strand and increasing strain on the bottom strand as would be expected from pulling up on the strand. It can be observed that many gages malfunctioned as

fatigue testing progressed. Most of the tests show only one strain value on top and bottom at each location. In these cases either there was only one strain gage on the outsides of the strands or the nearest gage no longer reported any measurements.

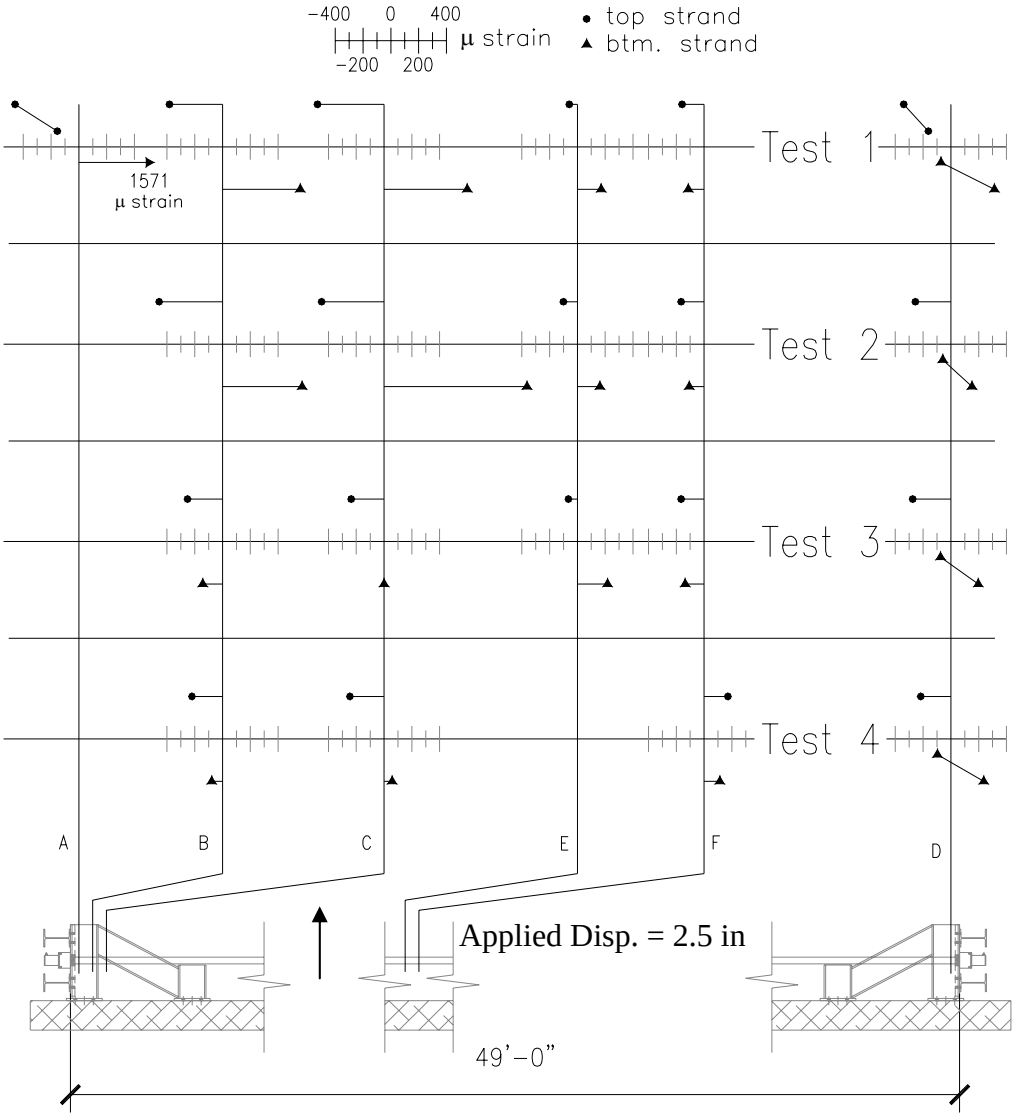

Figure 5-10 Summary of Measured Strains; Specimen 2– Static Tests 1 through 4

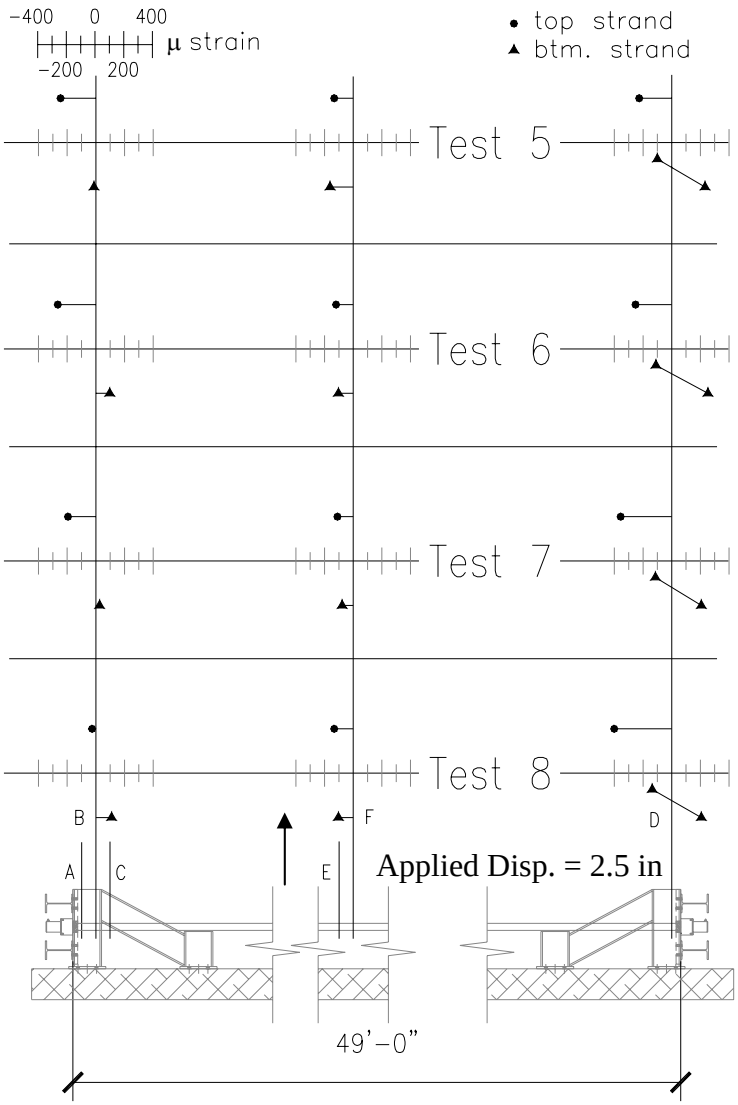

Figure 5-11 Summary of Measured Strains; Specimen 2 – Static Tests 1 through 8

5.4.3 Specimen 1

Strains were measured during the first three static tests. The first two tests conducted on successive days and the third test was conducted after 6 days of testing. All measured strain data are given in Appendix B.

For the force limits used in the fatigue tests for Specimen 1, none of the inferred stresses exceeded the threshold of 20 ksi. This was one of the reasons the actuator was moved from Position 1 to Position 2 after 3,484,840 fatigue cycles. Higher stresses were expected near the north anchor head with the actuator at Position 2. Most of the strain gages malfunctioned after the third static test. Therefore, it was not possible to continue static testing after the actuator position was changed.

Figure 5-11 shows the strains measured on lines A and B. It can be seen that the section experiences decreasing strain on the top of the strands and increasing strain on the bottom as would be expected from displacing the actuator in an upward direction.

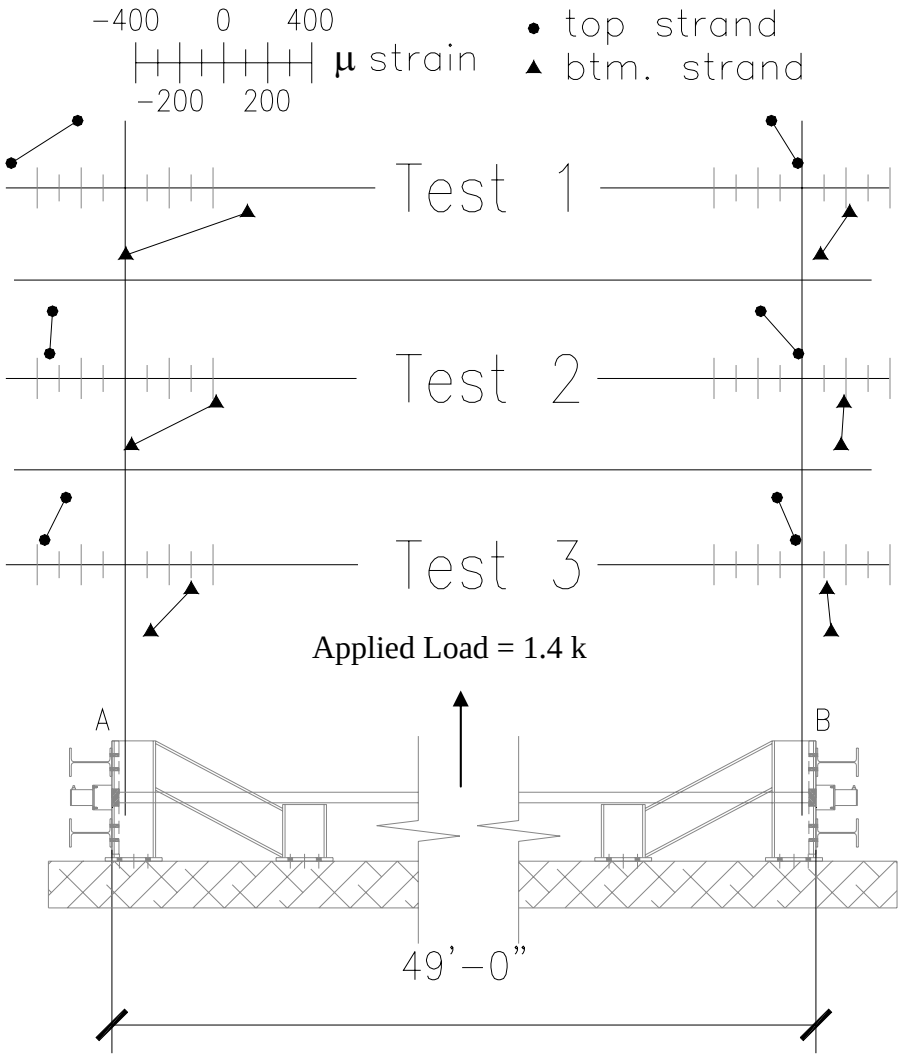

Figure 5-12 Summary of Measured Strains; Specimen1 – Static Tests 1 through 3

The strain measurements do not show a planar strain gradient within the cross-section. Cracking in the grout and small relative movements between the strands cause nonlinear strain change on the cross-section.

5.5 COMPARISON WITH PREDICTED RESPONSE

The decision to test the small-scale fatigue specimens was based on the analyses by Pebley (2005). Pebley developed a 3-D finite element model of the small-scale fatigue specimens and analyzed the response of the load applied at Position 1.

The results for Specimen 1 can be directly compared to Pebley's (2005) calculated values of actuator load, displacement, and strand stresses near the anchor head. Tables 5-14 and 5-15 summarize the results at three points in the vicinity of the maximum applied load during static test for the north and south ends. Pebley's calculations were based on an applied load of 1.35 k, but data were not recorded at this level. A least-squares approach was used to find values of the displacement corresponding to an applied load of 1.35 k. Because the strain response was nonlinear for Specimen 1, the stress range was taken as the maximum for the three measurements.

The results are compared with Pebley's predictions in Table 5-16. A similar approach was used for the data measured during static Test 2, and those results are summarized in Tables 5-17 through 5-19.

Table 5-14: Strain summary and calculated stresses of Specimen 1 - Test 1 North End

Test 1			Stress range inferred from strain measurements (ksi)			
Measurement	Actuator Load (k)	Displacement (in.)	A-T1	A-T2	A-B1	A-B2
1	1.260	3.249	-7.04	-17.90	15.30	2.26
2	1.361	3.496	-6.67	-16.00	17.22	0.07
3	1.459	3.729	-7.37	-15.46	18.96	0.71
Values for comparison	1.35	3.465	-7.4	-17.9	19.0	2.3

Table 5-15: Strain summary and calculated stresses of Specimen 1 - Test 1 South End

Test 1			Stress range inferred from strain measurements (ksi)			
Measurement	Actuator Load (k)	Displacement (in.)	B-T1	B-T2	B-B1	B-B2
1	1.260	3.249	-4.16	0.79	6.49	2.67
2	1.361	3.496	-4.25	0.61	6.71	2.55
3	1.459	3.729	-4.38	0.66	7.28	2.86
Values for comparison	1.35	3.465	-4.4	0.8	7.3	2.9

Table 5-16: Comparison of Pebley's Model and Specimen 1-Test 1

	Actuator Load (k)	Displacement (in.)	Maximum Stress Range at Anchor Head (ksi)
Pebley's Model	1.35	3.560	54.3
Maximum Values for Comparison	1.35	3.465	19.0
Error		2.7%	185%

Table 5-17: Strain summary and calculated stresses of Specimen 1 - Test 2 North End

Test 2			Stress range inferred from strain measurements (ksi)			
Measurement	Actuator Load (k)	Displacement (in.)	A-T1	A-T2	A-B1	A-B2
1	1.293	3.277	-11.91	-12.06	13.59	1.36
2	1.391	3.523	-9.00	-9.25	14.51	0.47
3	1.192	3.039	-10.07	-12.49	6.44	1.96
4	1.39	3.528	-10.64	-12.05	11.11	1.37
5	1.19	3.039	-10.24	-12.49	6.03	2.77
6	1.388	3.528	-10.97	-11.73	11.01	1.93
Values for comparison	1.35	3.277	-10.5	-11.4	11.7	1.4

Table 5-18: Strain summary and calculated stresses of Specimen 1 - Test 2 South End

Test 2			Stress range inferred from strain measurements (ksi)			
Measurement	Actuator Load (k)	Displacement (in.)	B-T1	B-T2	B-B1	B-B2
1	1.293	3.277	-6.01	-0.08	5.72	5.37
2	1.391	3.523	-5.50	-0.17	6.05	5.19
3	1.192	3.039	-5.60	-0.50	4.84	5.63
4	1.39	3.528	-6.13	-0.87	5.75	5.85
5	1.19	3.039	-5.69	-0.90	4.50	5.51
6	1.388	3.528	-5.91	-0.63	5.83	5.94
Values for comparison	1.293	3.277	-6.13	-0.90	6.05	5.94

Table 5-19: Comparison of Pebley's Model and Specimen 1-Test 2

	Actuator Load (k)	Displacement (in)	Stress at Anchor (ksi)
Pebley's Model	1.35	3.560	54.3
Maximum Values for Comparison	1.35	3.43	11.7
Error		3.7%	364%

The measured stiffness of specimen of Specimen 1 is very similar to the value predicted by Pebley. However, the maximum measured stress range was considerably less than predicted. Based on the strain data reported in section 5.4, significant deviations from the expected response were observed. The variations of the strain gages were nonlinear. The strains near mid-depth of the cross-section are larger than at the top or bottom (Figures 5-9 through 5-11). It is uncertain the reason for these deviations. Possible explanations include relative movement of the wires within the strand and the interaction of the grout and strands.

CHAPTER 6

Observed Damage after Conclusion of Small-Scale Bending Fatigue Tests

Following the completion of the bending fatigue tests, the small-scale specimens were disassembled. The locations of all wire breaks were measured and any other evidence of damage, such as cracking of grout or presence of corrosion, was noted. The results of these autopsy evaluations are summarized in Section 6.2. The locations of the actual wire breaks are also compared with those detected by SoundPrint during the fatigue tests.

Autopsies of the large-scale bending fatigue specimens (Poser 2001, Ridd 2004), indicated that most of the wire breaks were caused by fretting. This was also true in the small-scale bending fatigue specimens. An overview of the fretting process is presented in Section 6.1.

6.1 WIRE FRACTURES DUE TO FRETTING

Fretting occurs when two wires rub against each other repeatedly. A fatigue crack initiates at the contact point between the two wires. The fatigue crack grows gradually until the stress in the intact cross-sectional area exceeds the fracture strength of the material. At this point, the wire fractures.

In most cases, the contact point corresponding to the initiation of fretting (Figure 6-1) was located between two adjacent outer wires or between an outer wire and the center wire (Poser 2001, Ridd 2004). A detailed view of a contact point between two adjacent outer wires is shown in Figure 6-2. The distinction between the slow growing fatigue crack and the rapid fracture is visible on the fracture surface.

In a few cases the fatigue cracks initiated along an outside edge of an outer

wire. These wire breaks may be attributed to defects in the wire or damage that occurred during the stressing or grouting.

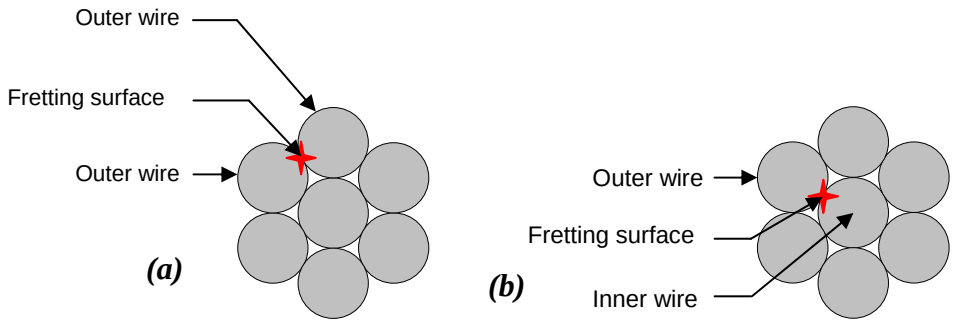

Figure 6-1 Initiation points for fretting fatigue: (a) Fretting between adjacent outer wires, (b) Fretting between center wire and outer wire (Ridd 2004)

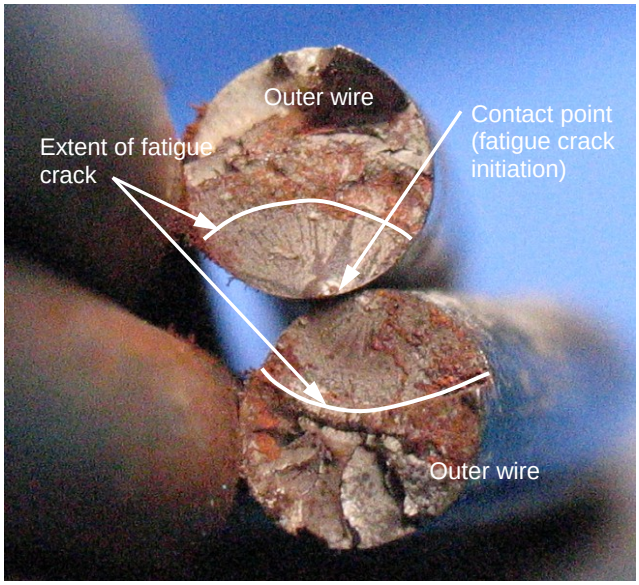

Figure 6-2 Fretting fatigue failure between two adjacent outer wires (Ridd 2004)

Each wire break observed in the small-scale bending fatigue specimens was classified using a two-character scheme based on the initiation point for fretting fatigue. Three terms are used: 'O' represents an outer wire, 'C' represents a center wire, and '?' indicates another source. The first letter in the

scheme identifies the wire with the break, and the second letter represents the adjacent wire or object that initiated the fatigue crack. For example, O-C means that the fatigue crack was initiated by fretting of an outer wire against the center wire.

6.2 AUTOPSY RESULTS

Following the completion of the fatigue tests, the specimens were disassembled and inspected for damage. To remove the stay from the reaction frames, the specimens were cut into three sections: north end, south end, and center region (area where the actuator was attached to the specimen). The post-tensioning duct was cut away to expose the grout. The grout was removed in regions of suspected wire breaks. The strands were then removed from the anchor heads. Special care was taken to preserve any regions where breaks occurred.

The results of the autopsy investigations are summarized in this section for Specimens 1 and 2. Fatigue tests are ongoing for Specimen 3; therefore, no data are reported.

6.2.1 Specimen 1

Specimen 1 failed abruptly after more than 5 million cycles. All fourteen wires failed in the vicinity of the north anchor head, and the specimen was completely separated from the north reaction frame (Figures 6-4 and 6-5).

Figure 6-3 North end of Specimen 1 at end of fatigue test

Figure 6-4 Fracture of all wires at north end of Specimen 1

During the autopsy, a total of 16 wire breaks were identified. Fourteen breaks occurred near the north anchor head and two wire breaks occurred in the top strand near midspan. The measured locations of all wire breaks are summarized in Table 6-1. The wires are numbered in Figure 6-6. All distances were measured from the inner face of the north anchor head. Positive numbers indicate that the wire broke along the free length and negative numbers indicate that the wire broke within the anchor head (Figure 6-5).

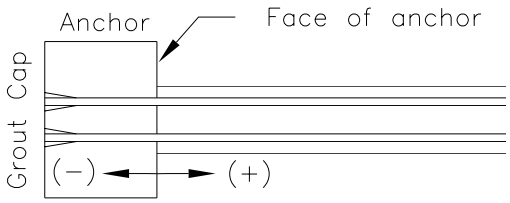

Figure 6-5 Sign convention used to locate wire breaks

Table 6-1 Measured locations of wire breaks – Specimen 1

Strand	Wire	Type of Wire Break		Distance from Face of North Anchor Head
Top	1	Tension	—	3/16 in.
	2	Fatigue	O-C	3/8 in.
	3	Fatigue	O-C	1-1/8 in.
	4	Fatigue	O-C	1-1/4 in.
	5	Fatigue	O-O	1-1/4 in.
	6	Fatigue	O-O	7/8 in.
	C	Fatigue	C-O	3/4 in.
	-	Fatigue	O-O	1 in. South of Midspan
	-	Fatigue	O-O	1 in. south of Midspan
Bottom	1	Fatigue	O-C	-7/8 in.
	2	Fatigue	O-C	-5/8 in.
	3	Fatigue	O-O	-3/8 in.
	4	Fatigue	O-O	-3/8 in.
	5	Fatigue	O-C	-3/8 in.
	6	Fatigue	O-?	-5/8 in.
	C	Fatigue	C-O	-5/16 in.

Photographs of the wire fracture surfaces near the north end are shown in Figure 6-6. All seven wires in the top strand fractured along the free length within 1.5 in. of the face of the anchor head. In contrast, all seven wires in the bottom strand fractured within the anchor head. For Specimen 1, the longest wires on the section of that separated from the anchor head were labeled as wire 1. The final positions of the wires were distorted by the sudden failure. All other wires were labeled as shown in Figure 6-6

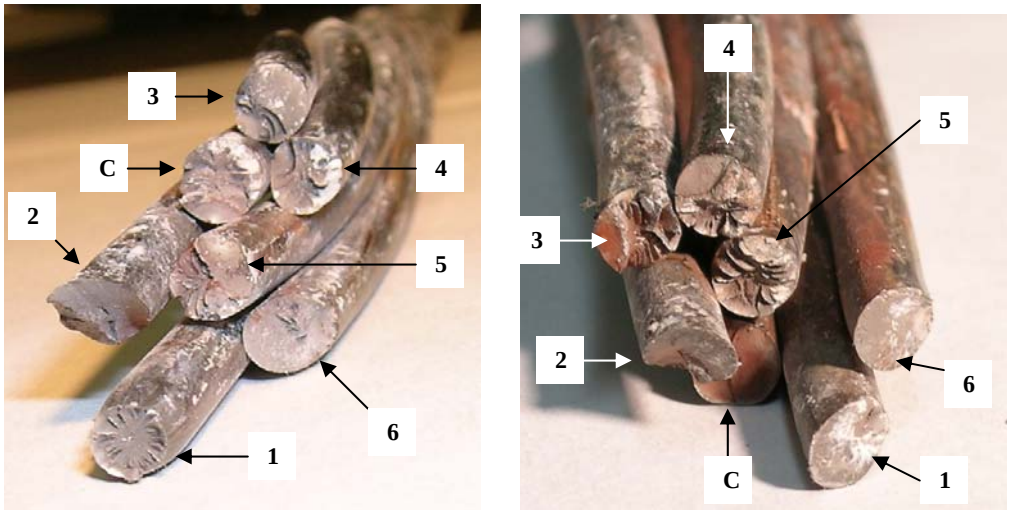

(a) *(b)*

Figure 6-6 Photographs of wire breaks at north end of Specimen 1: (a) Top strand, (b) Bottom strand

The shape of the failure surface for wire 1 in the top strand is clearly different from those of the other wires. The symmetric conical failure pattern and reduced cross section suggests that this wire failed in tension after necking. Evidence of fatigue crack growth was observed in all other wires.

It is not possible to compare the observed wire breaks directly with the wire breaks detected during the fatigue tests by SoundPrint. The SoundPrint readings provide a record of the time of the fracture and the approximate location along the length, but the strand that experienced the wire break can not be identified. In contrast, the autopsy records provide data on the actual location of each wire break, but the time of the wire break can not be determined.

However, comparing the locations of the wire breaks detected by SoundPrint with the distribution of actual wire breaks provides an indication of the accuracy of the acoustic detection system.

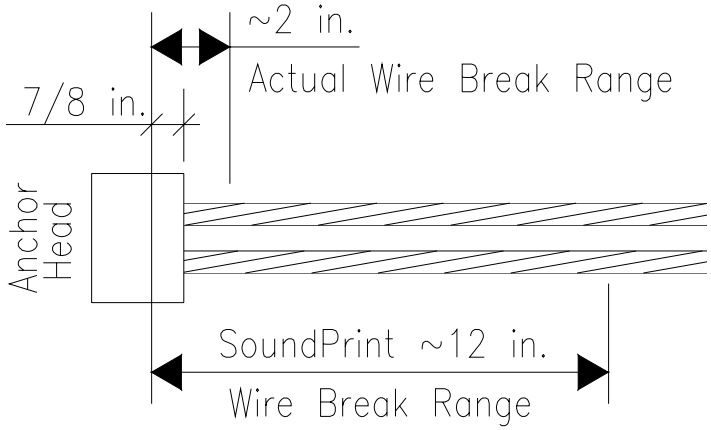

Figure 6-7 Comparison of wire breaks detected by SoundPrint with actual locations – Specimen 1 North End

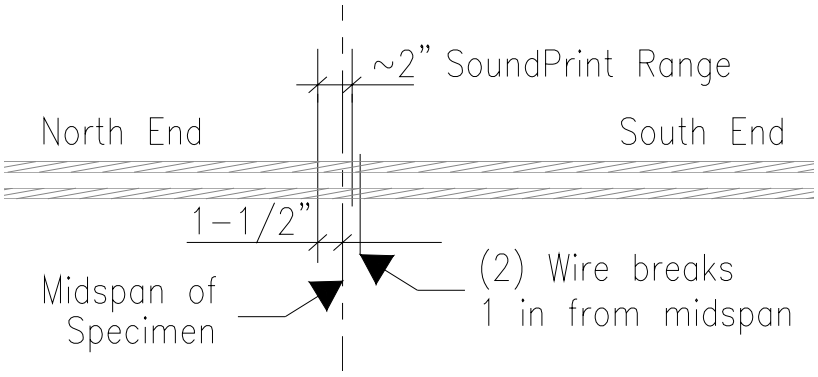

Figure 6-8 Comparison of wire breaks detected by SoundPrint with actual locations – Specimen 1 Near Midspan

At the north end of the specimen, all 14 wires fractured within 2 in of the face of the anchor head (Figure 6-7). SoundPrint identified twelve of the fourteen wire breaks. However, several wires may have fractured simultaneously when this specimen failed, so this difference is not considered to be significant. The SoundPrint records indicated that the breaks were distributed over the 12 in. range.

SoundPrint identified two wire breaks near midspan and two fractured

wires were detected. The locations detected by SoundPrint were within 2 in. of the observed fractures (Figure 6-8).

This correlation between the wire break locations detected by SoundPrint is similar to that observed for the large-scale bending fatigue specimens. The accuracy is higher away from the anchor heads, but all wire breaks were within 12 in. of the observed locations.

The autopsy also revealed a modest amount of corrosion on the surface of the strand in the vicinity of the wire fractures. Corrosion product was not observed on the surface the grout, however.

The grout appeared to be cracked near the anchor heads, at both ends of the specimen, but more cracks were observed at the north end. The cracks at the south end were small radial cracks. The grout at the north end appeared cracked in every way, and was pulverized near the strands.

The autopsy also indicated that the post-tensioning duct was not centered around the strands during the grouting process (Figures 6-8 and 6-9). As a result, the grout was more extensively cracked in regions where the strands were closer to the side of the duct.

Figure 6-9 Photograph of condition of specimen after fracture at north end of Specimen 1

Figure 6-10 Typical section through Specimen 1

6.2.2 Specimen 2

Specimen 2 sustained over 4.7 million cycles. The fatigue testing lasted thirty-eight days with no unexpected difficulties.

A total of 8 wire breaks were identified during the autopsy. All wires in the bottom strand fractured near the north anchor head. The center wire fractured at two locations. Two of the wire breaks occurred within the anchor head. The initiation point for one of these breaks on an outer wire was not caused by contact with another wire. The center wire also fractured within the anchor head. No wires fractured on the top strand. A summary of the wire break locations measured from the autopsy is given in Table 6-2.

SoundPrint reported 6 wire breaks. After ten days of testing, two wire breaks were detected; the remaining four breaks were detected in the last nine days of testing.

Table 6-2 Measured locations of wire breaks – Specimen 2

Strand	Wire	Type of Wire Break		Distance from Face of North Anchor Head
Bottom	1	Fatigue	O-?	-1/2”
	2	Fatigue	O-O	+6-5/8”
	3	Fatigue	O-O	+1/2”
	4	Fatigue	O-O	+1/2”
	5	Fatigue	O-C	+5/8”
	6	Fatigue	O-C	+5-7/8”
	C	Fatigue	C-O	+5-5/8”
	C	Fatigue	C-O	-1-5/8”

A comparison of wire break locations can be made between the observed breaks and the measured SoundPrint record. SoundPrint located the breaks within a few inches of the actual break locations (Figure 6-11).

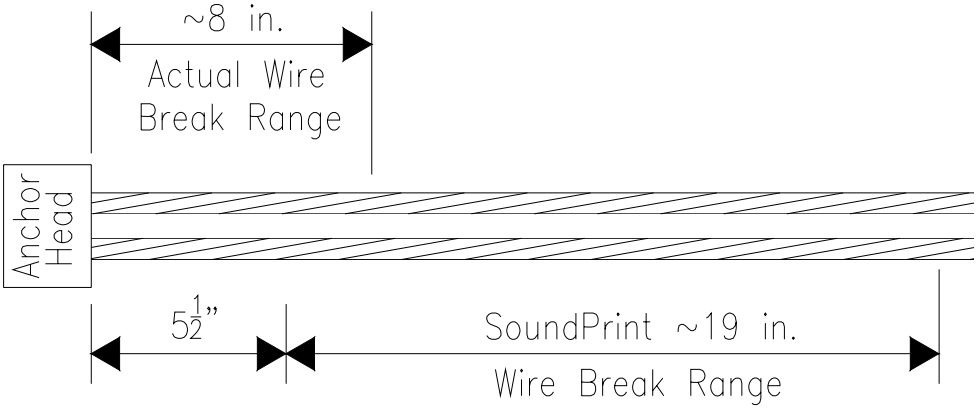

Figure 6-11 Comparison of wire breaks detected by SoundPrint with actual locations – Specimen 2 North End

The amount of corrosion on the bottom strand was more noticeable than in Specimen 1. The corrosion was only on the fractured strand in the regions where the breaks occurred. Figures 6-12 and 6-13 show the strands during the autopsy. In Figure 6-13 the corrosion from the fretting and wire breaks can be seen on the bottom strand.

Figure 6-12 Autopsy of specimen 2

Figure 6-13 Specimen 2 after grout has been removed

The grout appeared cracked in the anchorage regions. It was also noticed that the duct was not centered over the strands during the grouting process. During construction, the best efforts were made to be sure that the duct stayed straight and aligned with the strands, but this was almost impossible. After the duct was sealed, it was impossible to tell where the strands were within the duct. The duct was visually inspected for straightness before and after the grouting process.

CHAPTER 7
Summary and Conclusions

7.1 SUMMARY

Pebley (2005) developed the guidelines that were used to design the small-scale bending fatigue specimens discussed in this thesis. His calculations indicated that the large-scale bending fatigue specimens, which were modeled after the shortest stay on the Fred Hartman Bride, were more representative of beam behavior than cable behavior. Therefore, the length was increased and the diameter was reduced for the small-scale specimens. With this configuration, cable response was expected to dominate during the fatigue tests of the small-scale specimens, as it does for the stay cables on the Fred Hartman Bridge.

Three small-scale bending fatigue specimens were constructed as part of this investigation and the results from the first two specimens are reported in this thesis. Fatigue tests of the third specimen are on going. In addition, twenty-four individual strands were subjected to axial fatigue loading.

7.2 CONCLUSIONS

7.2.1 Axial Fatigue Response of Strand

Results of previous axial fatigue tests by Eggers (2003) and Ridd (2004) were confirmed. The results presented in Chapter 2 were essentially the same as those in the previous tests. Single strand, axial-fatigue tests resulted in an acceptable fatigue performance by Strand B and an unacceptable fatigue performance by Strand A. These tests were carried out according to PTI Guide Specifications Recommendations for Stay Cable Design, Testing and Installation (2001). Section 3.2.2.1.E of this guide details the required procedures.

The major difference between the two strand types was the cross-sectional area. Strand A had a smaller cross-section. Specifically, the individual wires of Strand A had smaller diameters than those of strand B, but their overall strand diameters were approximately the same. This difference made an impact in two ways. First, a larger cross-sectional area will increase the axial fatigue life of the prestressing strand. Second, the extra space created from the smaller diameter wires in Strand A provides room for relative movement between the wires. This movement leads to fatigue damage and a shorter fatigue life.

The results of the strand recovered from a bending fatigue test can be compared to Strand B results in axial fatigue to determine the impact of the presence of grout on axial fatigue life. Strand B satisfied the requirements for PTI fatigue testing and the recovered strand did not. In terms of cycle count, not much separated the two strands. The amount of variation between the results of the two strands can be attributed to scatter. More testing of this type would be needed to determine if grout decreases fatigue life.

7.2.2 Comparison of Small-Scale and Large-Scale

Overall response of small-scale and large-scale bending fatigue tests was similar. Most of the wires fractured near the anchor heads, but some also broke near the loading point. Periodically during the fatigue tests, static tests were conducted to evaluate changes in the specimen response. Similarly to the large-scale specimens, the lateral stiffness decreased as the number of wire breaks increased. However, the stiffness did not decrease linearly as the number of wire breaks increased.

7.2.3 SoundPrint System

The SoundPrint system was used to detect wire breaks during the fatigue tests. The accuracy of these measurements was similar to those obtained during the large-scale bending fatigue tests.

The record proved to be a general guide to number and location of wire breaks but the system did not record all of the breaks that occurred in the laboratory. One reason for this discrepancy may be the extensive amount of filtering that was required to eliminate laboratory noise.

7.2.4 Strain Gages near the Anchor Head

Unlike the large-scale specimens, strains in the wires were also measured during the static tests. As expected, the highest strains were recorded in the vicinity of the anchor head. However, it was not possible to evaluate redistribution of stresses as wires fractured because the strain gages attached to the most highly stressed wires did not survive more than 100,000 fatigue cycles.

The areas with high stress range were more severe environment for the gages. The gages stopped working from the repetitive movement of the strands or relative movement between the strand and the grout. The gages that continued to function were in area of lower stress ranges.

7.2.5 Comparison of Measured and Predicted Response

Pebley's 3-D finite element model provided an accurate estimate of he initial stiffness of the test specimens. However, the model overestimated the maximum stress in the strand near the anchor head. The strain gages did not measure strains at the anchor head, as Pebley's model did. A small change in strain is seen in the two inch distance, but not enough to verify the model.

APPENDIX A
Construction Details

A.1 REACTION FRAME

The small-scale bending fatigue specimens were supported by four reaction frames which were attached to the strong floor in the Ferguson Structural Engineering Laboratory. The reaction frames were constructed from W12x40 sections (Figure A-1 and A-2).

Figure A-1 Reaction frame

The frames stand 2'-10" high and are 5'-4" long. Two 1"x14"x12" plates were welded to the base of the reaction frames. The four frames hold the two yellow anchor supports at the correct locations.

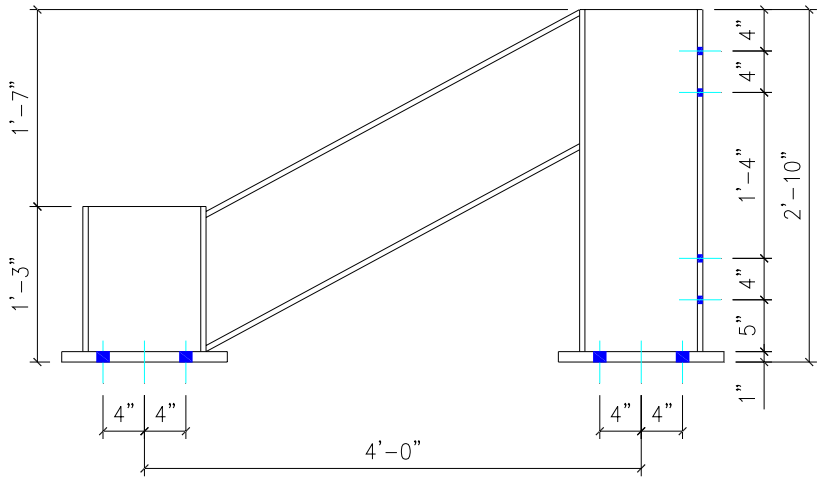

Figure A-2 Reaction frame drawing

A.2 ANCHOR SUPPORTS

The two yellow anchor supports span 4 ft between the pair of reaction frames at each end of the specimen. The anchor supports were also fabricated from W12x40 sections with a 2-in. plate bolted to the front of the support to hold the anchor head and to react against the prestressing strands (Figure A-3 and A-4).

Figure A-3 Anchor support

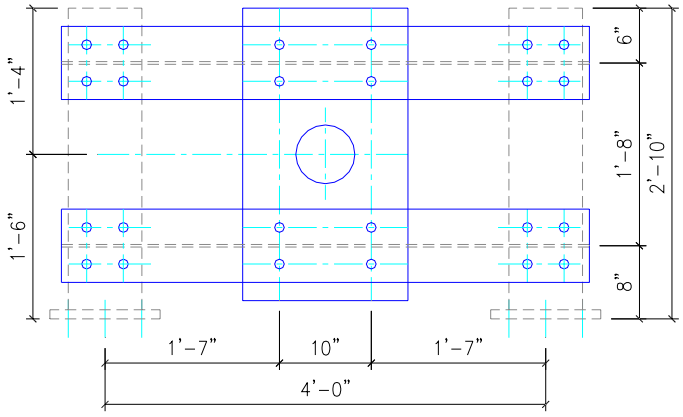

Figure A-4 Anchor support drawing

A.3 PREPACKAGED GROUT

SikaGrout 300PT was used to construct the specimens. The grout properties are given in the Table A-1. It is non-metallic and contains no chlorides.

Table A-1 Grout Properties (GTI, 2006)

SikaGrout 300 PT Typical Data	
Material and Curing Conditions	73°F and 50% R.H. Water used: 12.5 pints per 50 lb. bag
Shelf Life	Nine months in original, unopened bags.
Wet Density (ASTM C-138)	Approximately 125 pcf
Fine Aggregate	Contains none (sand-free)
Volume Change (ASTM C-1090)	24 hours 0.0% shrinkage
	28 days between 0 and +0.2% expansion
Expansion (ASTM C-940)	3 hours between 0.0 and +2.0%
Compressive Strength (ASTM C-942)	1 day 3,000 psi (20.0 MPa)
	3 days 5,000 psi (33.3 MPa)
	7 days 7,000 psi (46.7 MPa)
	28 days 8,000 psi (53.3 MPa)
Initial Set (ASTM C-953)	Approximately 3 to 12 hours

APPENDIX B

Results of Strain Measurements

The results of the periodic strain measurements were summarized and presented in Chapter 5. Additional data are presented in this appendix. All the strain data are shown in a single plot for each test. The same data are then grouped by location to provide more detailed information.

B.1 SPECIMEN 1

Strains were measured during the first three static tests for Specimen 1. Gage locations are shown in Figure 3-14. For each test the raw data are for all of the locations then divided into separate plots for location A (north end), location B (south end), and location C (midspan).

B.1.1 Test 1

Test 1 was conducted two days before the fatigue test began. The raw data are shown results for the north end, the south end, and the center.

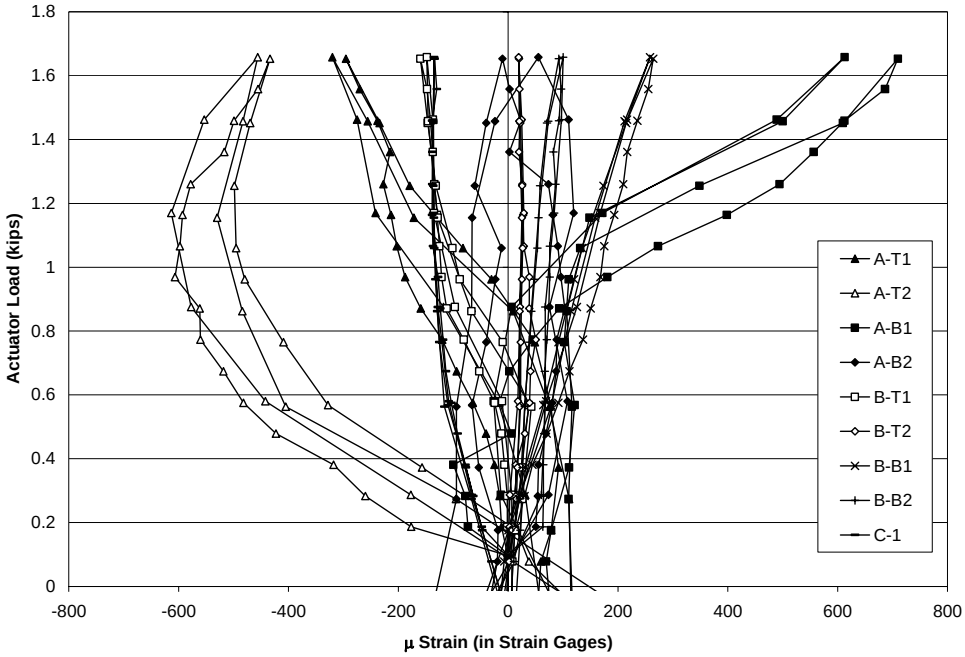

Figure B-1 Specimen 1 - Test 1- All strain data

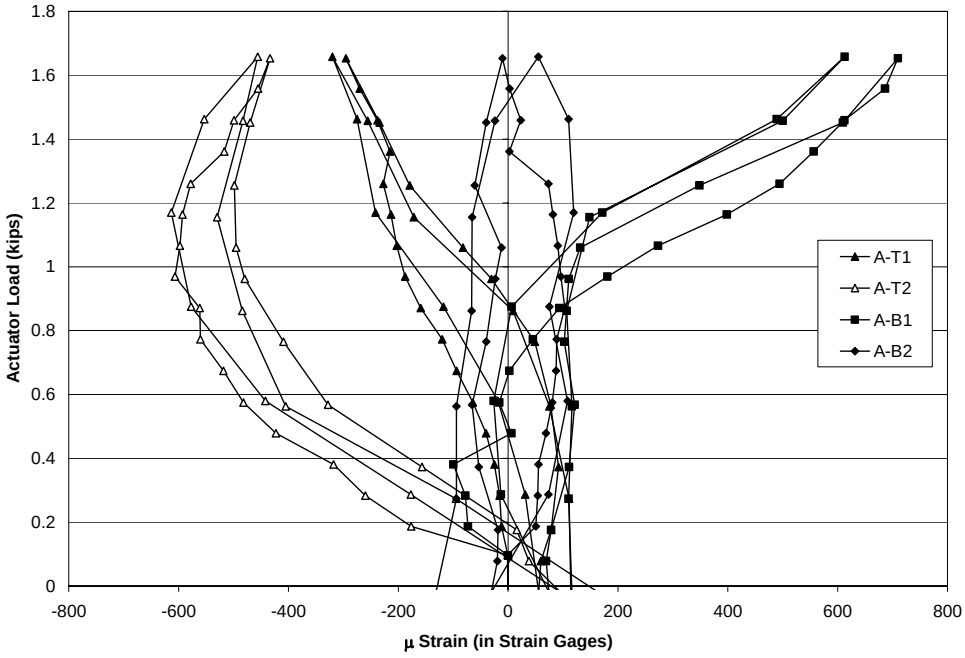

Figure B-2 Specimen 1 - Test 1- North end strain data

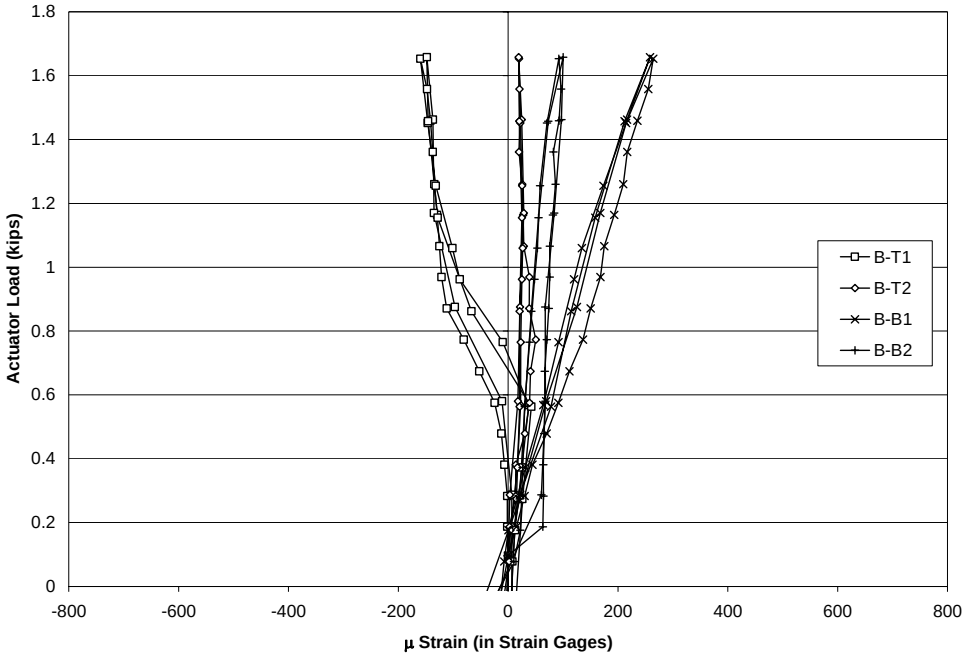

Figure B-3 Specimen 1 - Test 1- South end strain data

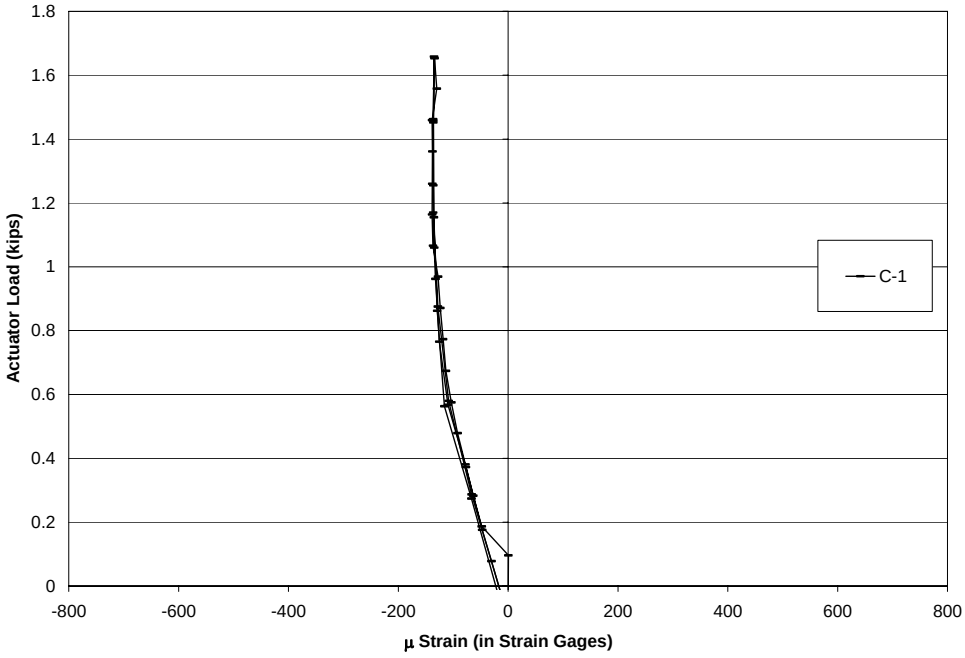

Figure B-4 Specimen 1 - Test 1- Center strain data

B.1.2 Test 2

Test 2 was conducted one day before the fatigue test began.

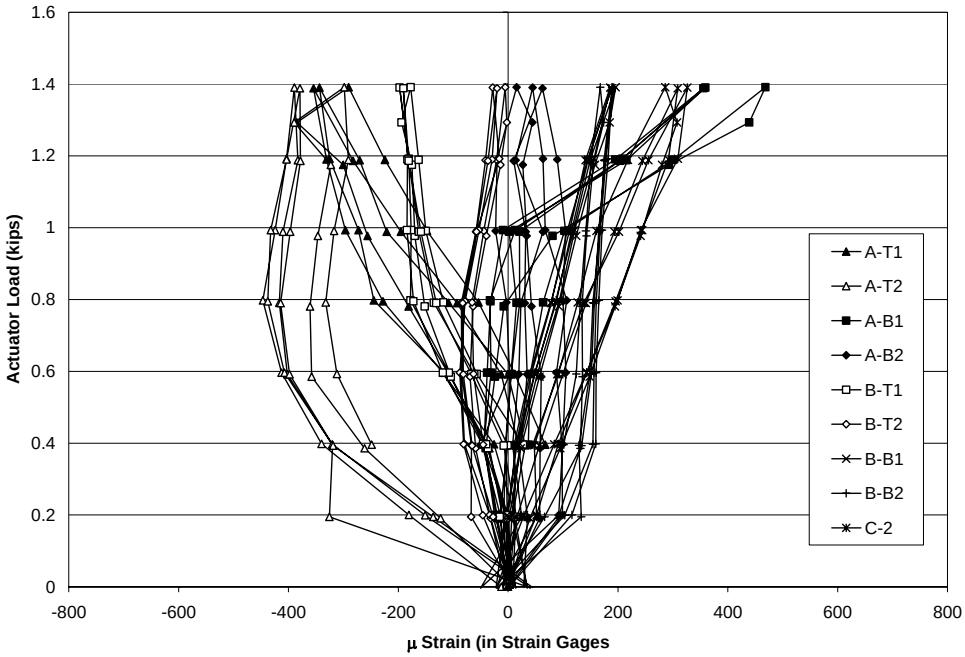

Figure B-5 Specimen 1 - Test 2- All strain data

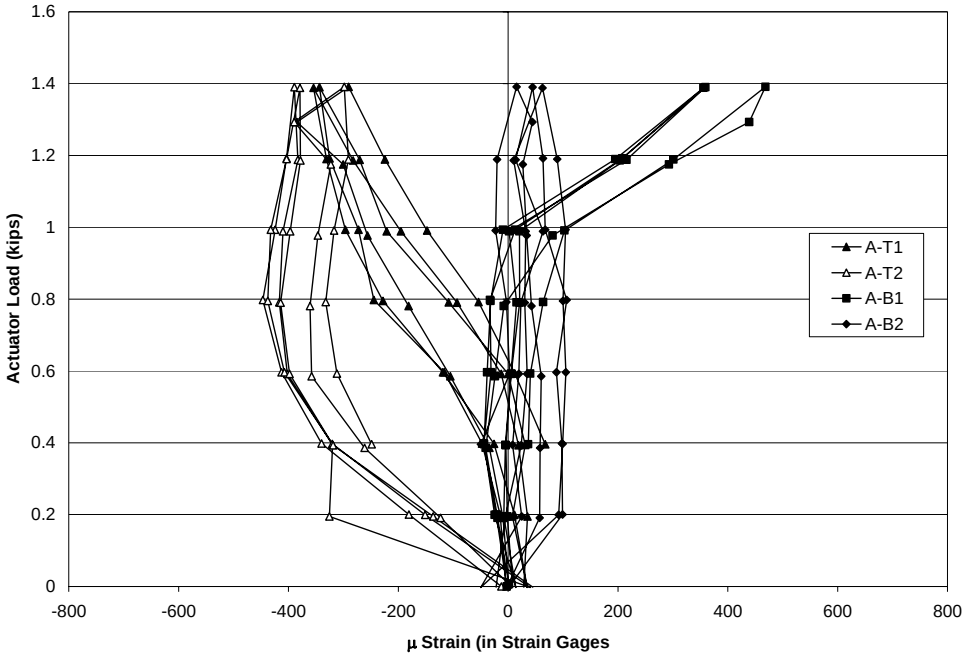

Figure B-6 Specimen 1 - Test 2- North end strain data

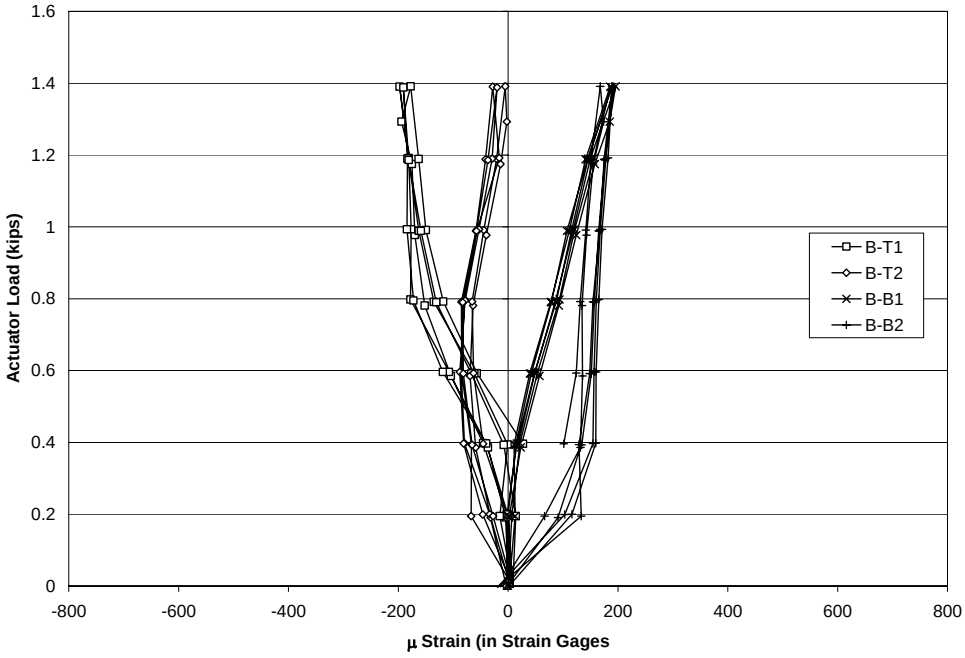

Figure B-7 Specimen 1 - Test 2- South end strain data

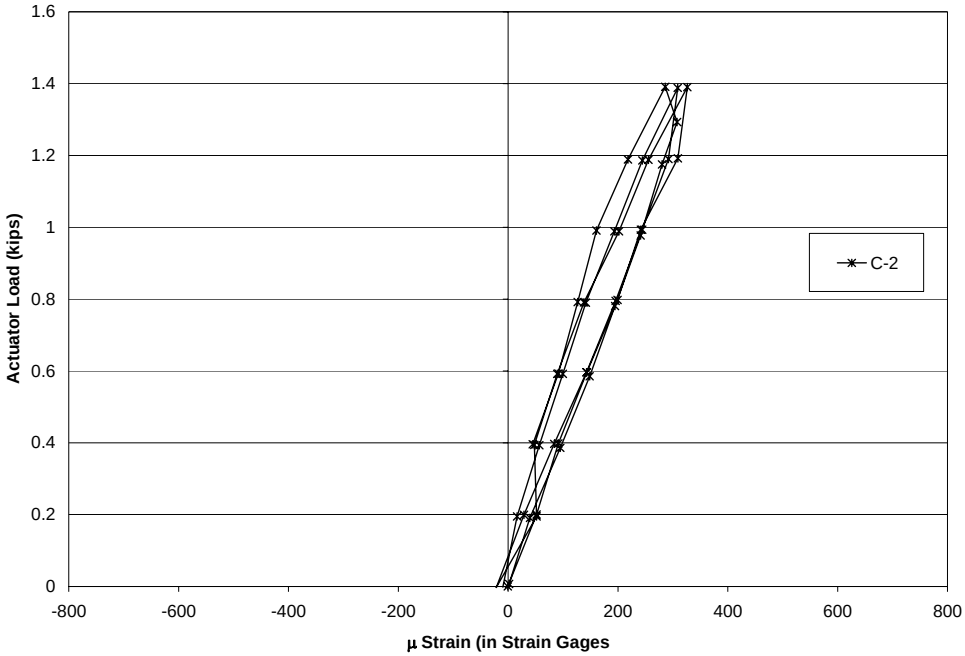

Figure B-8 Specimen 1 - Test 2- Center strain data

B.1.3 Test 3

Test 3 was conducted six day after the fatigue test began. The specimen had experienced 258,597 fatigue cycles at the time of the test.

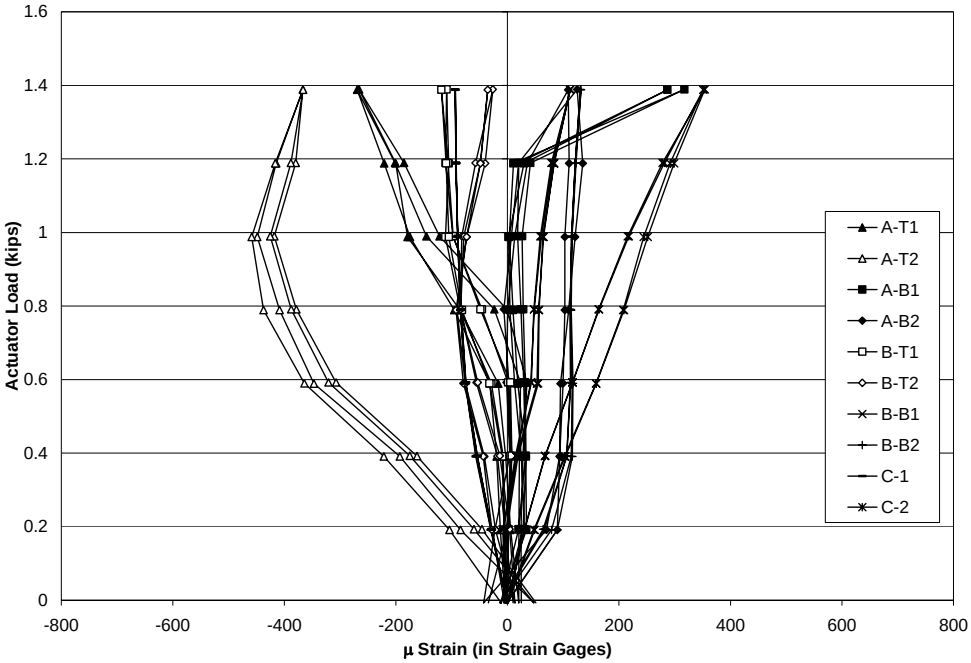

Figure B-9 Specimen 1 - Test 3- All strain data

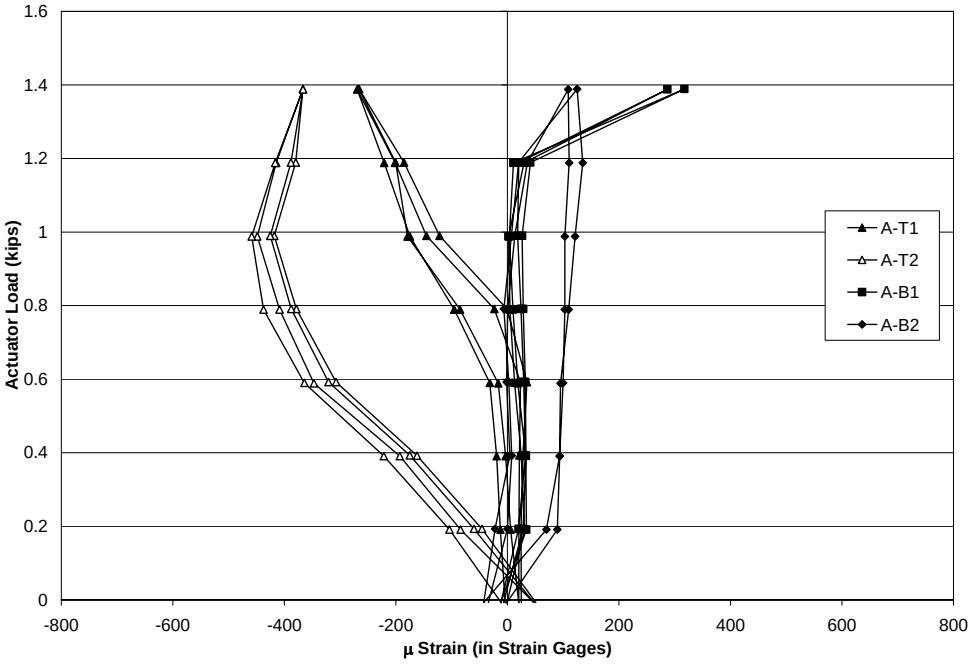

Figure B-10 Specimen 1 - Test 3- North end strain data

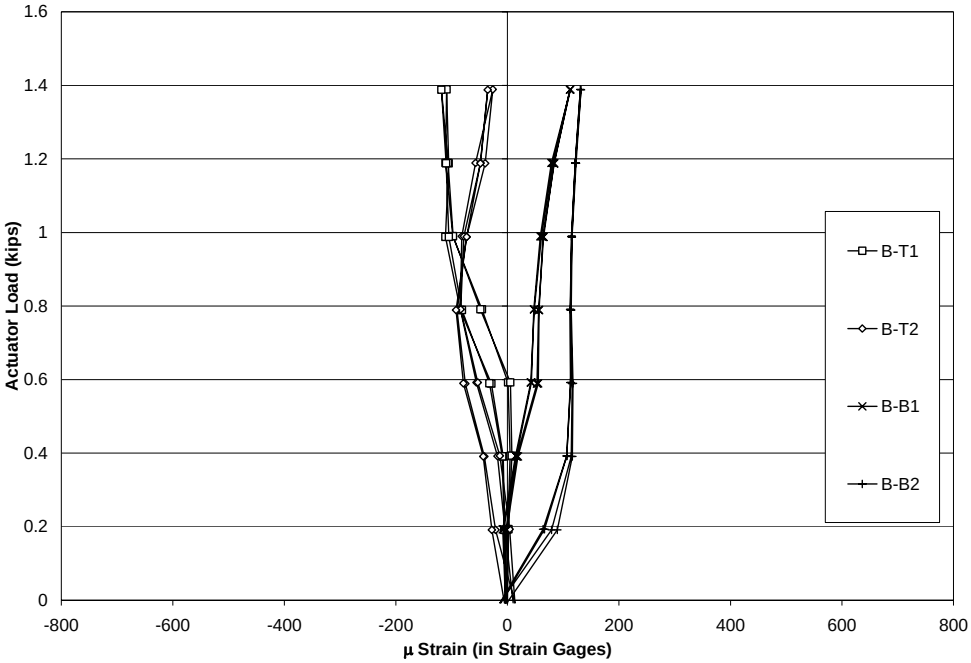

Figure B-11 Specimen 1 - Test 3- South end strain data

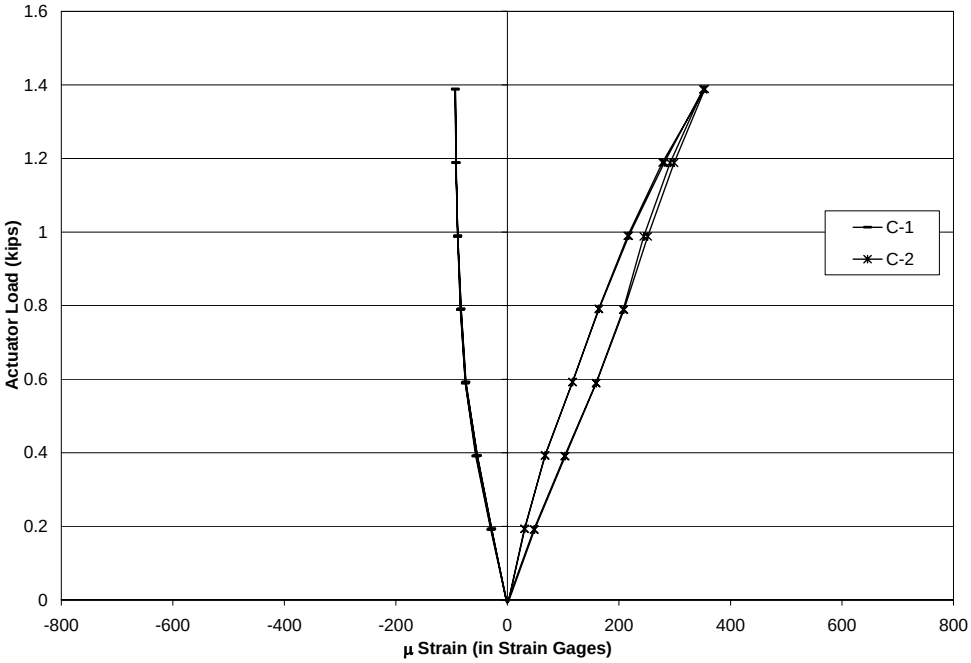

Figure B-12 Specimen 1 - Test 3- Center strain data

B.2 SPECIMEN 2

Strains were measured during all eight static tests for Specimen 2. Gage locations are shown in Figure 3-15. For each test, all data are shown in a single plot. The data recorded are grouped by location: north end (locations A, B, and C), south end (locations D and E), and near the point of load application (locations F and G).

B.2.1 Test 1

Test 1 was conducted immediately before the fatigue tests started.

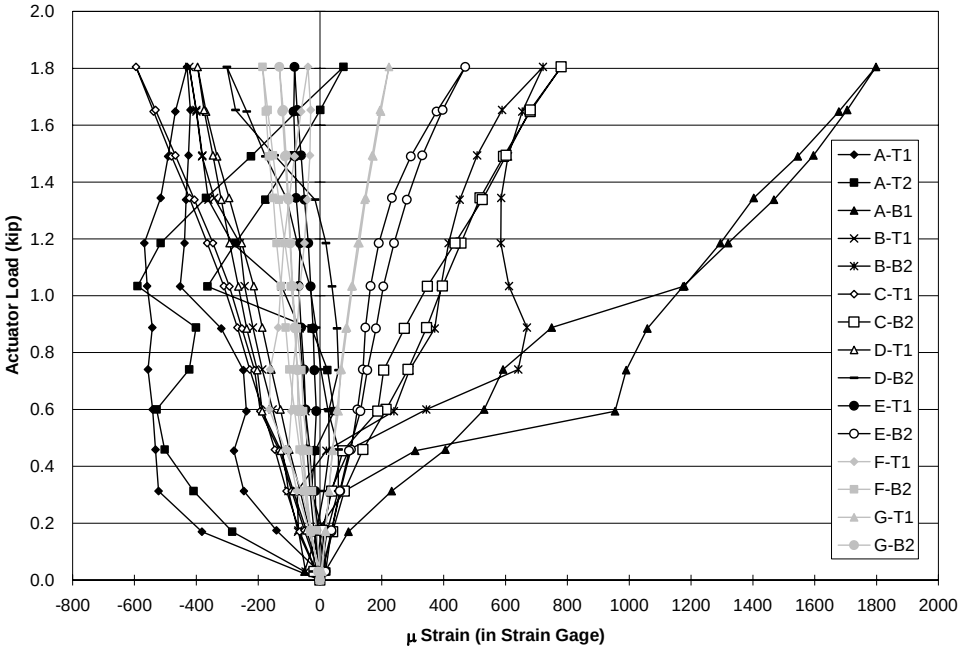

Figure B-13 Specimen 2 - Test 1- All strain data

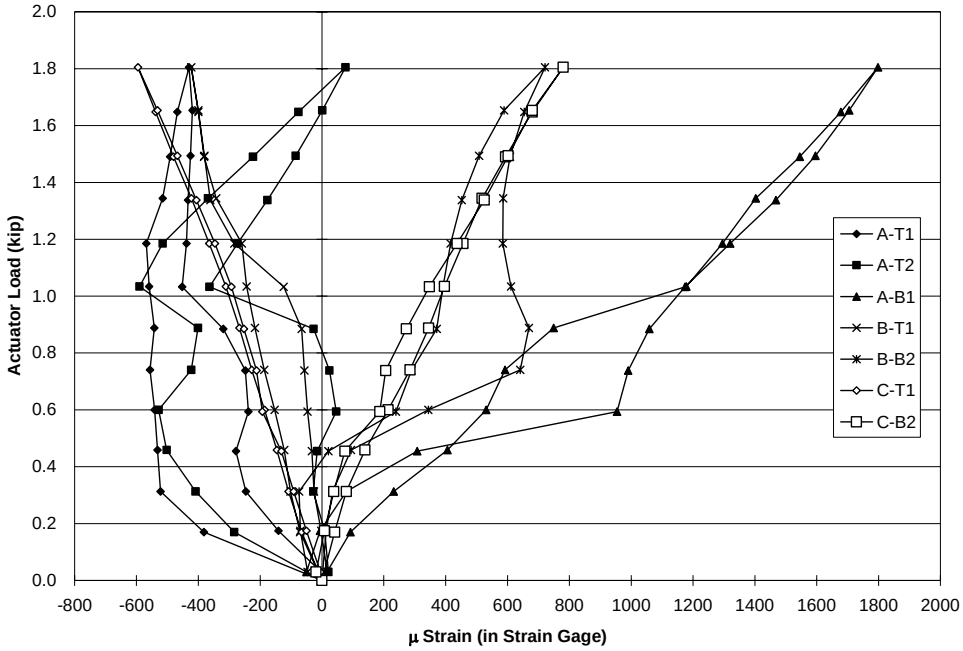

Figure B-14 Specimen 2 - Test 1- North end strain data

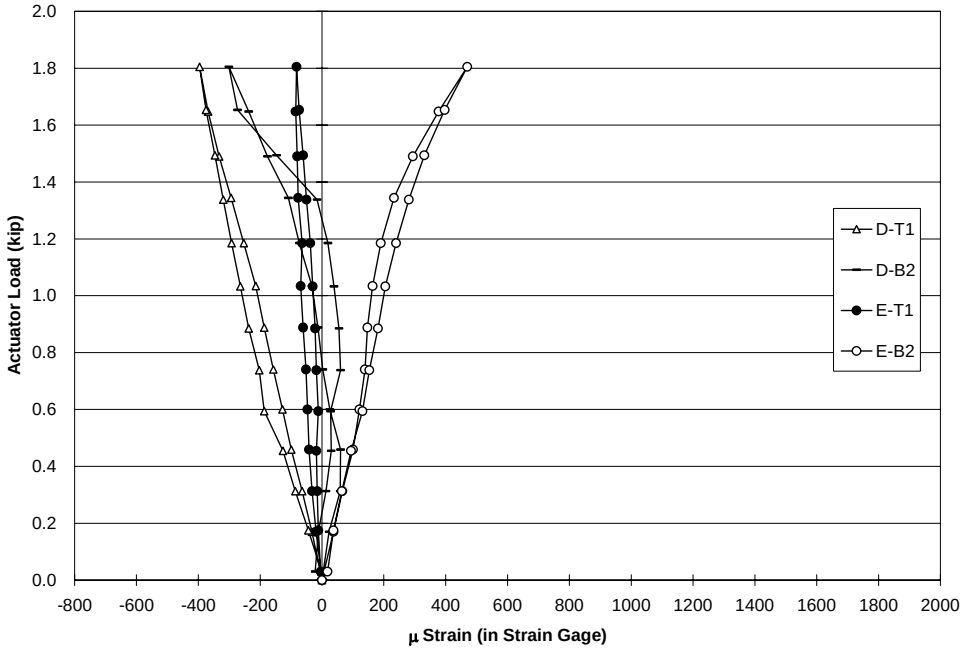

Figure B-15 Specimen 2 - Test 1- South end strain data

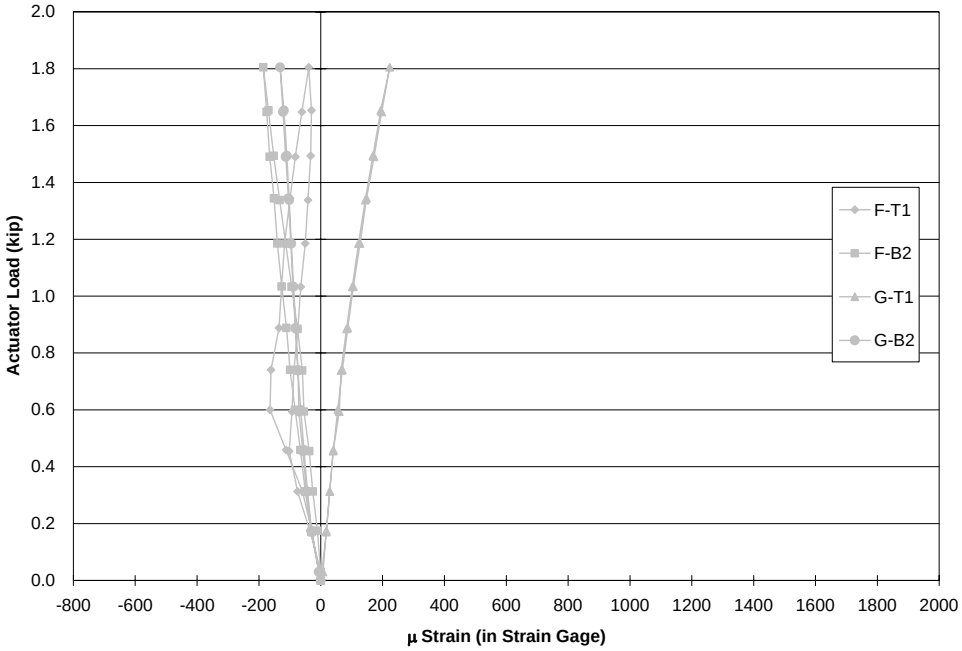

Figure B-16 Specimen 2 - Test 1- Center strain data

B.2.2 Test 2

Test 2 was conducted 7 days after the fatigue test started. The specimen had experienced 857,200 cycles at the time of the test.

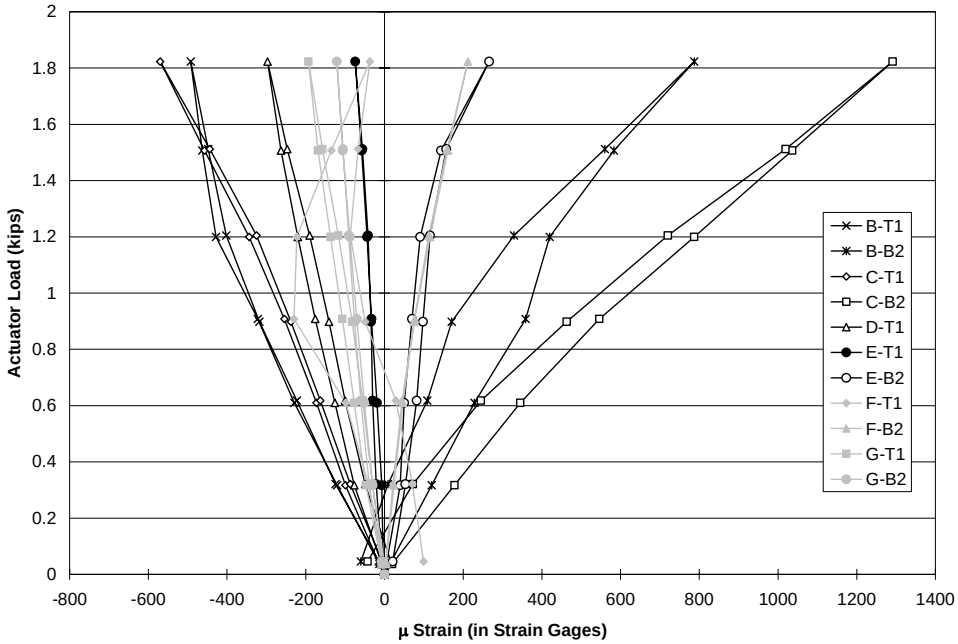

Figure B-17 Specimen 2 - Test 2- All strain data

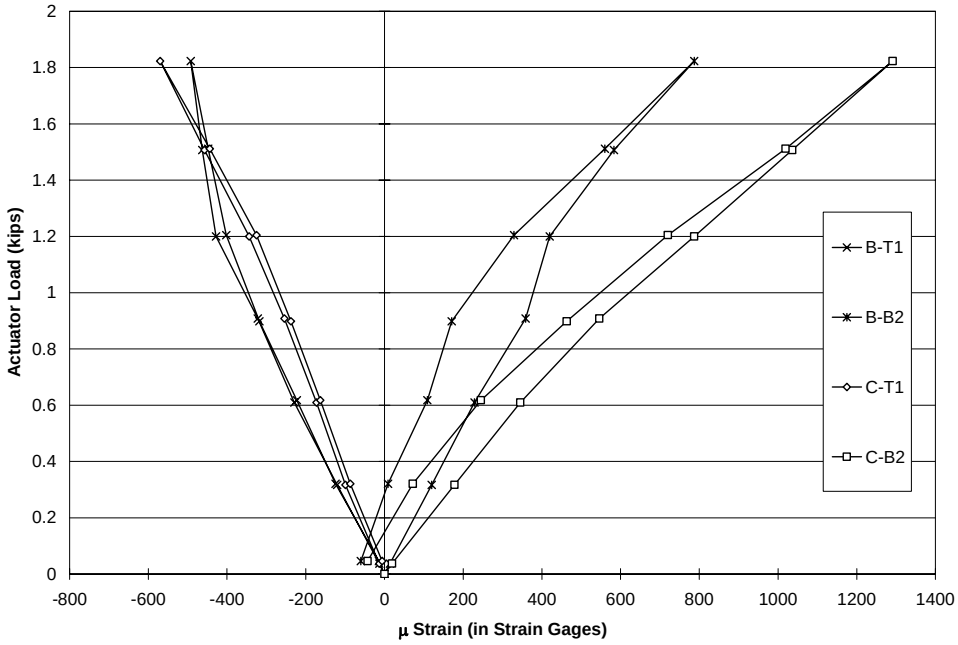

Figure B-18 Specimen 2 - Test 2- North end strain data.

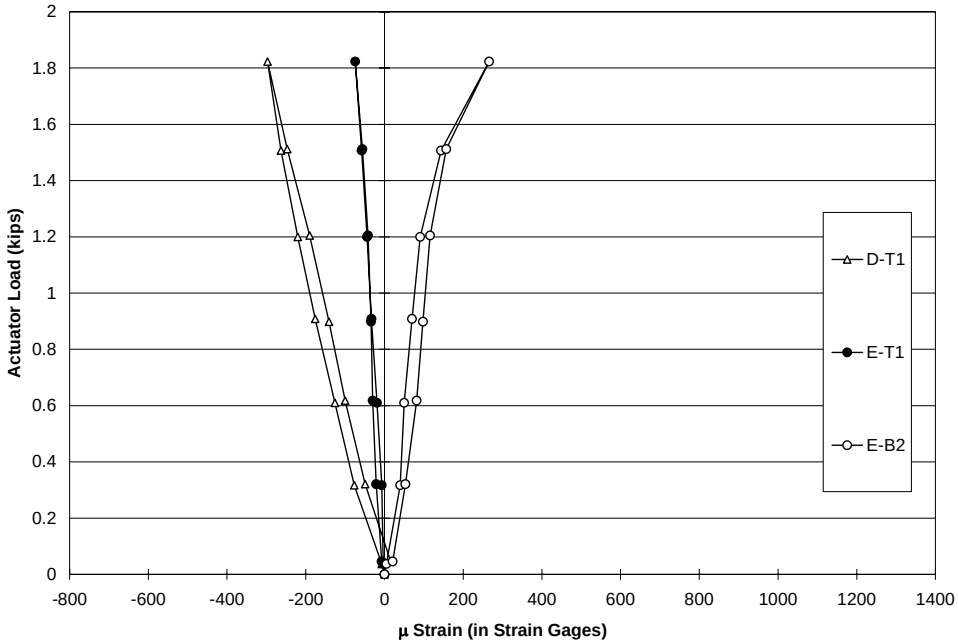

Figure B-19 Specimen 2 - Test 2- South end strain data

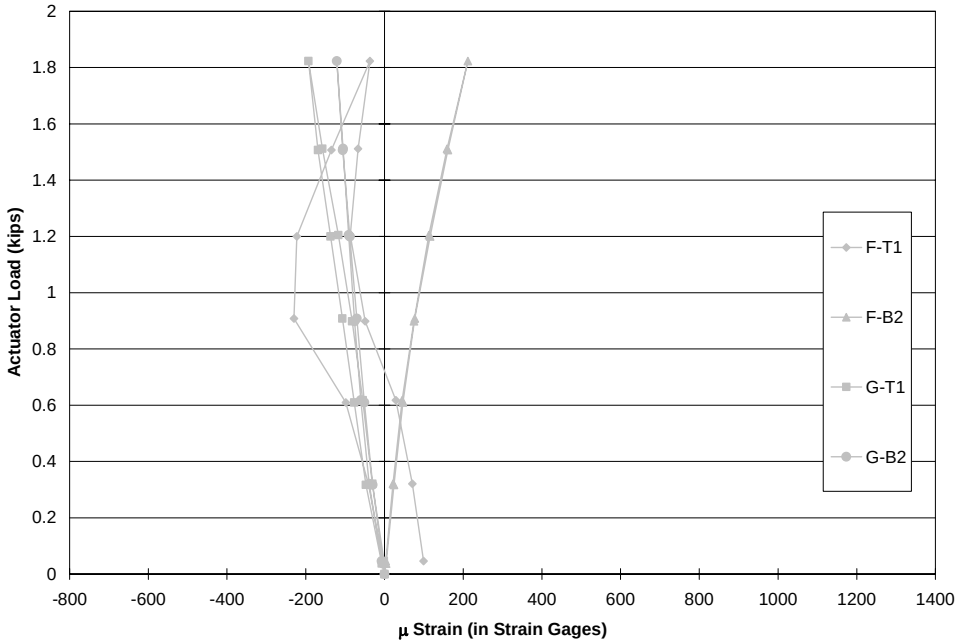

Figure B-20 Specimen 2 - Test 2- Center strain data

B.2.3 Test 3

Test 3 was conducted 15 days after the fatigue test started. The specimen had experienced 1,871,180 cycles at the time of the test.

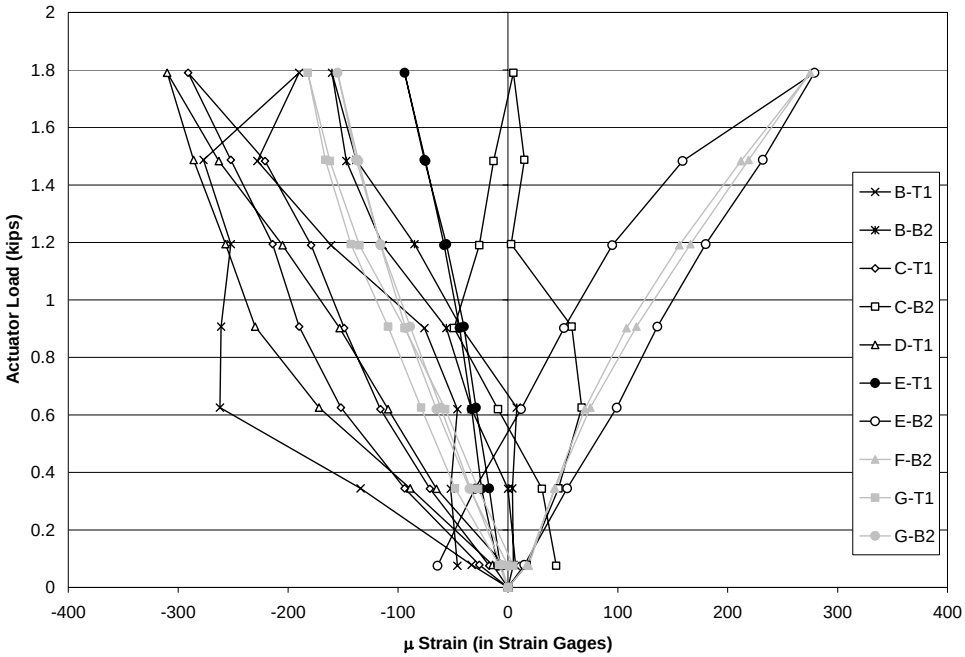

Figure B-21 Specimen 2 - Test 3- All strain data

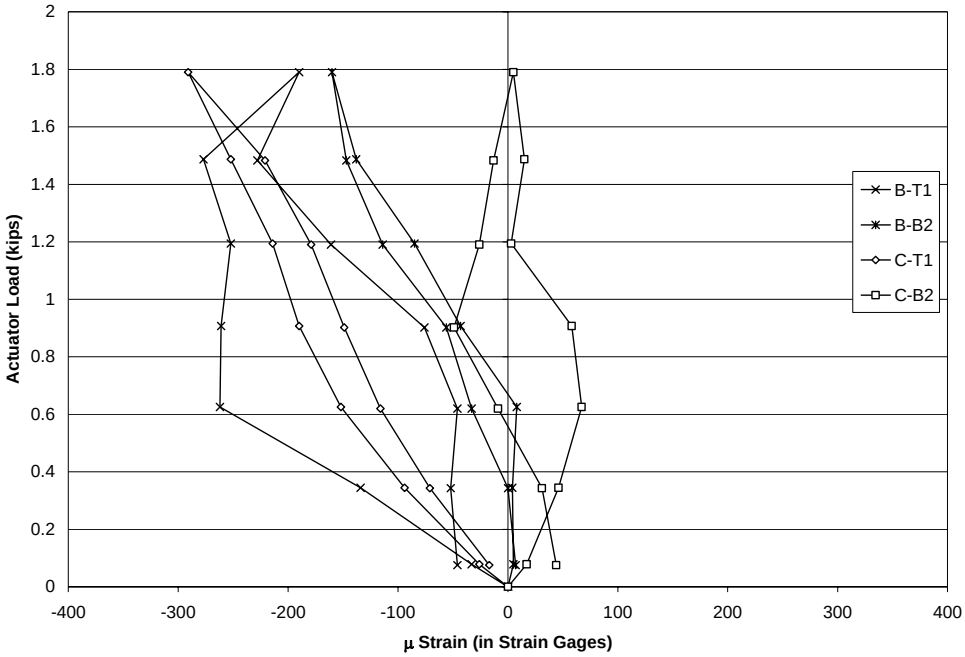

Figure B-22 Specimen 2 - Test 3- North end strain data

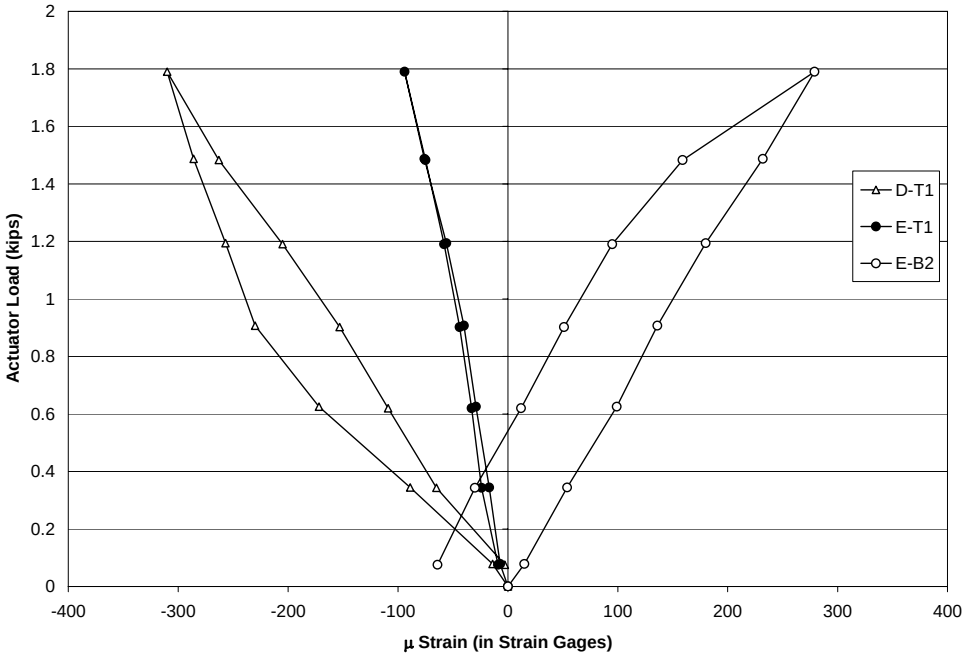

Figure B-23 Specimen 2 - Test 3- South end strain data

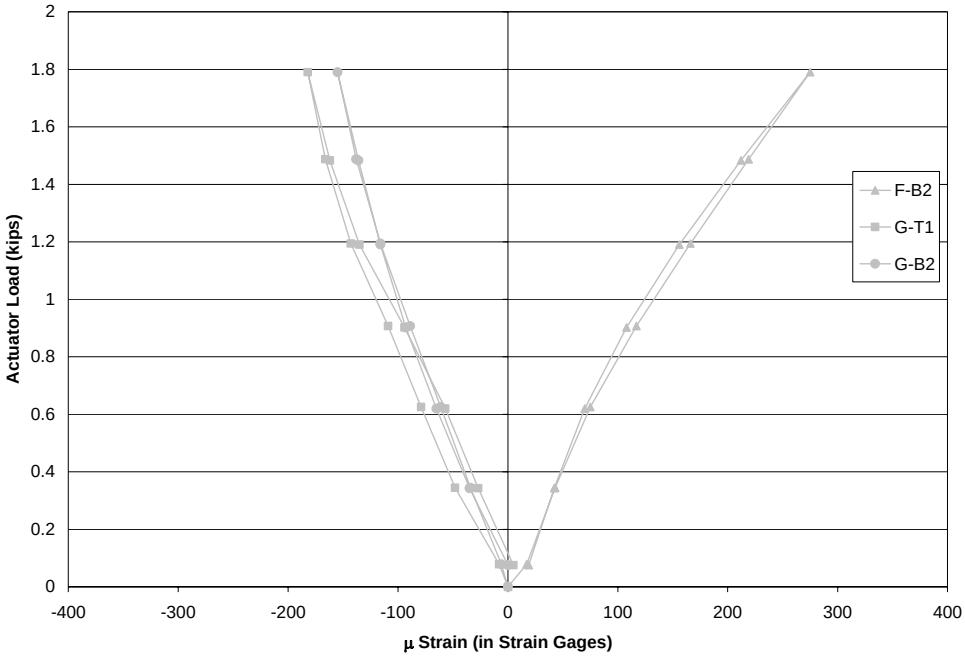

Figure B-24 Specimen 2 - Test 3- Center strain data

B.2.4 Test 4

Test 4 was conducted 22 days after the fatigue test started. The specimen had experienced 2,780,862 cycles at the time of the test.

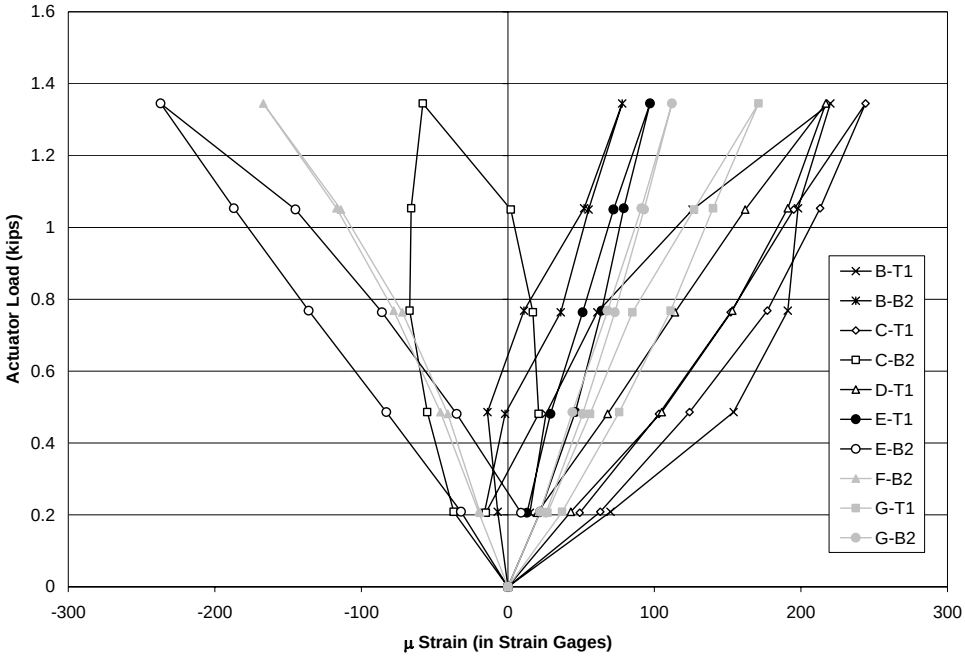

Figure B-25 Specimen 2 - Test 4- All strain data

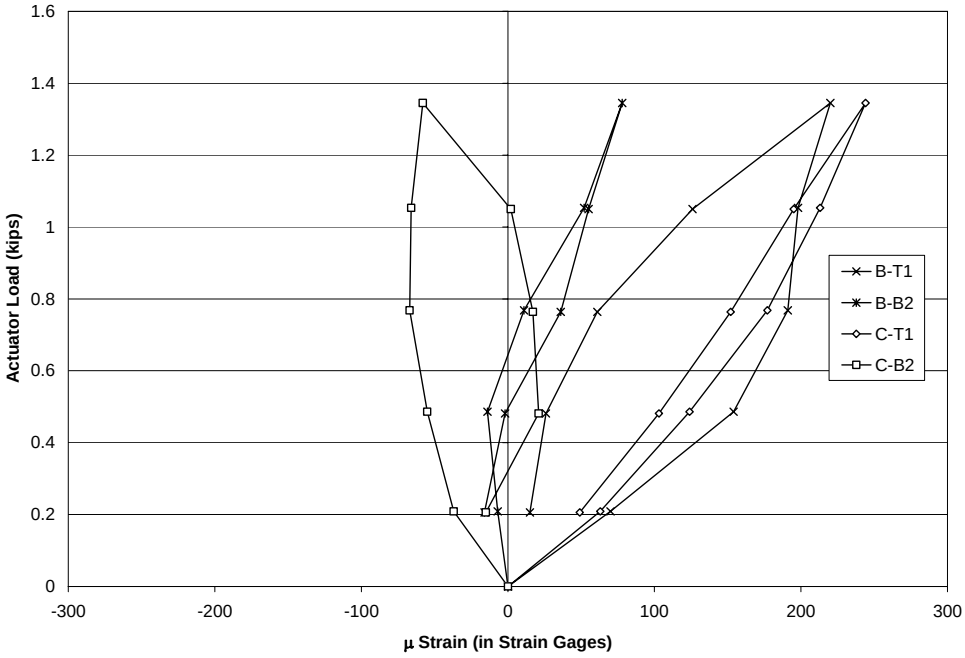

Figure B-26 Specimen 2 - Test 4- North end strain data

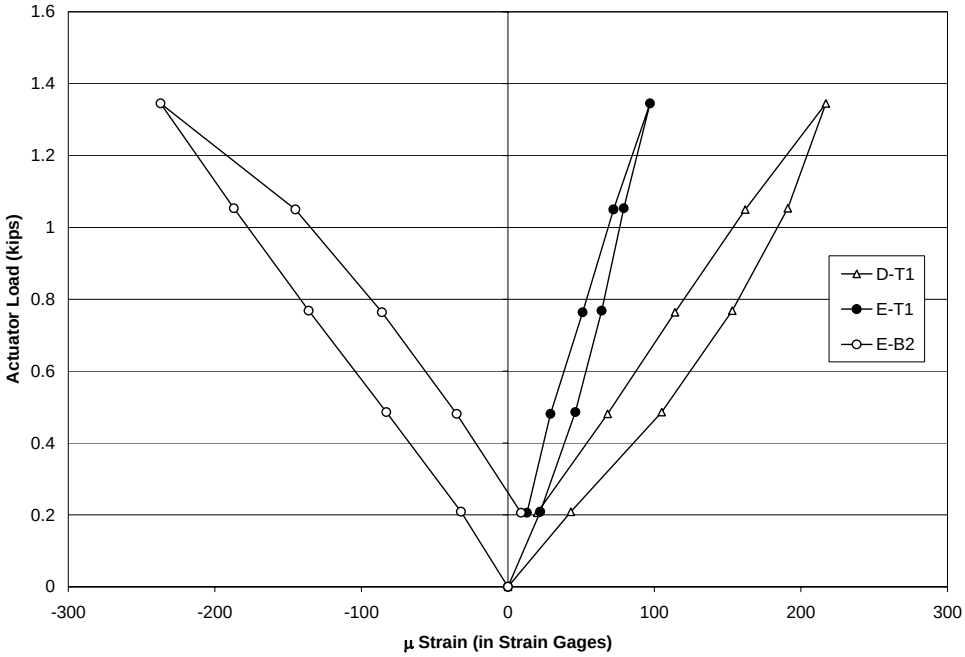

Figure B-27 Specimen 2 - Test 4- South end strain data

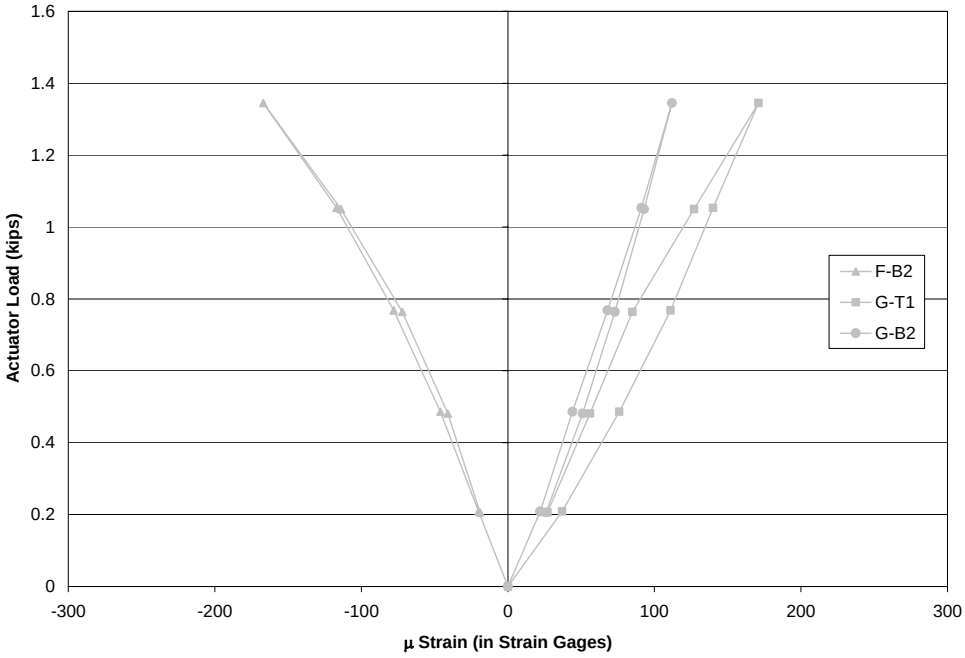

Figure B-28 Specimen 2 - Test 4- Center strain data

B.2.5 Test 5

Test 5 was conducted 28 days after the fatigue test started. The specimen had experienced 3,568,128 cycles at the time of the test.

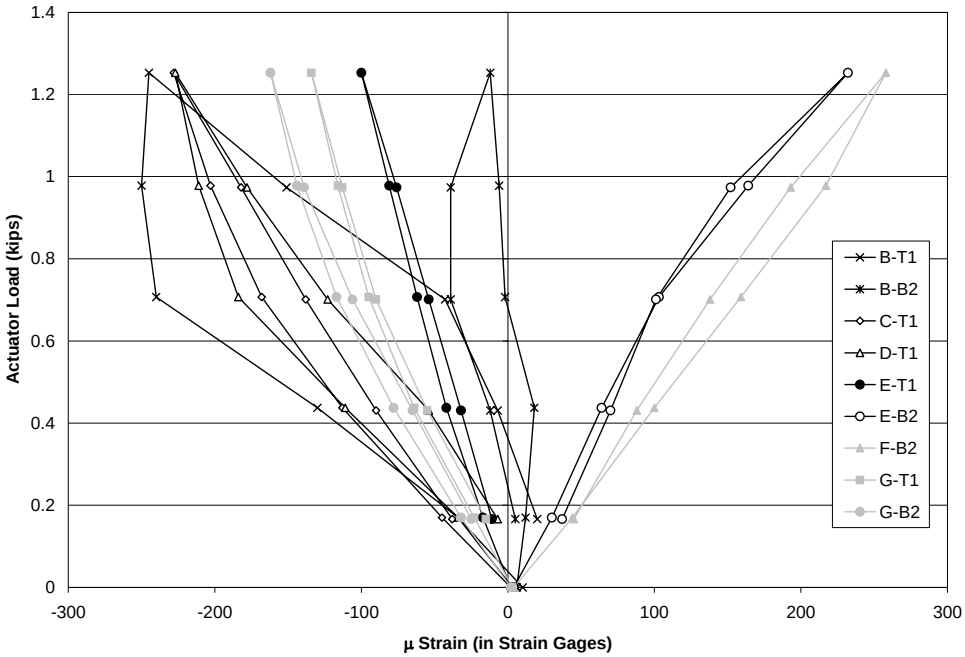

Figure B-29 Specimen 2 - Test 5- All strain data

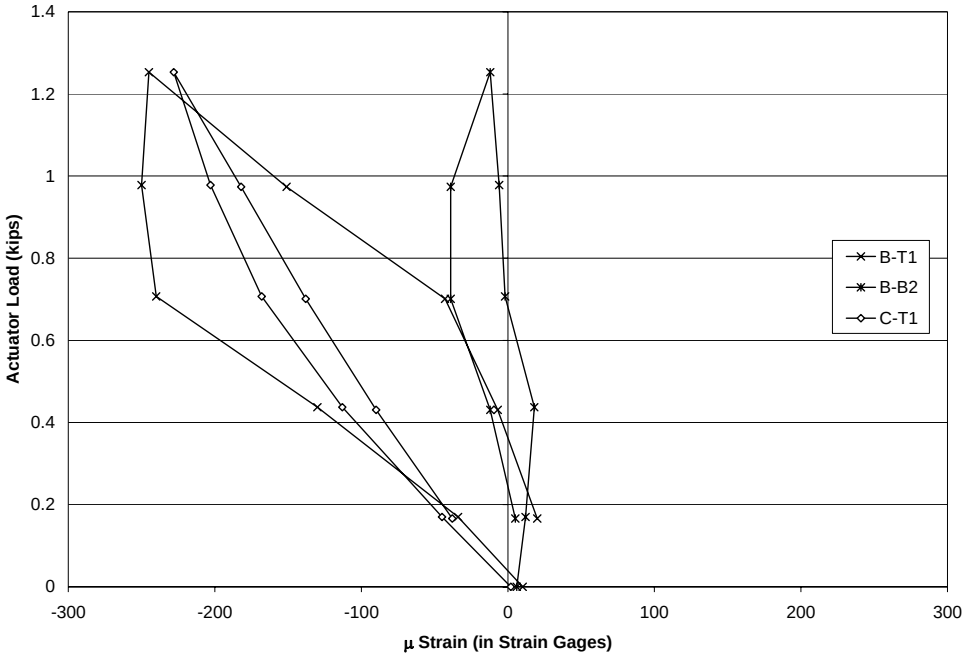

Figure B-30 Specimen 2 - Test 5- North end strain data

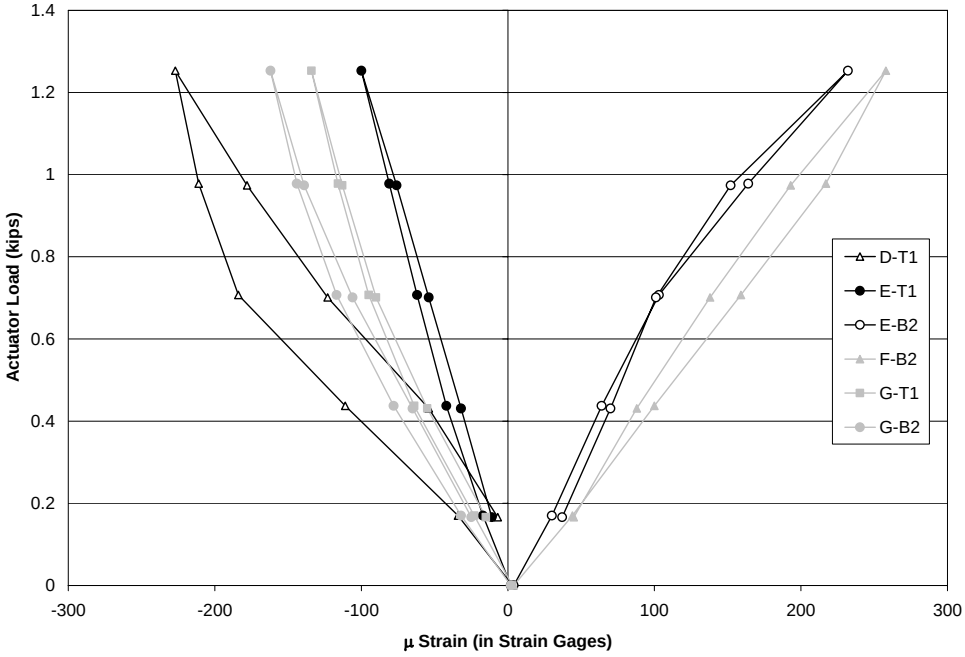

Figure B-31 Specimen 2 - Test 5- South end and Center strain data

B.2.6 Test 6

Test 6 was conducted 31 days after the fatigue test started. The specimen had experienced 3,924,975 cycles at the time of the test.

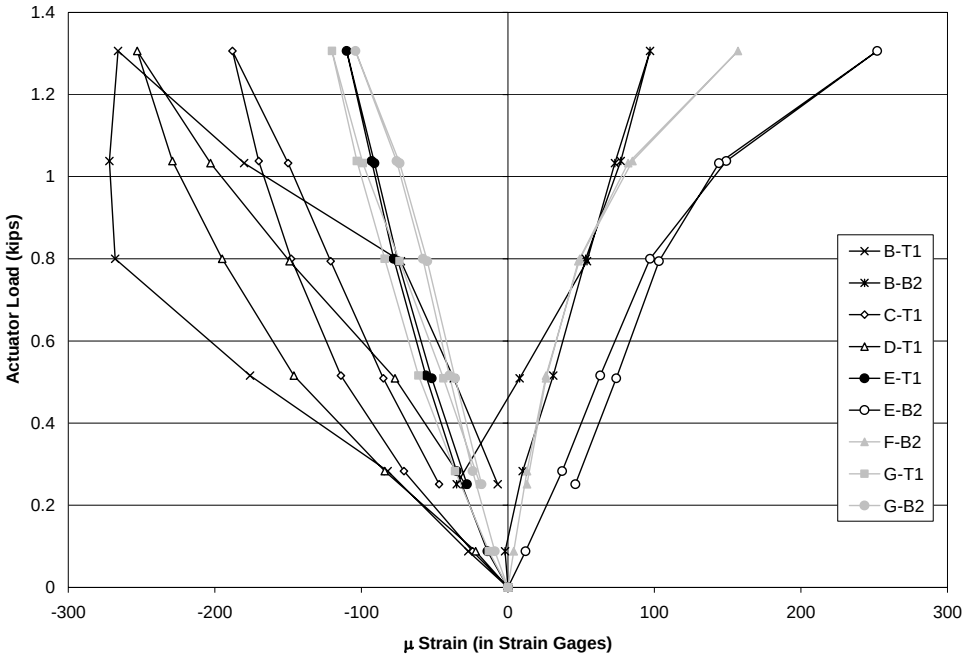

Figure B-32 Specimen 2 - Test 6- All strain data

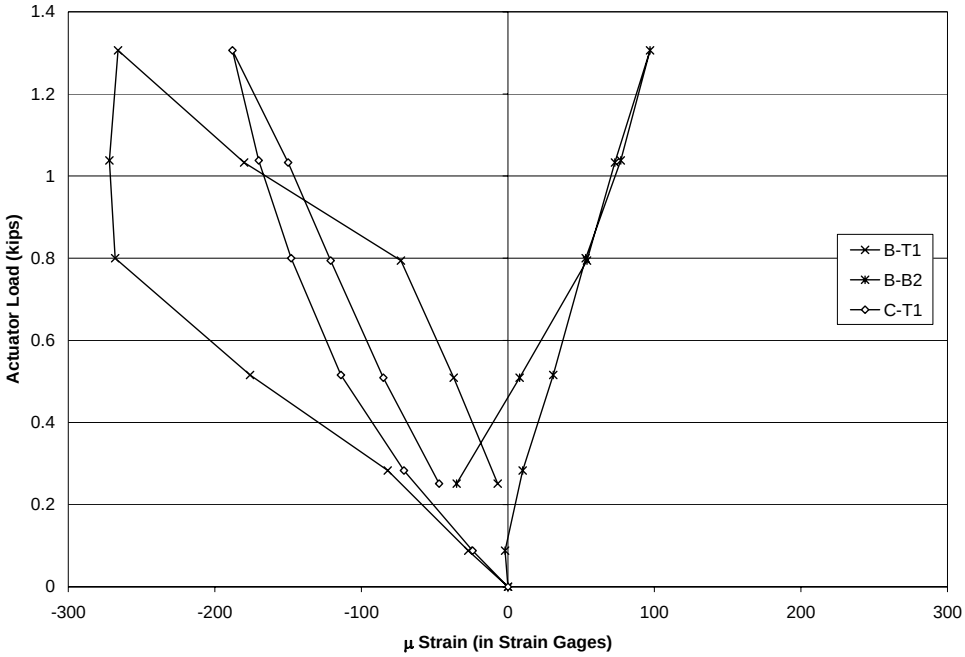

Figure B-33 Specimen 2 - Test 6- North end strain data

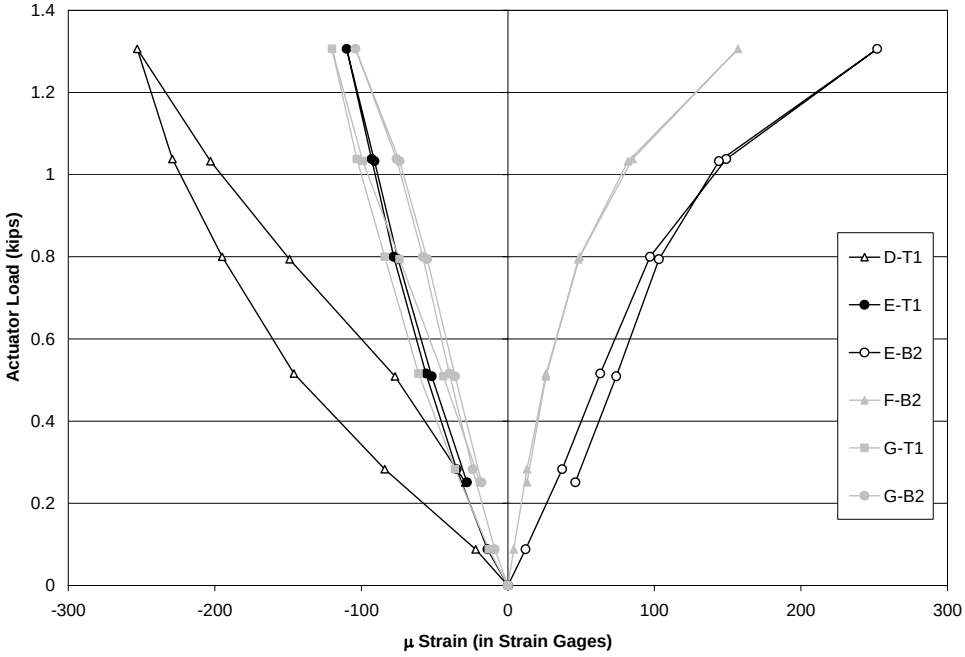

Figure B-34 Specimen 2 - Test 6- South end and Center strain data

B.2.7 Test 7

Test 7 was conducted 34 days after the fatigue test started. The specimen had experienced 4,323,526 cycles at the time of the test.

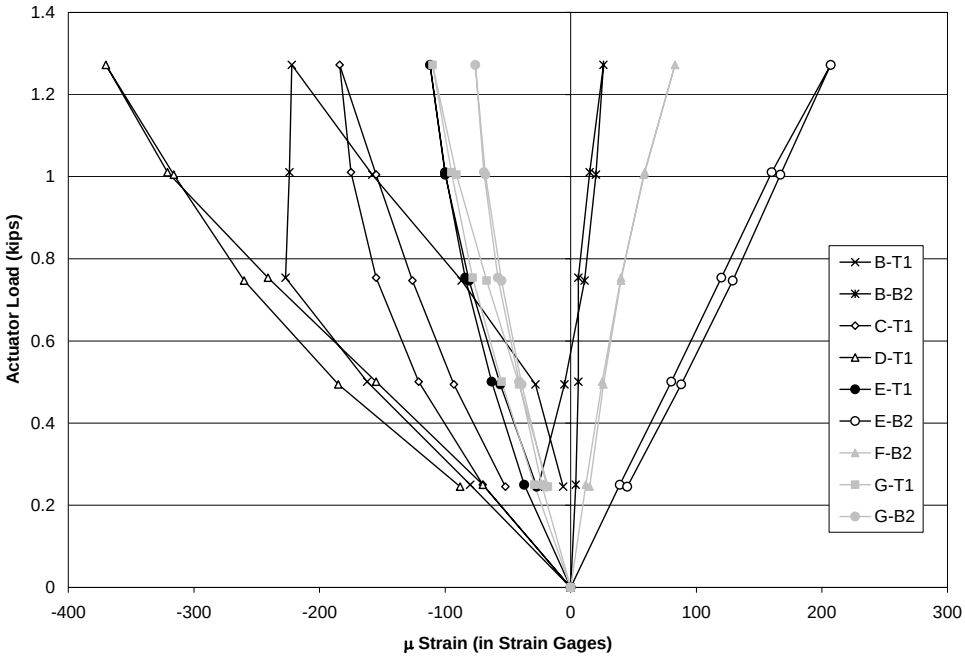

Figure B-35 Specimen 2 - Test 7- All strain data

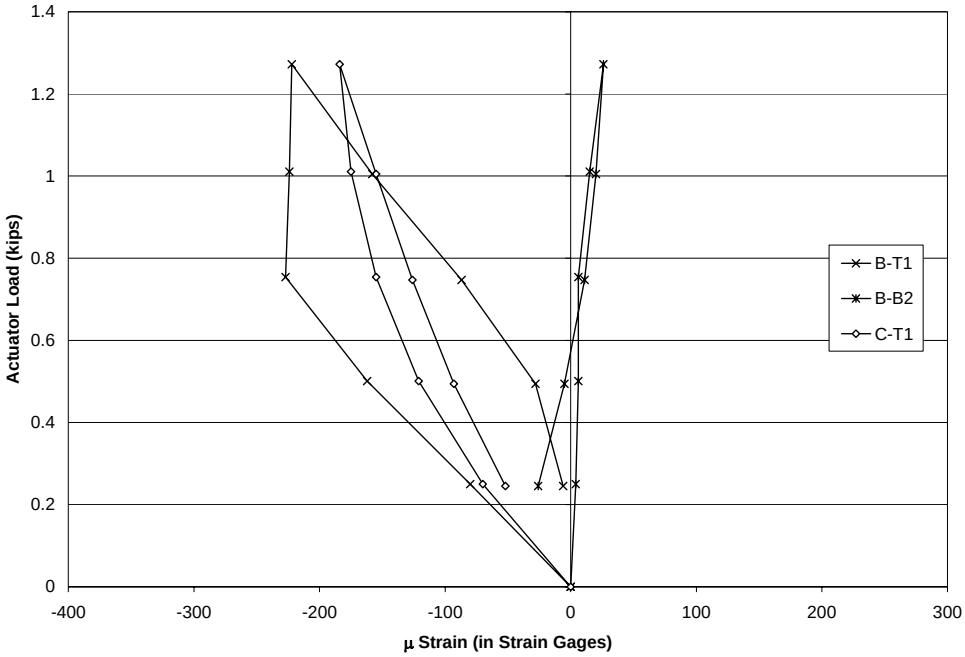

Figure B-36 Specimen 2 - Test 7- North end strain data

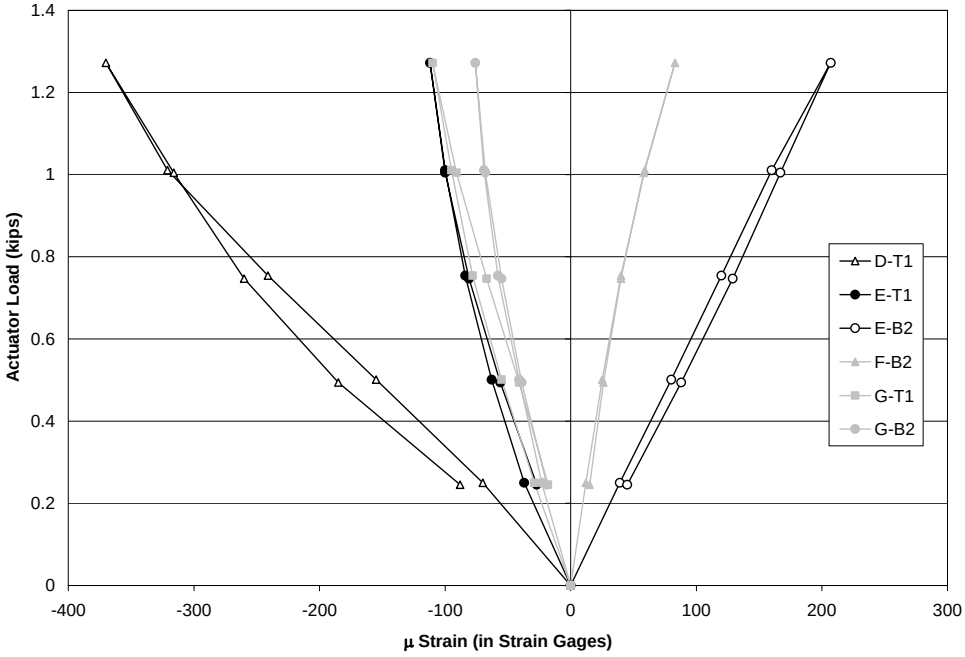

Figure B-37 Specimen 2 - Test 7- South end and Center strain data

B.2.8 Test 8

Test 8 was conducted 37 days after the fatigue test started. The specimen had experienced 4,603,980 cycles at the time of the test.

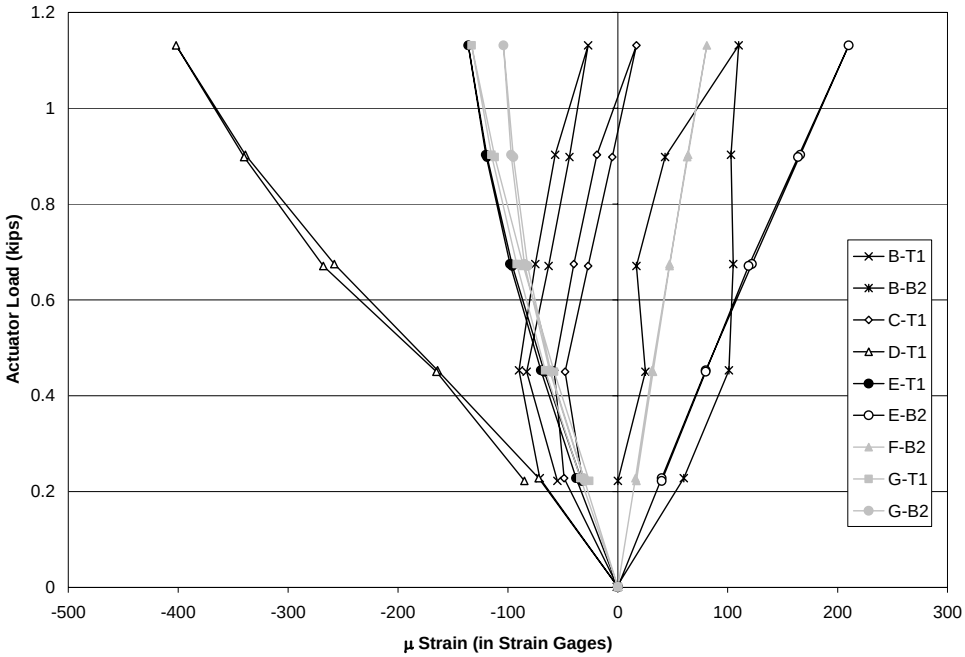

Figure B-38 Specimen 2 - Test 8- All strain data

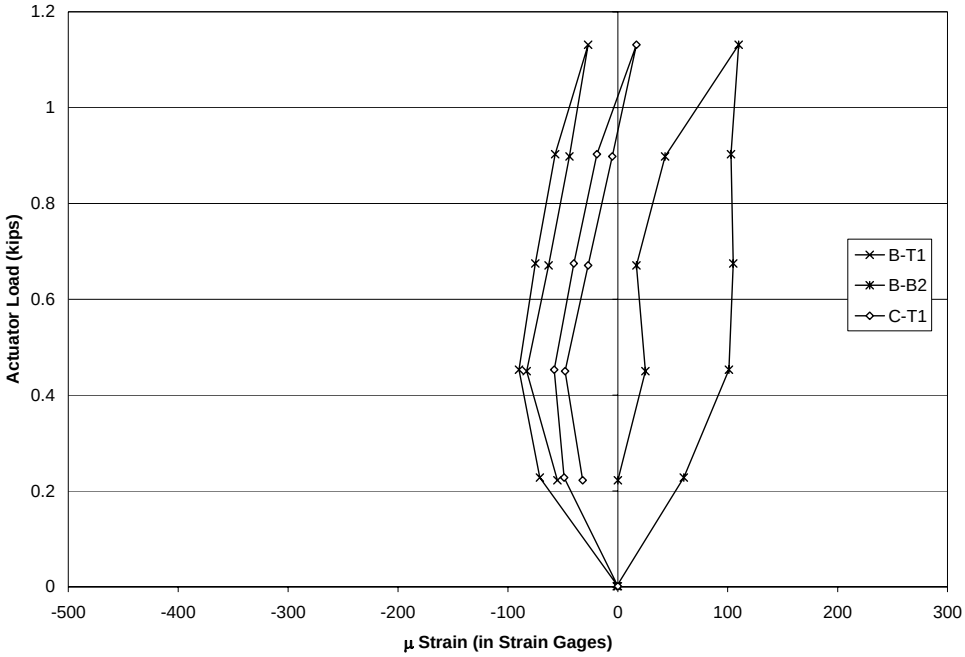

Figure B-39 Specimen 2 - Test 8- North end strain data

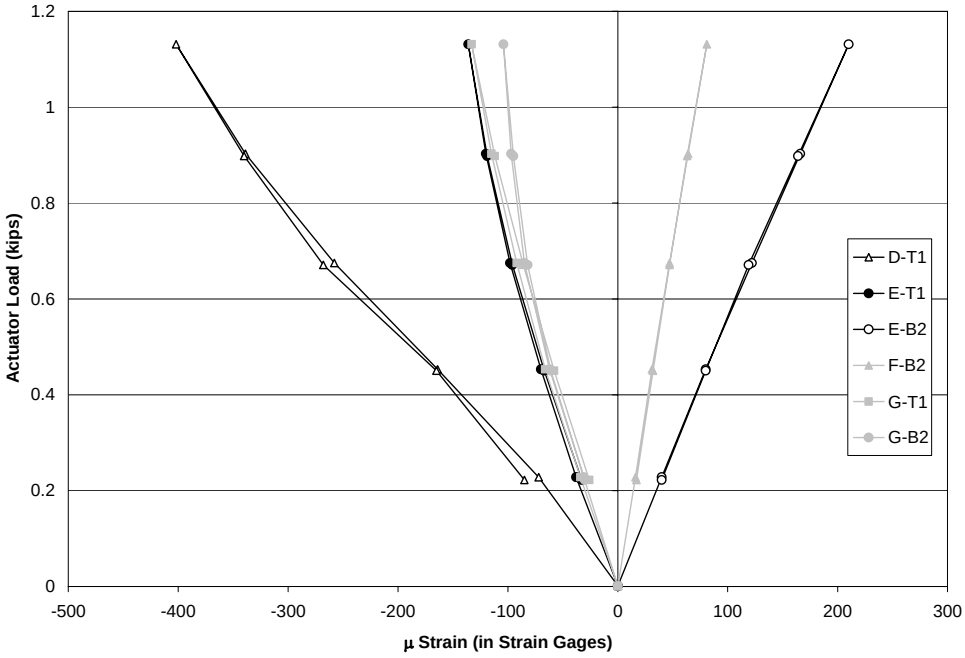

Figure B-40 Specimen 2 - Test 8- South end and Center strain data

B.3 SPECIMEN 3

The results shown here are from tests performed on specimen 3. See figure 3-16 for gage locations. For each test, all data are shown in a single plot. The data recorded are grouped by location: north end (locations A and B), north end (locations C and D), along the length of the specimen (locations E, F and G) and the south end (locations H and I).

Only one test was recorded for specimen 3. It was taken the same day as the beginning of the fatigue test.

B.3.1 Test 1

Test 1 was conducted immediately before the fatigue tests started.

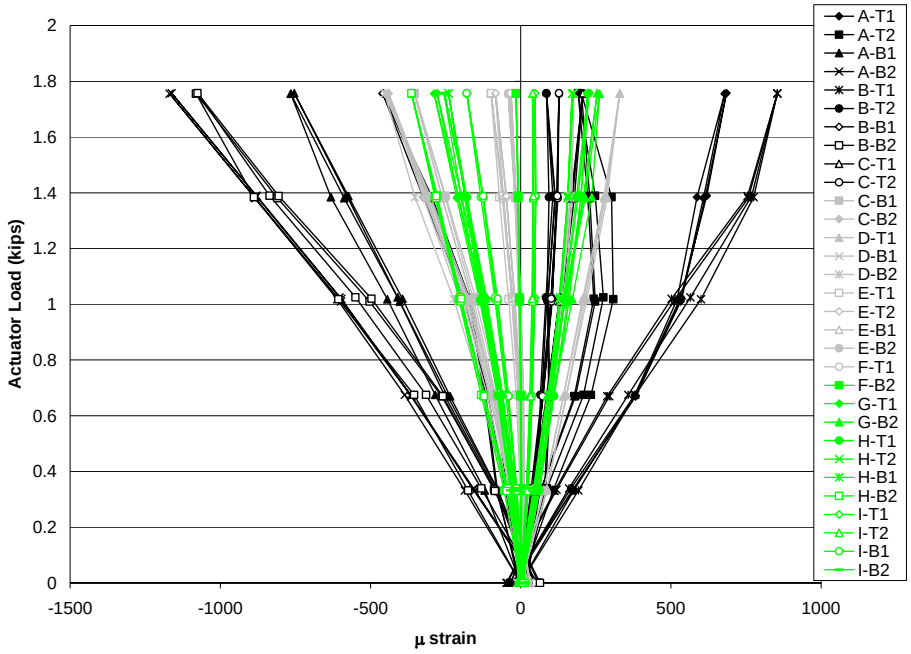

Figure B-41 Specimen 3- All strain data

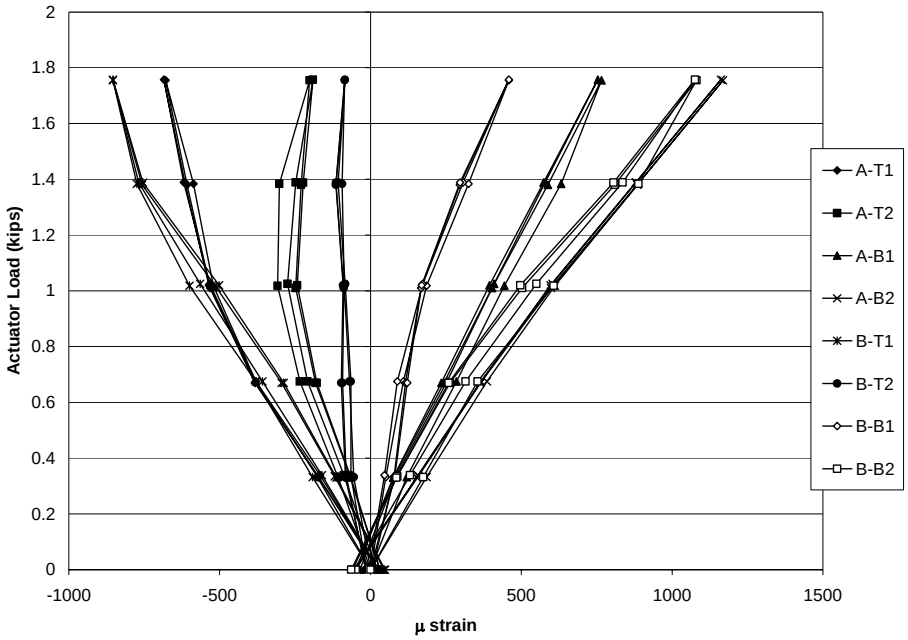

Figure B-42 Specimen 3- North end strain data at 2 in and 6 in

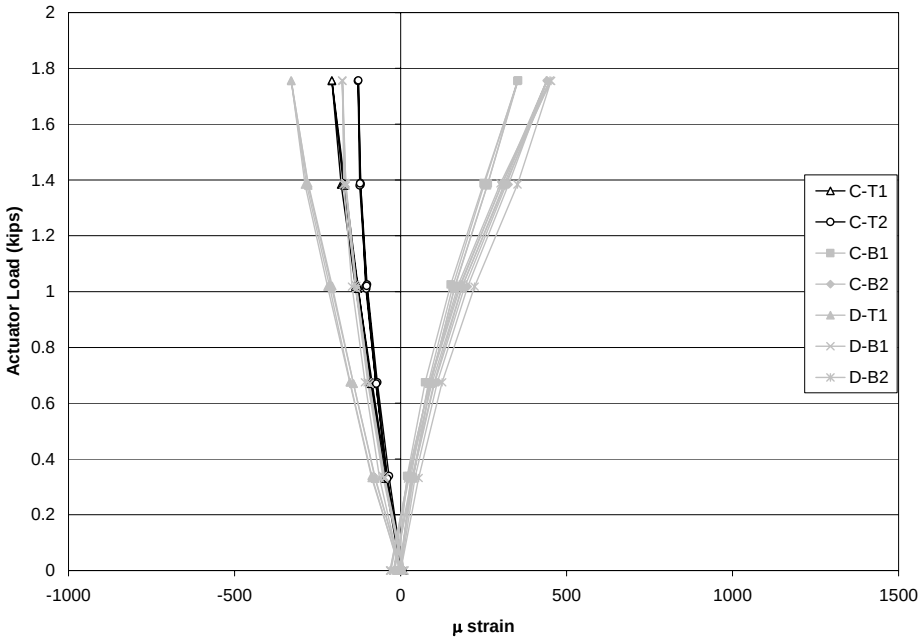

Figure B-43 Specimen 3- North end strain data at 12 in and 18 in

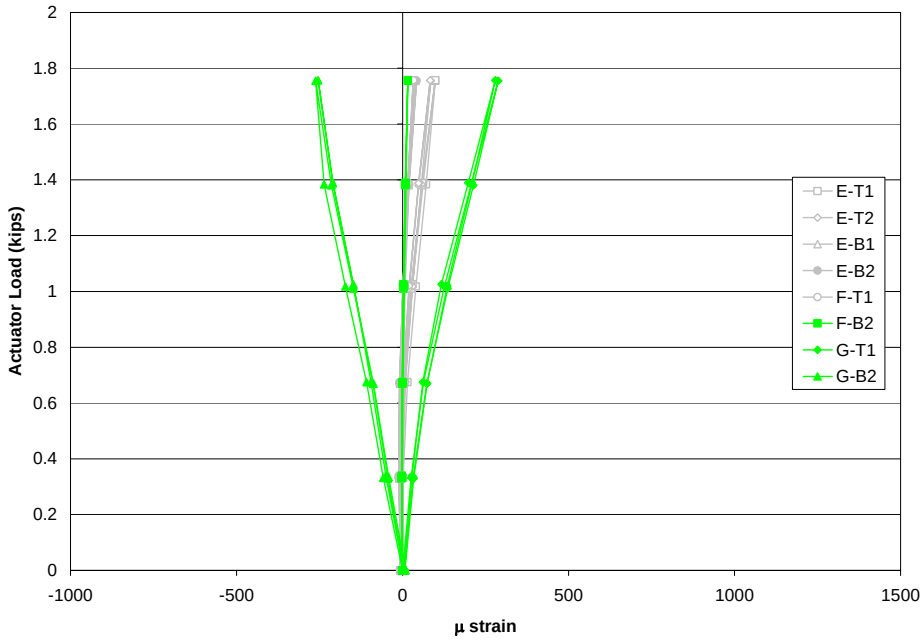

Figure B-44 Specimen 3- Center strain data

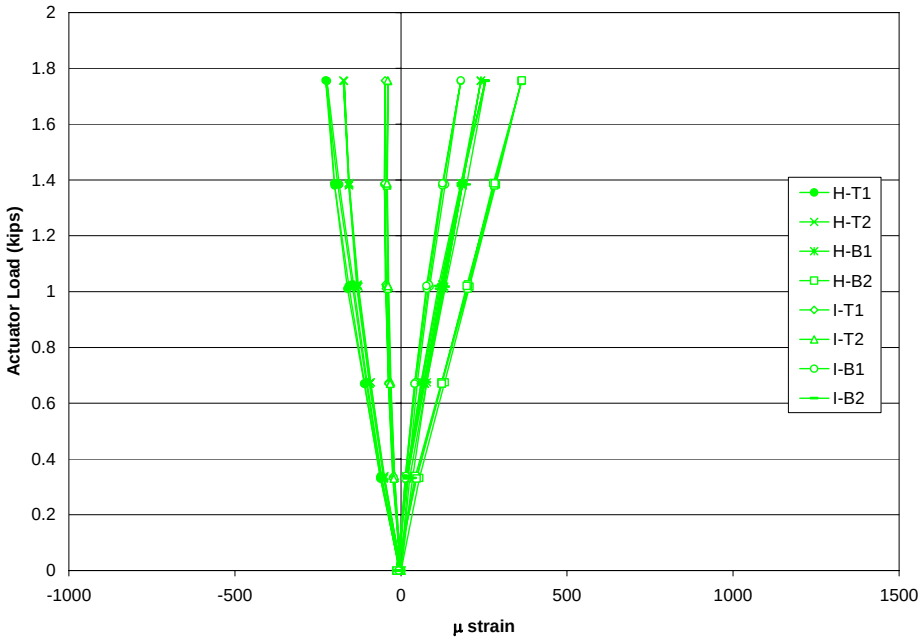

Figure B-45 Specimen 3- South end strain data

References

Dowd, Joseph A. (2001), "Response of Stay Cables to High-Amplitude Vibration", M.S. Thesis, Department of Civil Engineering, the University of Texas at Austin.

Eggers, John C. (2003), "Cable Stay Analysis for the Fred Hartman Bridge", M.S. Thesis, Department of Civil Engineering, the University of Texas at Austin.

"Fred Hartman, former BU journalist instructor." The Associated Press, July 28, 1991.

General Technologies, Inc., (2006). website: http://www.gti-usa.net/

Heller Bryan (2003), "Fatigue Response of Pretensioned Concrete Beams", M.S. Thesis, Department of Civil Engineering, the University of Texas at Austin.

Hornswell, Cindy. "Fred Hartman, 75, first a printer, now he 'owns the place'." Houston Chronicle May 29, 1983.

MacDougall, Collin and Bartlett, F. Michael (2003) "Tests of Unbounded Seven-Wire Tendon with Broken Outer Wires," ACI Structural Journal, September-October 2003.

Pebley, Aaron J. (2005), "Bending Stresses in Stay-Cables During Large-Amplitude Vibrations – A Fred Hartman Bridge Case Study", M.S. Thesis, Department of Civil Engineering, the University of Texas at Austin.

Poser, Marcel (2001), "Full-Scale Bending Fatigue Tests on Stay Cables", M.S. Thesis, Department of Civil Engineering, the University of Texas at Austin.

PTI Guide Specifications (2001), "Recommendations for Stay Cable Design, Testing and Installation", Post-Tensioning Institute, Phoenix, AZ.

Ridd, Jennifer (2004), "Fatigue Performance of Stay Cables", M.S. Thesis, Department of Civil Engineering, the University of Texas at Austin.

Texas Daily Newspaper Association, personal e-mail with Darla Thompson, Director of Member Services, January 13, 2006.

Texas Department of Transportation, personal e-mail with David Mraz, Bridge Engineer at TexDOT, January 17, 2006.

Texas Department of Transportation, images of video taken April 4, 1997 by TexDOT employee.

Virlogeux, Michel (1998), "Cable vibration in cable-stayed bridges", *Bridge Aerodynamics*, Proceedings of the International Symposium on Advances in Bridge Aerodynamics, Copenhagen, Denmark.

www.texasexplorer.net/hartmanbridge.htm, 2006.

Zuo, Delong and Jones, Nicholas P. (2005), "Stay-Cable Vibrations Monitoring of The Fred Hartman Bridge (Houston, Texas) and The Veterans Memorial Bridge (Port Arthur, Texas)," Final Report to: The Texas Department of Transportation and the University of Texas at Austin.

VITA

Matthew James Bean was born in Las Cruces, New Mexico, on September 20, 1978 to Brent and Vanita Bean. After high school, Matthew served a mission in the island nation of Fiji for the Church of Jesus Christ of Ladder-Day Saints. He attended New Mexico State University to earn a Bachelor's Degree in Civil Engineering.

Matthew and Stephanie were married December 28, 2000, in Albuquerque, New Mexico. After five years of marriage, Preston James Bean was born to them on January 27, 2006.

Matthew began his education at UT in August of 2004. He received his Master of Science in Engineering in May 2006 under the direction of Dr. Sharon Wood and Dr. Karl Frank.

Permanent Address
3702 Frankford Road #13105
Dallas, TX 75287

This thesis was typed by the author.